Transport of trace gases measured in the marine boundary layer in the tropical West Pacific during the TransBrom-Sonne campaign

Diploma Thesis
by
Sebastian Wache

Mathematisch - Naturwissenschaftliche Fakultät der
Christian - Albrechts - Universität zu Kiel
Erstellt am Leibniz - Institut für Meereswissenschaften
Forschungsbereich 1
- Maritime Meteorologie -

Kiel, November 2010

Abstract

This thesis describes the TransBrom-Sonne cruise and the evaluation of the transport of three different atmospheric trace gases, which were measured during the cruise. The campaign started in Tomakomai, Japan (42°N 141°E), sailed through the Western Pacific, and ended in Townsville, Australia (19°S 146°E). Because of their role in ozone depletion methyl iodide and bromoform as natural trace gases are investigated. Additionally methane as an anthropogenic trace gase is investigated as well.
To chase these air masses 5 day backward trajectories are calculated. First two independent trajectory models (Hybrid Single Lagrangian Integrated Trajectory [HySplit], British Atmospheric Data Centre [BADC]) using different meteorological input data (National Centers for Environmental Prediction - Global Data Assimilation System [NCEP-GDAS], operational European Centre of Medium-Range Weather Forecasts [opECMWF]) are compared with each other. Both models generally agree, although, the HySplit trajectories have a larger spread than BADC trajectories. The comparison of the whole cruise track reveals a good qualitative agreement, however, the BADC trajectories are often longer than the HySplit trajectories, which is due to higher wind speeds in the meteorological input data. Furthermore the onboard measured wind speeds and wind directions are used other way around to verify the high resolution opECMWF wind data. Overall, the opECMWF data show a good agreement to the observed wind fields. However, the maxima in wind speed, especially during storm/typhoon events, are underestimated in the opECMWF data. For the investigation of source regions the HySplit trajectories are used. The whole cruise and its adjacent regions are classified into 10 boxes based on their open ocean or mainland/island characteristics. The main difference is the separation due to anthropogenic and natural source regions. Additionally a separation is done by classification of different meteorological regimes. On the one hand three meteorological regimes were identified on the other hand 8 source regimes were used due to the observed bromoform characteristics during the cruise. The first part of the cruise was mainly influenced by northerly winds and mainland of Japan, East Russia and China leading to high concentrations of the three measured gases. Especially, the tropical storm events lead to high correlation of wind speed and methyl iodide concentration (coefficient of 0.56). Methane and bromoform show no such correlation with wind speed. In the middle part of the cruise weak easterly winds and the open ocean source lead to a steady concentration of the trace gases. The last part of the cruise was influenced by trade and southerly winds and coastal regions. Thus the amounts of bromoform and methyl iodide reach their maxima with 4 ppt respectively 1 ppt. In contrast, over the whole cruise, methane shows the typical global distribution with a gradient between the northern (NH) and southern hemisphere (SH) with 1860 ppb respectively 1750 ppb, due to more mainl and hence more anthropogenic influences on the NH.

Zusammenfassung

In dieser Diplomarbeit werden die TransBrom-Sonne Kampagne und die während der Fahrt gemessenen Spurengase analysiert. Die Kampagne startete in Tomakomai, Japan (42°N 141°E), durchquerte den westlichen Pazifik und endete in Townsville, Australien (19°S 146°E). Gemessen wurden zum einen Methan als überwiegend anthropogen verursachtes Gas, sowie Bromoform und Methyliodid, die hauptsächlich aus natürlichen Quellen entstehen. Methyliodid und Bromoform stehen außerdem im Zusammenhang mit der Ozonzerstörung in der Stratosphere. Um die Herkunft dieser Gase und ihren Weg bis zur Schiffsposition, an der gemessen wurde, bestimmen zu können werden Trajektorien berechnet. Die Trajektorien reichen dabei 120 Stunden (5 Tage) zurück.
Zuerst werden zwei verschiedene Trajektorienmodelle (HySplit, BADC) miteinander verglichen. Dafür werden zum einen 27-Trajektorien-Ensembles für Fallstudien untersucht, sowie Einzeltrajektorien über die gesamte Fahrtroute. Das HySplit-modell benutzt dabei NCEP-GDAS-Assimilationsdaten, das BADC-Modell operationelle ECMWF-Assimilationsdaten als Eingangsdatensätze. Beide Modelle zeigen im Vergleich ein ähnliches Verhalten und ähnliche Wegstrecken. Die HySplit-Trajektorien zeigen im Gegensatz zu den BADC-Trajektorien eine weitere Streuung. Die BADC-Trajektorien hingegen zeichnen sich durch längere Reichweiten aus, was für höhere Windgeschwindigkeiten in den Ausgangsdaten spricht.
Im weiteren Verlauf werden hochaufgelöste opECMWF-Daten mit den vom Schiff gemessenen Windgeschwindigkeiten sowie Windrichtungen verglichen. Insgesamt passen die assimilationsdaten gut zu den Messwerten, unterschätzen aber die extremen Windgeschwindigkeiten. Vor allem während den Taifunereignissen besteht ein Unterschied von mehr als 6 m/s. Für die Auswertung der Quellregionen mit Hilfe der Trajektorien wird das HySplit-Modell genutzt, da es eine einfache und schnelle Handhabung aufweist. Außerdem wurde das Modell auch in früheren Untersuchungen verwendet, wodurch eine Vergleichbarkeit geschaffen wird.
Zur genaueren Auswertung sind die gesamte Fahrt und die angrenzenden Regionen in 10 Boxen unterteilt. Dabei wird zwischen Festland/Inseln und offenem Meer unterschieden. Das Hauptaugenmerk liegt dabei auf anthropogenen und natürlichen Quellen. Dabei wird übergeordnet die gesamte Fahrt in drei meteorologische Regime eingeteilt. Diese basieren auf den gemessenen Windrichtungen. Zusätzlich wird eine feinere Einteilung basierend auf dem gemessenen Bromoformgehalt gemacht.
Der erste Teil der Fahrt ist durch nördliche Winde geprägt. Dabei kommen die Luftmassen hauptsächlich vom japanischen, ostrussischen und ostchinesischen Festland, was zu einer erhöhten Konzentration aller drei Gase führt. Vor allem während der Sturmereignisse sind die Konzentrationen erhöht. Methyliodid weist dabei die höchste Korrelation von 0.56 über die gesamte Fahrt auf. Bromoform und Methan zeigen dagegen keine hohen Korrelationswerte mit der Windgeschwindigkeit. Im weiteren Fahrtverlauf sinken die Konzentrationen, was auf den offenen Ozean und den schwachen alternierenden Wind zurückzuführen ist. Nach Überqueren des Äquators beginnt der Einfluss der starken Passatwinde und der südlichen Winde. Auch die Nähe zur Küstenregion von Papua Neuginea und Australien lassen die

Konzentrationen von Bromoform und Methyliodid wieder ansteigen mit Werten von 4 ppt, beziehungsweise 1 ppt. Der Verlauf des Methangehalts zeigt über die gesamte Fahrt den typischen NH-SH-Gradienten. Die Werte liegen dabei auf der NH mit 1860 ppt höher als auf der SH, wo sie bei 1750 ppt liegen. Durch mehr Festland auf der NH ist auch die Anzahl der anthropogenen Quellregionen höher.

Contents

Chapter 1

Introduction

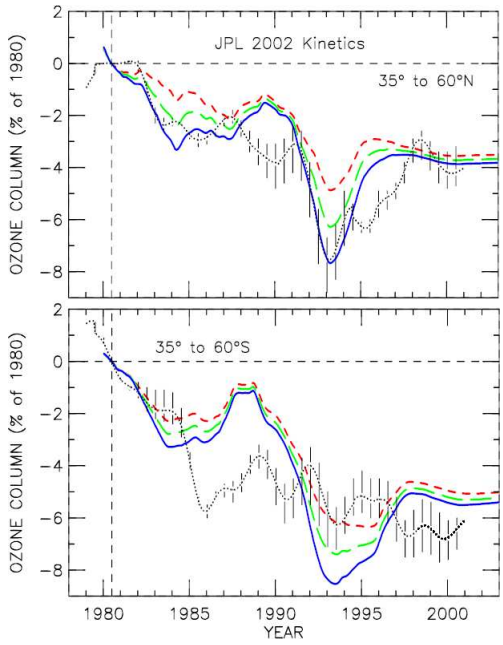

Figure 1.1: Calculated change in column ozone relative to 1980 (AER 2-D model) in the regions of 35°N - 60°N (top) and 35°S - 60°S (bottom). Stratospheric Br_y ^{VSLS} in different concentrations, 0 (red), 4 (green), and 8 (blue) ppt compared with observed trend in total ozone (black line) are shown (Salawitch et al., 2005).

In 2006 observations recorded the biggest ozone hole (in 13-20 km) since its discovery in 1985 (NASA, 2006). The decrease of ozone is mainly caused by anthropogenic chlorine and bromine compounds especially at the poles and mid-latitudes (WMO, 2007b) Recent findings suggest that natural halocarbons also play a role in ozone depletion in mid-latitudes. Total inorganic bromine measured in the stratosphere is

higher than can be explained by anthropogenic emitted bromine compounds (Dorf et al., 2006). Measurements show high emissions of reactive bromine and iodine in marine regions, especially in coastal and upwelling regions of the tropical ocean (Quack et al., 2004), which may be responsible for ozone depletion in the troposphere and stratosphere (Chameides and Davis, 1980). However, ∼5 ppt are missing. Model studies by Salawitch et al. (2005) accounts ∼65 % and ∼75 % of the observed ozone depletion in the 35-60°N and 35-60°S regions including 0 ppt of Br_y. A better overall agreement shows the model run including 8 ppt with ∼92 % of measured ozone loss in each hemispheres (Figure 1.1).
According to model simulations interaction of high emissions and strong convection processes can transport halocarbons into the stratosphere. In the tropical Western Pacific no measurements of marine short lived bromine compounds have been carried out before. The marine halocarbon production is related to the biological activity (e.g. macro algae) in the ocean. The influence of marine halocarbons in future can be higher due to climate change. Higher surface temperatures, changes in ocean and atmospheric circulations and a change in biological activity can all impact future VSLS emissions.
The goal of this thesis is to investigate the origin of air masses in the marine boundary layer, which were measured during the TransBrom-Sonne campaign in the Western Pacific. This study concentrates on the meteorological influence on three different trace gases bromoform, methyl iodide and methane, which are introduced in Chapters 2 and 3. The weather situations during the TransBrom-Sonne cruise and a meteorological intercomparison between ship measurements and operational ECMWF data are given (Chapter 5). Chapter 6 compares the air mass origin of VSLS with HySplit and BADC trajectory simulations. The last result chapter of this thesis includes the analysis of the air masses along the cruise track, classified in meteorological and source regimes (Chapter 7). Finally a conclusion and outlook is drawn in Chapter 9.

Chapter 2

Fundamentals

In this Chapter the fundamentals which are relevant for the TransBrom-Sonne cruise are explained. First the structure of the atmosphere is introduced with a detailed view on the troposphere and the stratosphere. Afterwards the general global wind circulation is shown. The last section gives an overview of the tropical meteorology with its characteristics.

2.1 Structure of the atmosphere

The typical classification of separate parts of the atmosphere is done by the temperature gradients. Classifications by ionization, friction or compound are acceptable as well. In this section the typical separation by temperature is explained.
In the planetary atmosphere three heating layers, which have three temperature maxima, exist:

- The lowermost heating layer (the earth's surface) due to absorption of the sun light between 0.3 μm and 5 μm of wavelength.
- The middle layer up to 50 km because most of the UV radiation is absorbed by ozone and heats the layer.
- The highest heating layer above 100 km due to the absorption of extreme UV radiation by oxygen.

Chasing a temperature maximum, the temperature gradient is negative during increasing altitude until the temperature minimum between the layers is reached. Then the vertical temperature gradient reverses its sign between the minimum and the next heat layer, whose can be seen in Figure 2.1 . Because of this temperature profile the atmosphere is divided into five spheres. Between theses spheres boundaries exist, which

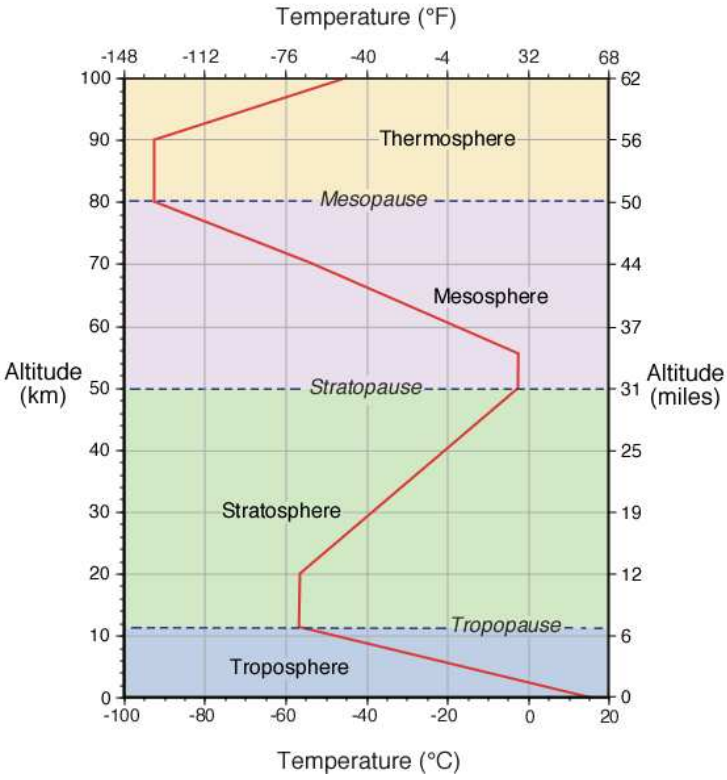

Figure 2.1: Temperature structure of the atmosphere against the altitude with corresponding spheres (Pidwirny, 2010)

notations end with the word “pause“, e.g. tropopause or stratopause (Deutscher Wetterdienst, 1987; Haeckel, 2005).

2.1.1 Troposphere

The troposphere is named after the Greek word “tropein“ , which means rotate, and characterizes the activity of turbulence and therefore rotation of air masses in this sphere. The earth’s surface absorbs insolation, becomes warmer and releases the heat to the lowermost air layer. The transport to higher altitudes takes place by convection and turbulence. Due to a convection-equilibrium, the temperature decreases with increasing height. The warmer air raises. Because of decreasing pressure and density with increasing altitude, the air expands and therefore becomes colder. The energy for this work comes just from the air itself (latent heat), thus the internal energy decreases. Because of the available amount of heat between the boundary layer and the tropopause in the tropics, the tropopause is higher and colder in warmer regions. In the tropics it reaches up to 18 km and -90°C compared to the lower and relative warmer tropopause at mid-latitudes (12 km and -60°C) and polar regions (7 km and -60°C). The troposphere includes round 100% of water vapor and 3/4 of atmospheric mass. The larger amount of water vapor in this sphere is the reason for the weather events, e.g. clouds and rain (Deutscher Wetterdienst, 1987; Haeckel, 2005).

2.1.1.1 Boundary Layer

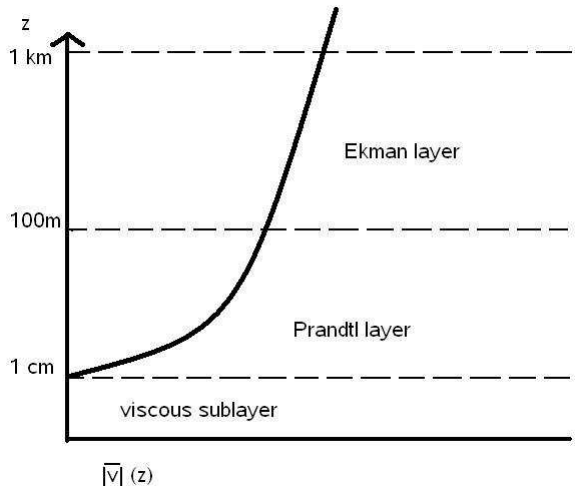

Figure 2.2: The Boundary Layer is classified into three different layers. In addition the wind speed increase with increasing height is shown (Etling, 2008).

The Boundary Layer (BL) is the lowermost layer in the troposphere. Within the BL mainly friction matters. The friction on the surface leads to a turbulence and deflection of the wind and hence, it induces a change in direction and speed of flow. Turbulence starts by more than 3 m/s windspeed. Near the surface, the wind flows in an angle up to 30° in a low pressure system due to friction, depending on the surface conditions. Over water the angle lies between 10° to 20°. With increasing altitude and decreasing friction the wind flows more clockwise and become stronger until ∼1000 m where it flows parallel to the isobars (lines of equal atmospheric pressure). Above the BL the geostrophic wind (balance of pressure gradient and Coriolis force) flows approximately laminar, without any surface impacts. Energy is dissipated throughout the BL due to turbulent mixing in vertical and horizontal directions. There are three classifications in the BL (Figure 2.2).The lowest layer is the laminar (viscous) layer within the first cm, the second is the Prandtl layer, named after L. Prandtl (1904), between 1 cm and 100 m altitude and the last and highest one is the Ekman layer, named after W. Ekman (1902), until 1000 m altitude (Etling, 2008). In the lowermost laminar layer transports of impulses, heat and moisture of molecular activity are the main processes. In the Prandtl layer turbulence increases from 20 m to 100 m altitude. The shearing stress and the exchange of impulses, sensible and latent heat are constant in the Prandtl layer and lead to a logarithmic wind distribution within this region. Already 50% to 70% of geostrophic wind is reached at the top of the Prandtl layer (Deutscher Wetterdienst, 1987). The main difference between the Prandtl and Ekman layer is that the exchange of transport in the Ekman layer depends on height.
In general, emissions of pollution, which could be anthropogenic trace gases, but also natural compounds, heat and energy transfer can influence the development of the BL.

2.1.1.2 Tropopause

The tropopause is the region of the atmosphere that lies between troposphere (2.1.1) and the stratosphere (2.1.2). Within the tropopause the lapse rate changes from being positive (in the troposphere) to negative (in the stratosphere). The exact definition used by the World Meteorological Organization (WMO) is as follows:

The lowest level at which the lapse rate decreases to 2°C/km or less, provided that the average lapse rate between this level and all higher levels within 2 km does not exceed 2°C/km (Roe and Jasperson, 1981).

It is also possible to define the tropopause by chemical composition due to the ozone amounts of the troposphere (low ozone) and the stratosphere (high ozone). It is a boundary varying in height depending on altitudes and hence, the height of the troposphere. At the poles it lies on an averaged altitude of ∼11 km and raises up to ∼17 km

over the equator. In the tropics convective overshoot can transport trace gases in and through the tropopause directly into the stratosphere, where they can deplete ozone (WMO, 2007b).

2.1.2 Stratosphere

The stratosphere (lat. stratus = layered) is a stable stratified sphere with slow vertical motion of warm and dry air masses due to absorption of ultraviolet radiation in the ozone layer in 15-50 km altitude (radiative equilibrium). The maximum of ozone is in 25 km height and has a close relationship to the temperature maximum in 50 km height. In the higher altitudes more absorption takes place than in lower, therefore the temperature increases with height. The maximum temperature, at the top of the ozone layer, lays between 47 km and 51 km. This layer is the end of the stratosphere and hence, it is called stratopause. The temperature of the stratosphere is also dependent on the angle of solar radiation and the ozone distribution within the stratosphere itself. These factors describe the diurnal of stratospheric temperatures in mid latitudes and polar regions. Hence, the highest temperatures are reached in the summer phases on each hemisphere. Therefore, a temperature gradient between both poles develops. The stratosphere is categorized into three vertical sections (U.S. Standard Atmosphere, 1976) (Figure 2.1):

- Isothemal layer from 15 km to 20 km (tropopause region).
- Increase of temperature of 1 K/km up to 32 km height.
- Increase of temperature about 2.8 K/km up to the stratopause (round 50 km), where temperatures lies at 0° C.

The water vapor content in the stratosphere is much less than in the troposphere (Section 2.1.1). Not only ozone plays an important role in the stratosphere, O_2, CO_2, H_2O, NO_2, and other green house gases control the earth's energy budget (Deutscher Wetterdienst, 1987; Haeckel, 2005).

2.2 General Circulation

The oldest theory of the General Circulation (GC) was developed by Woeikow (1874). The newer descriptions of the GC were created by Hermann Flohn and Sverre Petterssen in the beginning of the 1950s (Flohn, 1950a; Petterssen, 1950).

The main accelerator for the GC is the solar radiation. Based on more insolation in the tropics than in the polar regions there is an imbalance which has to be compensated. In Figure 2.3 it can be seen, that the warmer air at the equator rises and generates a

low pressure zone, which is called the Intertropical Convergence Zone (ITCZ, Section 2.2.1). The loss of equatorial air mass has to be filled up by surface flows, which are named the trade winds. Due to the Coriolis force the trade winds are diverted to the right in the NH and to the left in the SH. Therefore the trade winds come from the northeast in the NH and from the southeast in the SH and converge at the equator. Due to upward motion the air masses develop a high pressure system in specific height, they flow against trade winds (antitrades) and sink at ca. 30° north and south because of the subtropical ridge and less space in the height due to the sinking of the tropopause from the tropics to the polar regions. This is a closed and direct thermal cell, which is called the Hadley cell. Due to the fact that the earth rotates two more cells develop. If the earth would not rotate just one big cell from the tropics to the polar regions would exist. One of the two cells is the polar cell. It is also a direct thermal cell, where the cold air sinks at the poles and stabilizes the system at the surface. The point (∼60°N/S), where the polar cold air and the subtropical warm air converge, is called polar-front. It leads to pronounced weather phenomena, e.g. precipitation, strong westerly winds, and thunderstorms. The cell between the polar and Hadley cell is called the Ferrel cell, it is a indirect thermal one due to the existence of the two direct thermal cells and the circulation is in the opposite direction.

2.2.1 Intertropical Convergence Zone

At the equator solar insolation reaches its maximum. Warm air masses rise, loose density and cool down during its ascend. Therefore the ITCZ is a continuous band of converging air mass and hence, a low pressure band. If the dewpoint is reached during rising, convective clouds are build. By further rise of air mass, in such convective cloud systems precipitation and thunderstorms develop. Very occasionally the convection is high enough to penetrate the tropopause and reach the stratosphere (Liu and Zipser, 2005). The tropopause can be regarded as a barrier for the air and is driven to diverge. These air masses are then directed the way to the north or to the south. At 30° N/S (horse latitudes and regions of deserts) the air sinks and gets warmer and dryer. Due to the fact that mass has to be conserved, the air converges on the surface at the equator. These appearing winds are called trade winds (Section 2.2). Because of following the zenith, the ITCZ shifts either north of the equator during the northern summer, or south during the boreal winter (Figures 2.4 and 2.5).

2.3 Walker Circulation

The Walker Circulation (WC), named by Jacob Bjerknes after Sir Gilbert Walker (Bjerknes, 1969), is a zonal atmospheric circulation parallel to the equator. The WC

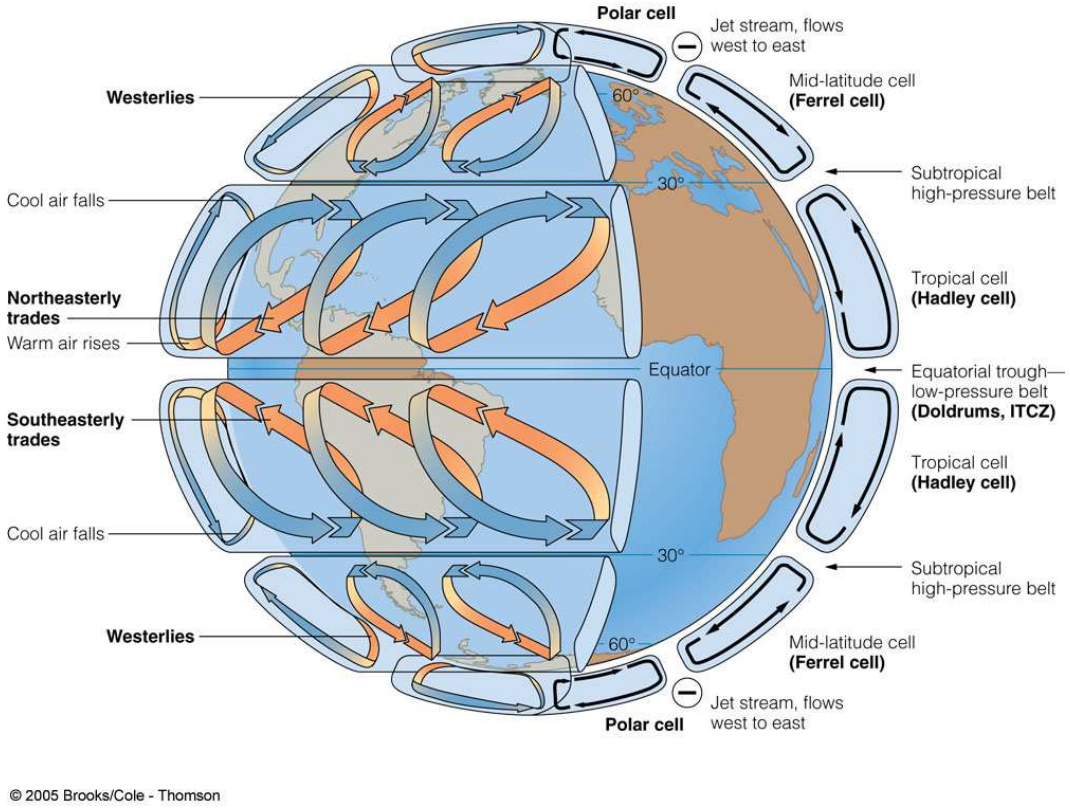

Figure 2.3: The general circulation at the surface and troposphere are drawn alongside the globe. Source: http://science.kennesaw.edu/∼jdirnber/oceanography/LecturesOceanogr/LecCurrents/0813.jpg

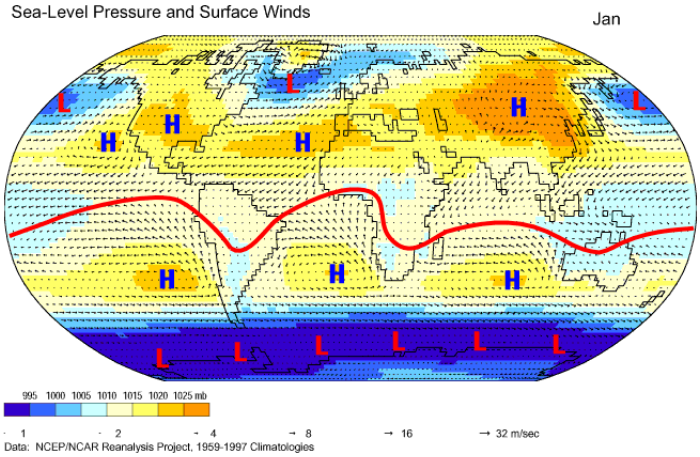

Figure 2.4: ITCZ (red line), horizontal winds and pressure systems during January, based on a climatology from 1959 - 1997 (NCEP/NCAR reanalysis). Source: Climate Lab Section of the Environmental Change Research Group, Department of Geography, University of Oregon

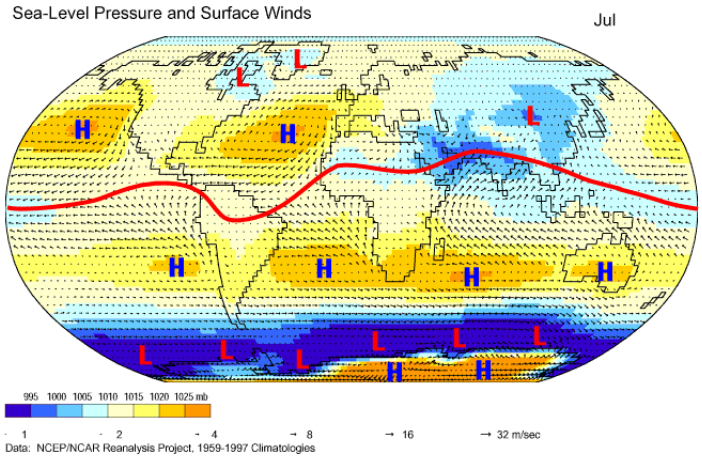

Figure 2.5: ITCZ (red line), horizontal winds and pressure systems during July, based on a climatology from 1959 - 1997 (NCEP/NCAR reanalysis). Source: Climate Lab Section of the Environmental Change Research Group, Department of Geography, University of Oregon

overlays the meridional Hadley cell at both hemispheres. The oceanic Humboldt current flows along the South American westcoast to the north and gets into the equatorial current. From east to west the water becomes warmer. Near Indonesia the warm water accumulates, leading to increased convection and precipitation. The oceanic counterpart is upwelling of cold deep water in the eastern part of the Pacific. This leads to sinking of air masses, high pressure and droughts (e.g. Atacama dessert at 22°S and 69°W). Because of these combined effects in the ocean and in the atmosphere a circulation (Walker Circulation) is developing, occurring between Australia and South America (Figure 2.6). Temporarily the WC can be weakened or even reversed and El Niño phenomena develops (Section 2.5).

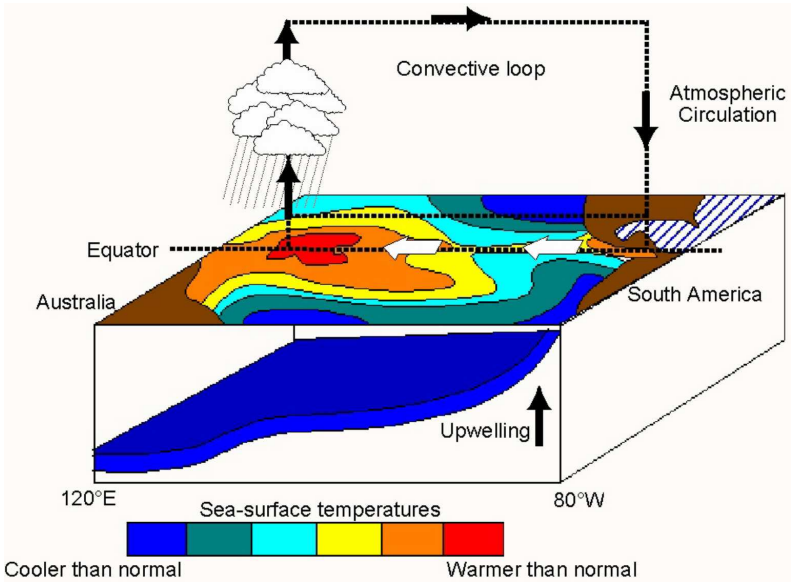

Figure 2.6: The atmospheric circulation along (zonally) the equator is called the Walker Circulation. Source: http://old.weathersa.co.za/References/elnino_ENSO1.jpg

2.4 El Niño-Southern Oscillation

The theory was developed by Bjerknes (1966, 1969) and one of the first persons who described the oscillation was Walker (1923, 1924).El Niño-Southern Oscillation (ENSO) is a quasi-periodic climate pattern that occurs every three to 7 years across the tropical Pacific Ocean. It is characterized by variations in the Sea Surface Temperatures (SST) of the tropical Eastern Pacific. If the Pacific is warmer than normal, so called El Niño (Spanish for the Christ Child) event develops and if it is colder it is an La Niña event. For an indication of these two events different indices exist to observe ENSO. One is the

NIÑO3 index, which is the temperature average over the region from 5° S to 5° N and from 150° to 90° W. Another one is the Southern Oscillation Index (SOI) (Figure 2.7), which is defined as the difference of the normalized mean sea level pressure Tahiti minus Darwin (Troup, 1965; Koennen et al., 1998). ENSO has an important global impact. Especially during the warm phase (El Niño) the Western Pacific region becomes dryer (Figure 2.10).

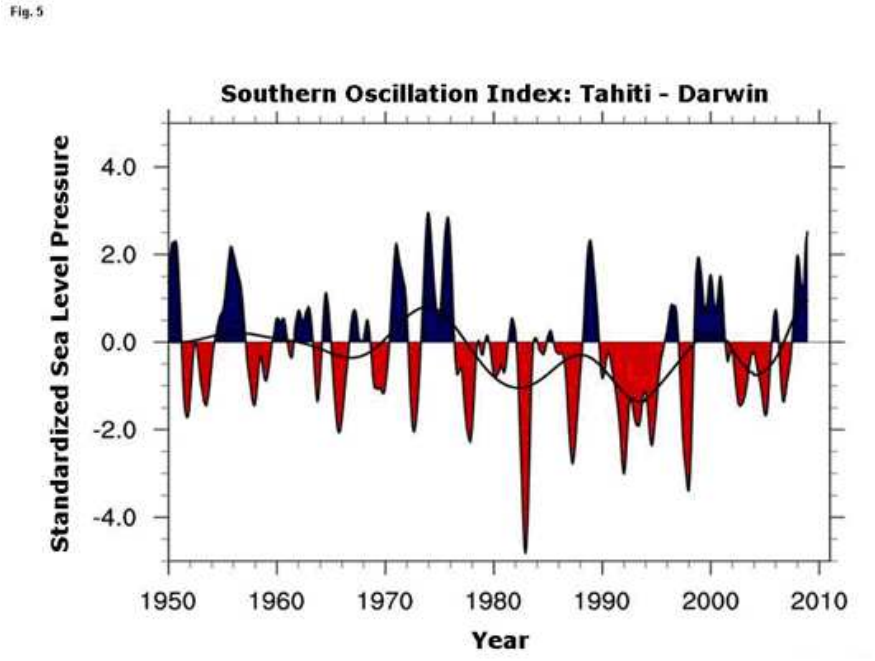

Figure 2.7: The Southern Oscillation Index, in standardized units of sea level pressure, shows monthly values. Red are the positive sea level pressure anomalies at Darwin and hence El Niño conditions. The black curve shows decadal variations. Source: http://jonova.s3.amazonaws.com/graphs/g/fig-5-soi-darwin-web.gif

2.5 El Niño / La Niña

El Niño was first detected by Peruan fishers. Every three to 7 years during Christmas time the cold Humboldt current was replaced by a weak warm current. If the pressure gradient between the Eastern and the Western Pacific decreases, consequently the Pacific trade winds have to decrease. Due to the replacing of cold water by a warmer current along Peru's coast the atmosphere gets unstable and convection develops. Unusual periods of precipitation takes place at the West coast of South America,

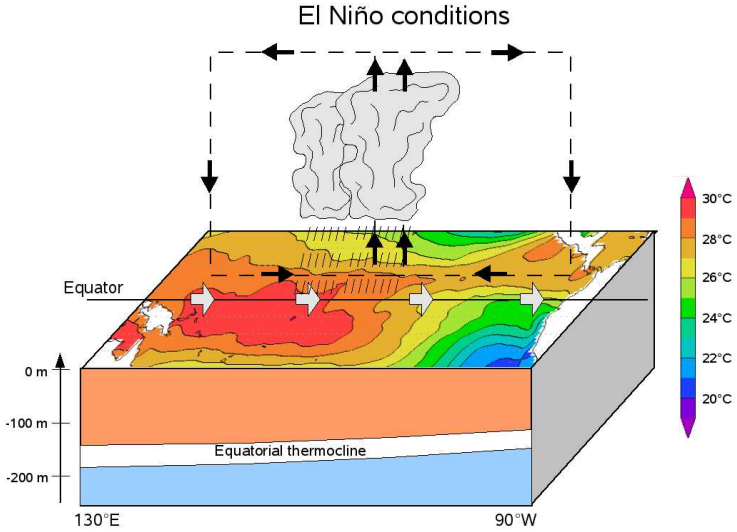

Figure 2.8: The ocean state for El Niño. The thermocline and the motion of air (black arrows) is illustrated. The red shading indicates warm water (Frauen, 2010).

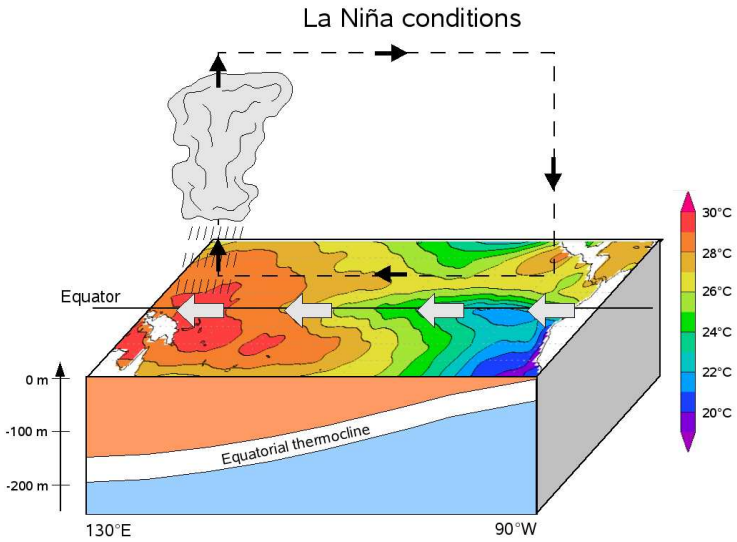

Figure 2.9: The ocean state for La Niña. The slope of thermocline and the motion of air (black arrows) is illustrated. The blue shading indicates cold water (Frauen, 2010).

occasionally leading to rain fall in the Atacama desert. In contrast the Western Pacific becomes dryer, which is seen in Figures 2.8 and 2.10.
La Niña (Spanish for girl) is a counterpart to El Niño and is distinguished by negative SST anomalies (Figure 2.9). Superior high pressure between South America and Indonesia leads to stronger trade winds in the Pacific ocean. Therefore, warm water is driven to the western part of the Pacific. Consequently, the temperatures over Peruan Pacific regions are colder, the thermocline is rising and more aridity exists, because of more stable atmospheric conditions. In contrast the convective center shifts to the west. Due to higher temperatures more convection develops, which leads to more precipitation over Australia and Indonesia.

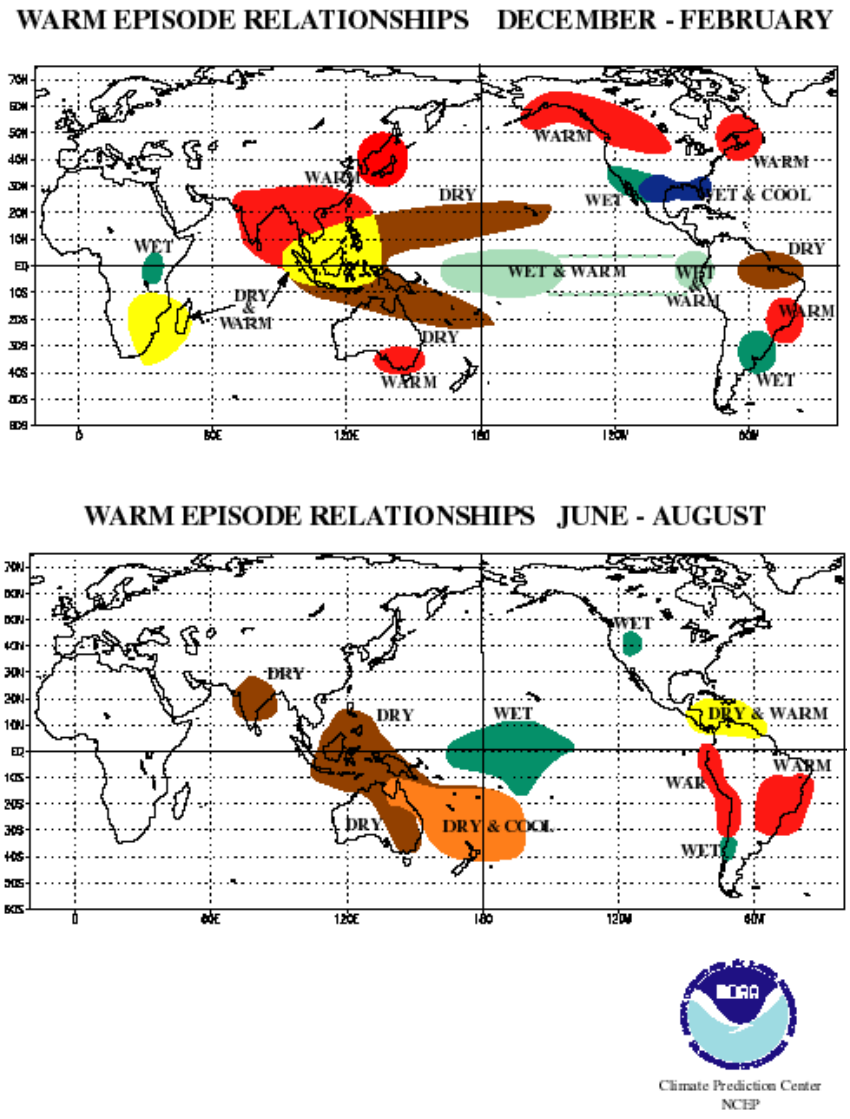

Figure 2.10: El Niño has climate impacts the over globe. The upper picture shows these impacts during boreal winter. The lower picture shows it during boreal summer. Source: http://www.knmi.nl/research/oceanography/enso/nino/

2.6 Typhoon

Typhoons, also known as hurricanes (North Atlantic / Northeast Pacific), Willy-Willy (Australia) or cyclones (India), are heavy storms which develop in tropical and sub-tropical regions. Six different regions of origin exist:

- Bay of Bengal
- Cape Verdes
- Central Indian Ocean
- Coralsea
- Northeast Pacific (southerly region)
- Northwest Pacific / Phillippine Sea
- South Chinese Sea

The origin of round 80 tropical storms per year lies between 5° and 22° N/S. Between the equator and 5° the Coriolis Force is missing or too weak for developing storms. A trough of "Easterly Waves" serves as a disturbance in the atmosphere, advancing cloud clusters and rotation of the air masses which have enough Coriolis Force. In most cases cloud clusters of thunderstorms induce the tropical storm formation. Additionally, a weak vertical wind shear not exceeding 10 m/s is necessary between the 950 hPa and 200 hPa layers. However, the main important factors are the SSTs. For developing tropical storms SSTs of round 27° C or higher are needed. Latif et al. (2007) reported that the SST difference between the tropical Indo-Pacific and North Atlantic region has an impact on the wind shear over the Atlantic, influencing the hurricane development. In a study by Gray (1979) using more than 20 years of observation, the origins are recognized where tropical depressions intensify and change to tropical storms with a maximum surface windspeed from 20 m/s to 25 m/s. In storms warm and wet air masses raise and condensate at higher altitudes. During condensation potential energy, detracted from the ocean before, becomes released and sinks. The surface pressure decreases, the air column looses density and gets warmer, leading to an increase of more warmer and wetter air for the developing typhoon. This self intensifying cyclone forces the structure to a tropical storm. Windspeeds of 8 Beaufort (Bft) to 11 Bft mark a tropical storm. From 12 Bft on the depression is called a typhoon (or hurricane) and will be classified by the Saffir-Simpson-Scale (Table 2.6). However, the classification of this scale partly varies with small deviations in the different basins (WMO, 1993).

Typhoon category	**Wind speed (km/h)**
Tropical depression	< 63
Tropical storm	63 - 118
Category 1	119 - 153
Category 2	154 - 177
Category 3	178 - 209
Category 4	210 - 249
Category 5	> 250

Table 2.1: The Saffir-Simpson-Scale divides typhoons in five categories by its strength. Source: http://coolgeography.co.uk/GCSE/Year11/Managing Hazards/Tropicalstorms/tropical-storms.htm

To keep typhoons alive the Coriolis Force is needed, else, the amount of air which flows into the storm would balance the pressure gradient after a certain time. Due to the Coriolis Force a rightward drift on the NH and a leftward drift on the SH leads to a rotation of storm systems, leading to a counterclockwise/clockwise rotation on the NH/SH. Because of this fact the air flows in spirals to the center of the storm, building a high wall of clouds, named “Eyewall“. The rotation speed in such a wall is too fast for the air to reach straight the center. The air converges and is forced to raise. The highest precipitation and highest wind speeds are observed in such walls. Directly in the center of the storm the air sinks, becomes warmer and dryer. This leads to a dissipation of clouds and development of the typical “eye“ (Figure 2.11). Such an eye is cloudless, calm and 10° C to 15° C warmer than the surrounding area of the typhoon. Tropical storms move along the tropospheric winds, especially the trade winds. Most of the time they chase the direction of of the strongest energy input, which is mainly given by the SST of 27° C or higher. As soon as the tropical storm/typhoon reaches colder regions or land masses it damps, because of missing energy and an increasing friction over land. Thus the tropical storm could change into an extra tropical storm (Anthes, 1982).

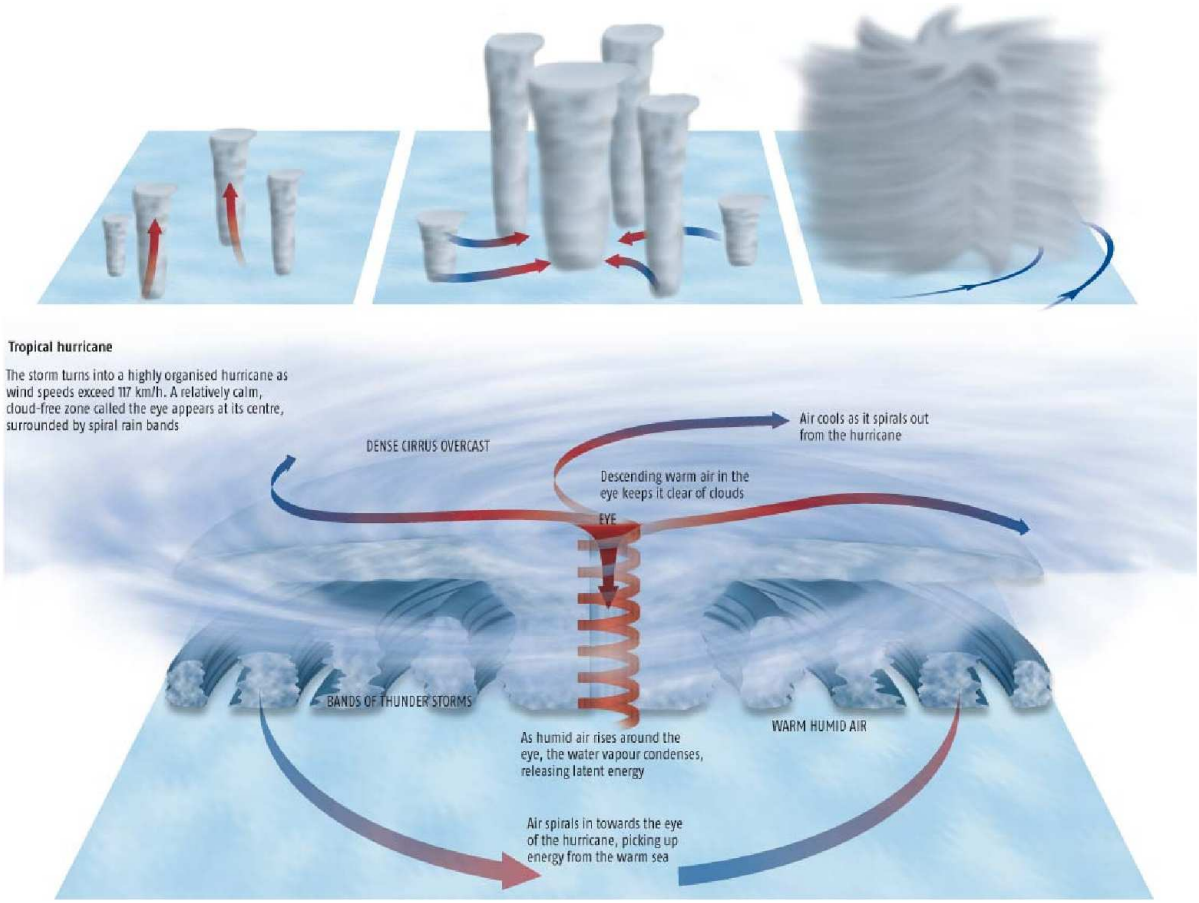

Figure 2.11: Development from a tropical disturbance to a typhoon. Source: http://www.newscientist.com/data/images/archive/2528/25281301.jpg

Chapter 3

Chemistry

3.1 Very short lived substances

In this Chapter the very short lived substances (VSLS) are introduced. Especially bromoform and methyl iodine are examples for natural sources of VSLS.
A third more anthropogenic trace gas, methane, is examined in Section 3.2.1.

Atmospheric trace gases are generally classified into "long lived" and "short live substances" while this classification is not well defined. Short lived trace gases include trace gases with lifetimes of less than 1 or 5 years. VSLS are defined as trace gases, whose local tropospheric lifetimes are comparable to or shorter than tropospheric transport time scales, so that their tropospheric distributions are non-uniform. VSLS have atmospheric lifetimes of less than 6 months (WMO, 2007b).

3.1.1 Bromoform

The largest source of organic bromine into the atmosphere is bromoform ($CHBr_3$). It has a lifetime of two to three weeks and releases very short lived bromine radicals into the troposphere and stratosphere, where they contribute to photochemical reactions, especially ozone depletion. The concentration of bromoform ranges from less than 1 ppt in the open ocean and often <10 to 400 ppt in coastal regions (Quack and Wallace, 2003). In the open ocean phytoplankton is considered to be the main source for bromofrom of ocean waters and atmosphere. In coastal regions macro algae are a major source of $CHBr_3$. $CHBr_3$ also has anthropogenic sources like the disinfection of coolant, bath or drinking water (Blake et al., 2003). All forms of chlorinated and ozonated water contain bromoform, while coastal power stations contribute the most to the anthropogenic source of 0.3 Gmol/yr and are locally very important. However natural oceanic emissions contribute with 9-13 Gmol/yr many times more to the atmosphere: 13-17 % from coastal regions, 34-43 % from the open ocean and 44-48 % possibly from

shelf seas. Special regions of importance for atmospheric $CHBr_3$ and for reactive Br-species may be the tropics and subtropics (Quack and Wallace, 2003; Warwick et al., 2006). Butler et al. (2007) and Quack et al. (2004) reported the highest $CHBr_3$ fluxes in upwelling water regions, especially near the equator, and at oceanic fronts.

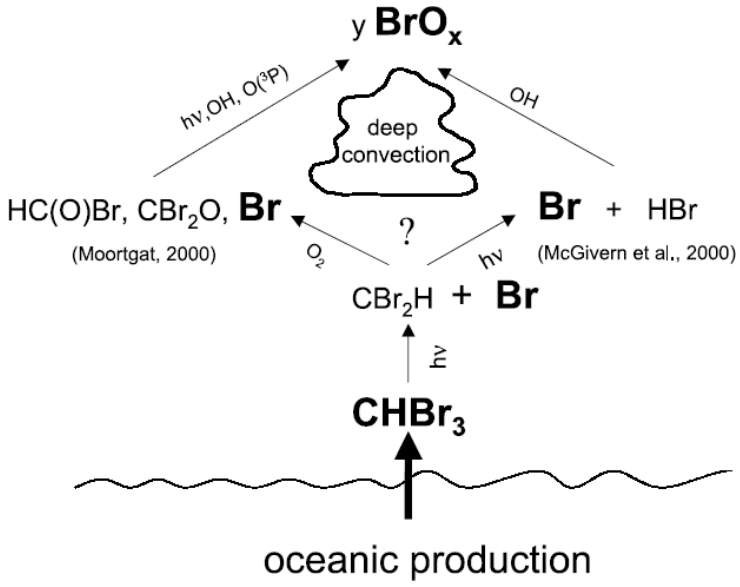

Figure 3.1: Entrainment of bromoform from oceanic production into the troposphere and stratosphere. (Quack and Wallace, 2003)

Bromoform and methyl iodide (see 3.1.2) are produced e.g. in the upper layers of the open ocean and are emitted into the atmosphere and especially entrained by deep convection to the upper troposphere and the lower stratosphere. Chemical decay of $CHBr_3$ in the atmosphere includes photolysis and reactions with oxygen (Figure 3.1). Ozone depletion caused by bromine radicals are 50-70 times higher than ozone depletion by chlorine radicals. In addition bromine and chlorine radicals support each other in the cycle of ozone depletion, which is thus 20 % higher.

3.1.2 Methyl iodide

Methyl iodide (CH_3I) has different sources. Marine natural emissions dominate the global atmospheric input, primarily through phytoplankton activity (Moore and Tokarczyk, 1993; Manley and dela Cuesta, 1997) and photochemical reactions in surface sea water (Richter and Wallace, 2004). Wet lands, peat lands (Dimmer et al., 2001), biomass burning (Andreae et al., 1996) and rice fields (Lee-Taylor and Redeker, 2005) also contribute to the atmospheric burden. Chameides and Davis (1980) showed that methyl iodide may catalytically deplete ozone in the troposphere, where it is rapidly

destroyed by ultra violet radiation leading to a lifetime for CH_3I of about 5 days (Lovelock et al., 1973; Zafiriou, 1974). It also plays an important role in other atmospheric processes as the formation of marine aerosols and cloud condensation nuclei (Chameides and Davis, 1980; Solomon et al., 1994; Davis et al., 1996; McFiggans et al., 2000; O'Dowd et al., 2002). High amounts near coastal areas and above biologically productive oceans and typical background concentrations of 0.2-2 ppt have been reported. The highest concentrations are found in the tropics and subtropics (Rasmussen et al., 1982; Blake et al., 1999; Butler et al., 2007). Li et al. (2001) measured values up to 4.9 ppt during their research cruise in the tropics of the Western Pacific. Yokouchi et al. (2008) reported that the concentration in marine boundary air at mid-latitudes correlates well with SST.

3.2 Long lived substances

3.2.1 Methane

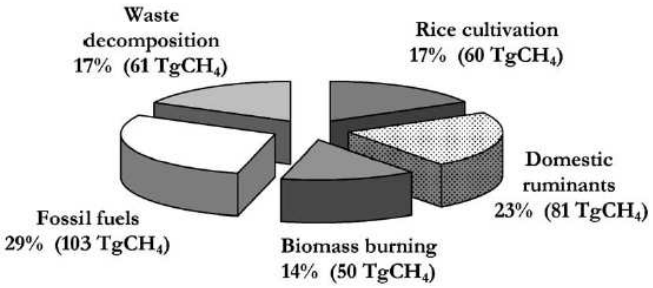

Figure 3.2: Distribution of anthropogenic sources of total methane emission (Wuebbles, D.J. and K. Hayhoe, 2002).

Methane (CH_4) has a long atmospheric lifetime (of 8 to 12 years). Hence, it shows a good horizontal and vertical mixing in the atmosphere up to the tropopause region. Methane's reactivity is important for tropospheric and stratospheric chemistry, because methane is the most abundant reactive trace gas in the troposphere. Its warming potential is 25 times higher than the CO_2 potential over a 100-year period (IPCC, 2001). Above the tropopause the mixing ratio decreases rapidly. The global average mixing ratio for 2004 at the surface was 1777 ppb (parts per billion) (Globalview CH4, 2005). This is a strong increase compared to glacial values of 400 ppb (Spahni et al., 2005) and 700 ppb in 1800 AD (MacFarling-Meure, 2004). The main reason for this high amount of methane is an increase of emissions related to biomass combustion, fossil fuel extraction, and agriculture (Figure 3.2). Fossil fuels such as natural gas,

coal, and petroleum and domestic ruminants are the leading sources, but additionally waste disposal, including enteric fermentation, animal and human waste, rice paddies, and biomass burning have the same weighting in the distribution.

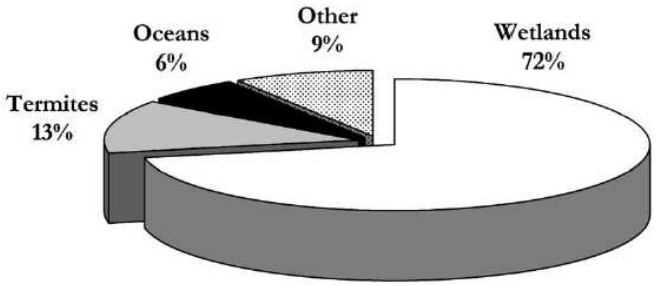

Figure 3.3: Distribution of natural sources of total methane emission (Wuebbles, D.J. and K. Hayhoe, 2002).

Natural emission sources are mainly boreal and tropical wetlands, followed by termites and other wild ruminants, oceans, and hydrates (Figure 3.3). The global growth rate decreased from about 14 ppb/yr in 1985 to almost zero in 2000 because of a steady state between a constant total of global sources and constant strength of sinks (Dlugokencky et al., 1998). The predictions of the total CH_4 in the atmosphere for the year 2100 range from 1575 to 3730 ppb (IPCC, 2001), depending on the emission scenario of the broad range of CH_4 sources (roughly half anthropogenic, half natural). Possible changes in the amount of CH_4 emissions due to melting of Arctic permafrost are not included, which adds uncertainties to the future predicts.

Chapter 4

Trajectory models, data and methods

In this Chapter the used data are introduced. Trajectory models are a good tool to investigate where air masses are come from or where they are go to. In the meteorology the pathway of an air parcel is called trajectory (lat. path). Every air parcel in a flow field **u** is moved along a pathway and changes its position **x**(t) based on following equation:

$$\frac{d\mathbf{x}(t)}{dt} = \mathbf{u}(\mathbf{x}(t), t) \tag{4.1}$$

The result of the differential equation 4.1 is the pathway of a trajectory. Local conditions influence these trajectories and hence, they are used to investigate the chemical and physical evolution of air parcels. Trajectories are a very important tool in meteorological analysis. Basics of these trajectory calculations are different models using different meteorological input data. In this study, 5 day backward trajectories of 2 different models based on assimilation data are calculated. These both models (NCEP-GDAS and opECMWF) are compared to check the discrepancy between the input data (Chapter 6).

4.1 HySplit model using NCEP-GDAS data

The HySplit-model (Version 4.9) is used to compute backward trajectories. Detailed technical information can be found in Draxler and Hess (2004). It is a complete online tool. The model runs are based upon 3D-VAR meteorological assimilation data which are sourced from the Global Data Assimilation System (GDAS, 3-hourly data archive) maintained by the National Centers for Environmental Prediction (NCEP, http://www.noaa.gov). It is a global T126 operational model. The parameters used in

this study are the u- and v-wind. The NCEP-GDAS is run 4 times a day, 00, 06, 12, and 18 UTC and model output is in GRIdded Binary (GRIB) format in a temporal resolution of 3 hours. The Gaussian grid is a 1° x 1° resulting grid. The vertical layers are separated into 24 levels from 1000 hPa to 20 hPa.

Investigating the source regions of air masses (Chapter 7) 27 trajectories ensembles are calculated 120 hours backward. Beginning at 00UTC every 6 hours an ensemble of trajectories is started for each air sampling. The starting altitude is 10 m to be as close as possible to the ship. Hence, the starting point lies within the boundary layer. For the intercomparison between HySplit and BADC trajectories (section 6.2), the HySplit trajectories are started in 500 m altitude corresponding to the requested[1] start level of 950 hPa for the BADC trajectories.

4.2 BADC model using opECMWF data

The BADC is an online tool to calculate trajectories of different models from different meteorological data center, e.g. ECMWF, NCEP, MetOffice. In this thesis operational data (opECMWF) from the ECMWF (http://www.ecmwf.int) are used. The 4D-VAR assimilation model is regularly updated. In 2009 the model resolution was T511 which corresponds to a horizontal resolution of T255. For the BADC trajectories the meteorological input is restricted to a grid spacing of 1.125° x 1.125°.
Hence, the number of grid points are 320 along zonal direction and 160 for meridional direction. It has 320 grid points encircling the earth at each latitude and is symmetric about the equator with 80 latitudinal points in each hemisphere. The vertical resolution includes 60 levels up to 0.1 hPa. The temporal resolution is up to 3 hours. The parameters used in this study are the u- and v-wind. The trajectories were calculated 120 hours backward. They were started every 6 hours beginning at 00UTC. Just one trajectory were started for each time step.

A detailed comparison between both models follows in Chapter 6.

4.3 Origin of air masses

For evaluation of the air mass origins in more detail the Western Pacific region is separated into different source regions. 10 different boxes with individual characteristics are defined, mainland and coastal regions as anthropogenic source regions and open ocean regions as natural source regions are the main categories. The NH includes boxes 1 to 6 (Figure 4.1) The SH includes the boxes 7 to 10 (Figure 4.2). The definitions are

[1]The starting height parameter in HySplit needs metric values (isolines) and in BADC pressure values (isobaric) are needed.

orientated towards the calculated trajectories and their range plus the anthropogenic and natural source regions. The colors are chosen with respect to the meteorological regimes. A more detailed declaration is shown in Chapter 7. The reddish boxes represent the first regime, the greenish the second and the bluish the third meteorological regime.

Box 1 is the biggest box in the NH. It includes parts of East Russia and East China. Consequently, anthropogenic sources are captured. The dimension of this box is 45°N to 70°N latitudes and 120°E to 160°E in longitude. This box lies outside of the TransBrom-Sonne cruise.

Box 2 includes mainly Japan and its coast towards the Pacific side and the Sea of Japan. Some eastern parts of Korea and China are also included to capture Japan and its adjacent water regions. The edges of the box reach from 30°N to 45°N and from 127°E to 145°E. This box includes first parts of the cruise track.

Box 3 is defined as an open ocean source. Its dimension, reaching from 20°N to 45°N and from 145°E to 170°W, is chosen to cover no mainland or islands. The box covers a big part of the Western North Pacific and is the last box in the first meteorological regime including the west wind zone and the ex-typhoon "Melor" and tropical storm "Nepartak". These two also influence the boxes 1 and 2.

The following box is number 4 lying in the second meteorological regime. It is slightly smaller than the boxes before. It covers the coordinates from 12°N to 20°N and from 142°E to 170°W. This box catches not only the open ocean but also the cruise track and the regions in the West of it. The Western part includes the islands of the Northern Mariana Islands and Guam which can have an possible anthropogenic influence.

More interesting is box No. 5. It covers the island of the Federated States of Micronesia. Thus this box is not an open ocean region, but it is possibly anthropogenic influenced by the islands. The box dimensions are 12°N to 2°S in latitude and 150°E to 175°W in longitude. A more detail view within the box can be find in Section 7.2 during the evaluation of the air mass origin.

Box 6 is more Western of Box 5 (142°E to 150°E), but it has the same latitudinal coordinates. In this box the islands of Palau are included. The cruise track touched this box just at its north eastern tip. Box 5 and 6 are the last boxes which are influenced by the second meteorological regime (Chapter 7).

Box 7 is the first box on the SH and is representative for the region of Papua New Guinea and their islands which are possible anthropogenic source regions. Its dimension includes the area from 2°S to 8°S and from 146°E to 180°E. In this box the change from meteorological regime 2 to 3 takes place.

The 8^{th} box mainly includes the region of the Coral Sea and therefore it can be a potential candidate for natural sources of measured traces gases in comparison to all

other boxes. It lies within the third meteorological regime. Its wideness reaches from 8°S to 19°S and from 146°E to 160°E. The cruise track crosses the box directly. Most of the time the course is diagonal through this box.

Boxes	**Latitude**	**Longitude**
Box 1	70°N - 45°N	120°E - 165°E
Box 2	45°N - 30°N	127°E - 145°E
Box 3	45°N - 20°N	145°E - 170°W
Box 4	20°N - 12°N	142°E - 170°W
Box 5	12°N - 2°S	150°E - 175°W
Box 6	12°N - 2°S	142°E - 150°E
Box 7	2°S - 8°S	146°E - 180°E
Box 8	8°S - 19°S	146°E - 160°E
Box 9	19°S - 50°S	140°E - 160°E
Box 10	8°S - 50°S	160°E - 180°E

Table 4.1: The coordinates from box 1 to box 10.

Box 9 is a southern and a long latitudinal box. It covers Eastern parts of Australia and Tasmania beginning at 19°S and ending at 50°S. The longitudinal range reaches from 40°E to 160°E. This box covers also the Great Barrier Reef, which has the potential to be a natural source region of halogonated trace gases. The covering of mainland includes the biggest cities of East Australia (e.g. Sydney, Melbourne, Brisbane, Canberra), which can be a potential anthropogenic source area.

The last box (10) is the biggest box on the SH and has the dimensions of 8°S to 50°S latitudinal and 160°E to 180°E longitudinal. It covers many islands of New Caledonia, Vanuatu and Fiji in the North. In the South there is New Zealand being a possible anthropogenic source region and having coasts for possible natural source regions. On the Western side of this box the open ocean of the South Pacific dominates this part.

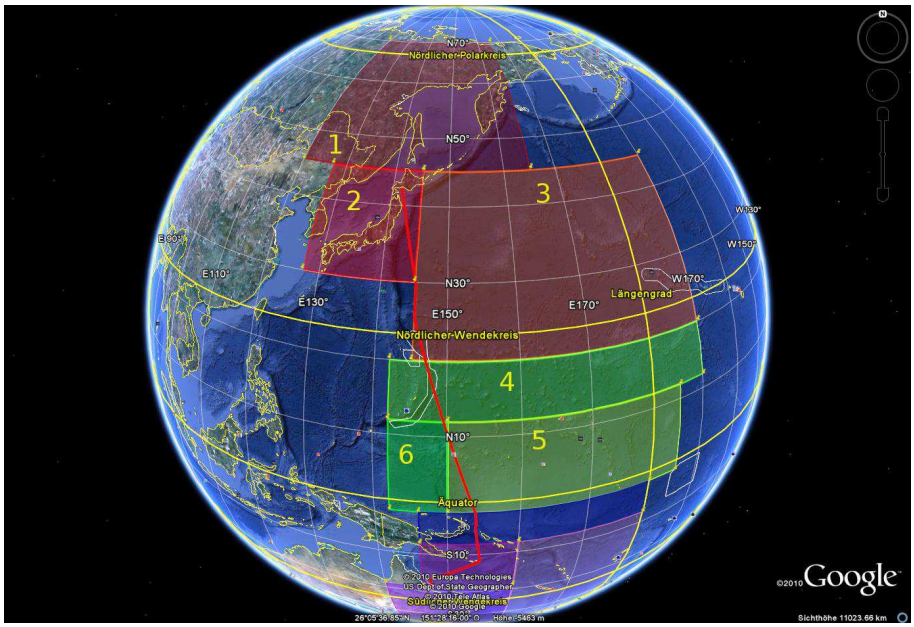

Figure 4.1: Boxes of the northern hemisphere for the trajectory analysis illustrated in Google Earth.

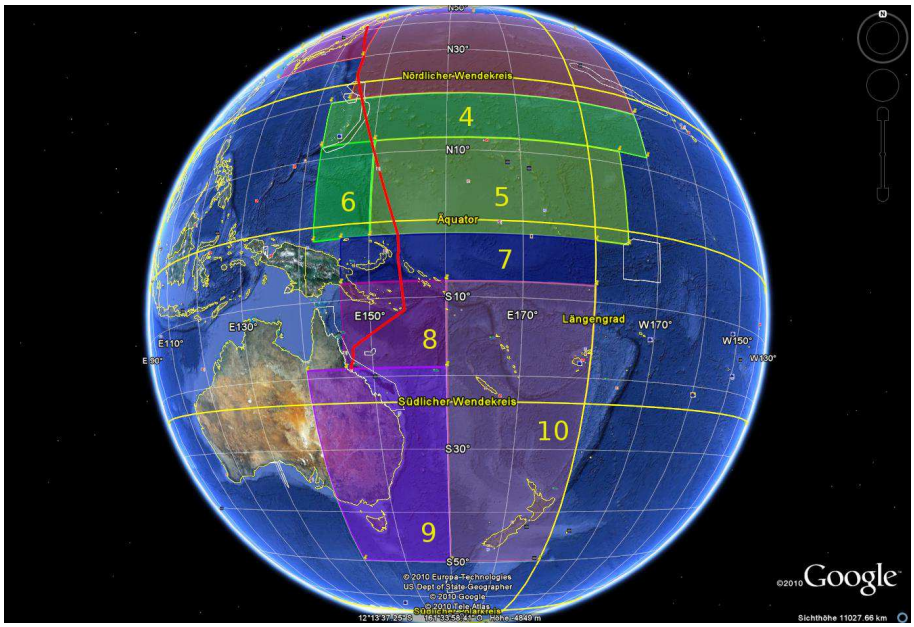

Figure 4.2: Southern hemisphere boxes for the trajectory analysis illustrated in Google Earth.

Chapter 5

The ship cruise

In this Chapter an overview about the TransBrom-Sonne cruise is given. First the meteorological measurements, especially the radio sondes on board are introduced and examples are shown. In the following part the cruise including the meteorological regimes and the weather phenomena is described. Last the ship measurements of wind speed and wind direction are compared with operational ECMWF reanalysis data.

5.1 GRAW radio sondes

Radio sondes, ozone sondes and snow white/cobalt sondes were launched to measure vertical profiles of the lower and middle part of the atmosphere, providing meteorological input data for trajectory and radiative calculations.

The highest point theses sondes reach under perfect conditions mostly lies between 30 km and 35 km altitude. The radio sondes (Graw Radiosonde DFM-06) record pressure, temperature and humidity. The pressure is calculated by GPS-height, the ground pressure and the vertical profile of humidity and temperature. More information can be found under http://www.graw.de. Based on the GPS signal, wind speed and wind direction are retrieved as well. Every day at 00, 06, 12, and 18UTC radio sonde measurements were carried out (Figure 5.1). The first start of ozone sondes was on October 10, 6UTC. From this date these sondes were launched every 24 hours. These more difficult and complex ozone sondes had to be calibrated 48 hours before start. This is a routine to eliminate pollution and to guarantee the same background conditions for the instruments. For every calibration step it is important to have checked the range of tolerance (Fujiwara, 2007). Cobalt/snow white sondes which detect water vapor in the stratosphere were launched only on October 13, 14, 19 and 22, 12UTC.

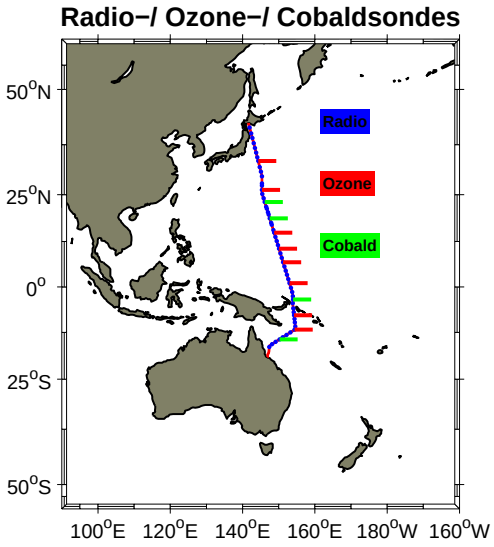

Figure 5.1: Starting points of radio sondes (red dots), ozone sondes (blue lines) and cobalt/snow white sondes (green lines) during the TransBrom-Sonne cruise.

5.2 Cruise report/meteorological conditions

The TransBrom-Sonne cruise which was carried out by the "Research Vessel (RV) Sonne" started in Tomakomai (42°N 141°E), Japan and ended after 4030 nm (7,500 km) in Townsville (19°S 146°E), Australia. The whole cruise passed the typical meteorological regimes of the westerly winds, the trade winds and the Intertropical Convergence Zone (ITCZ). Wind speed and direction are measured with the ship instruments (Figure 5.3, 5.2). The westerly winds of the NH were not directly measured at the ship track because of passage by the extratropical storm "Melor". The complete cruise track is shown in Figure 5.1.

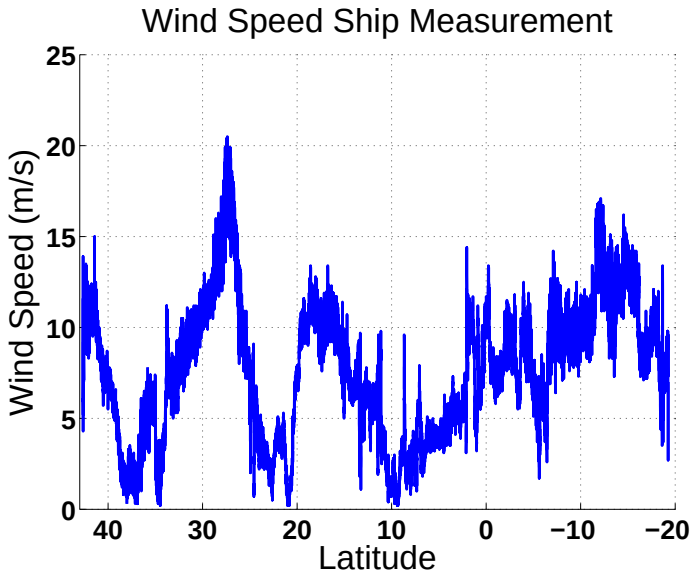

Figure 5.2: The blue curve shows the real measured wind speed during the whole track of the TransBrom-Sonne campaign from October 9 to 24, 2009.

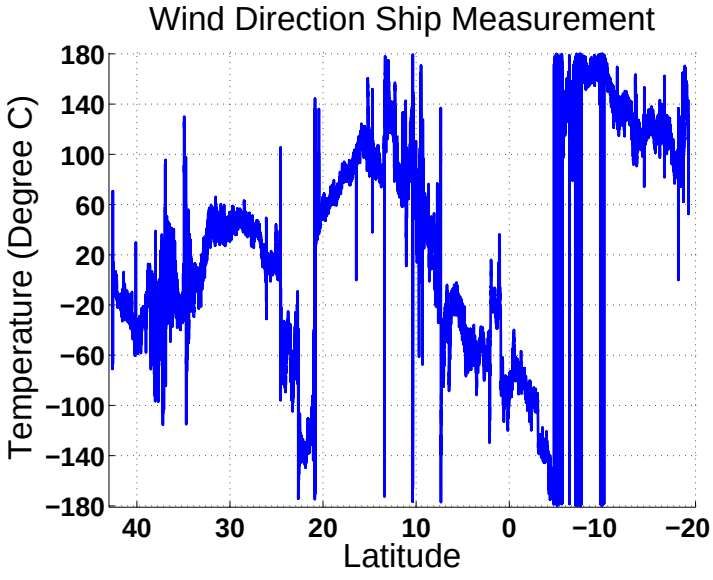

Figure 5.3: The blue curve shows the real measured wind direction during the whole track of the TransBrom-Sonne campaign from October 9 to 24, 2009.

5.2.1 NH extra tropics

The beginning of the TransBrom-Sonne cruise was on October, 9 2009 at Tomakomai harbor. During the night of October, 9 ex-typhoon "Melor" passed Tomakomai with a pressure of 980 hPa (Figure 5.4). A few hours before, after reaching Japan's mainland and colder regions, "Melor" changed from a typhoon into an extratropical storm. However, heavy rain and heavy storm were still observed by the scientific crew at night. In the harbor of Tomakomai the ship instruments measured winds of 7 Bft, until 10 Bft during gusts and 11°C. During its strongest periods "Melor", located south east of Japan, had a pressure of 910 hPa and an averaged wind speed of round 200 km/h and more than 280 km/h in gusts. It was a category 4 typhoon, a super typhoon (see Table 2.6) with an averaged movement of 26,6 km/h.

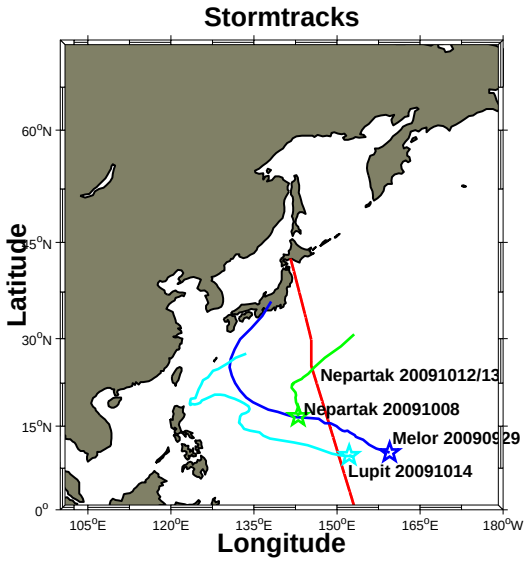

Figure 5.4: The storm tracks of all three tropical storms passing the cruise track. The date and the star indicate the birthday and birthplace of each tropical depression. The second date of "Nepartak" gives the date, when the RV Sonne crossed its pathway.

A NASA's satellite picture shows "Melor" and "Parma" which was another super typhoon at the same time very close to "Melor" (Figure 5.5). Both cyclones could interact if one approaches the other. One kind of interacting is called the Fujiwhara Effect (Fujiwhara, 1923, 1931), in which they are drawn together and begin to circle each other. In this case "Parma" was drawn towards the stronger "Melor". Stronger typhoons absorb weaker typhoons. This did not happen as "Parma" moved to Indonesia (not shown here) and "Melor" moved to Japan (Figure 5.4). In this thesis "Melor" and the following tropical depressions and storms during our cruise track are playing a role in the trajectories calculations (Section 7).

After a short delay of 4 hours, due to the extratropical storm “Melor“ RV Sonne started the cruise at 9 am (local time). The sky was overcasted, it drizzled and the wave height decreased slowly (Figure 5.6).

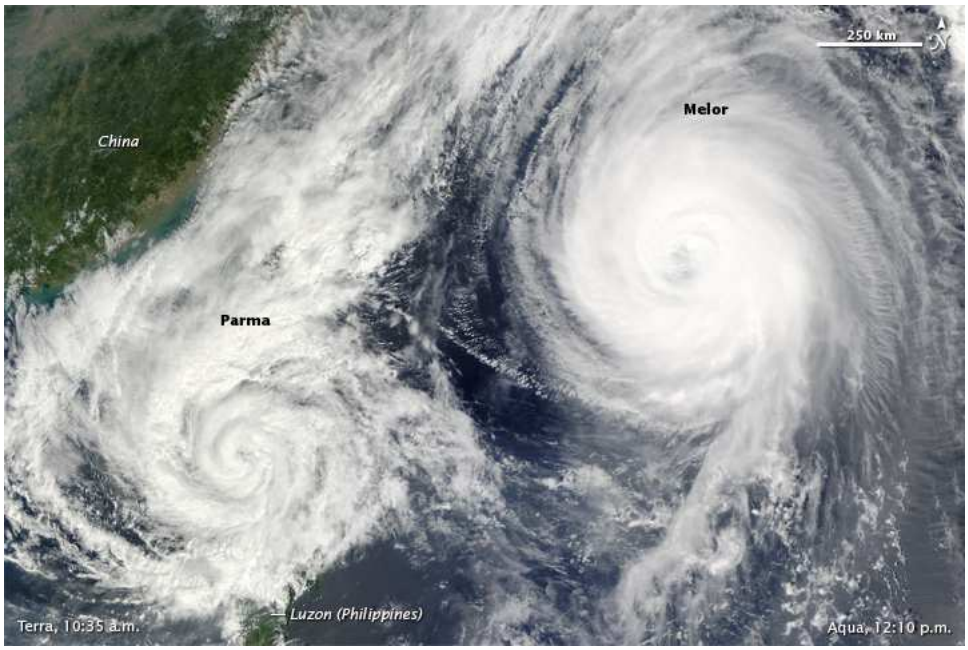

Figure 5.5: Super typhoon “Parma“ and super typhoon “Melor“ on October 6, 2009 very close to each other, observed by the satellites “Terra“ and “Aqua“. Source: http://earthobservatory.NASA.gov/IOTD/view.php?id=40615

On October 9, 2009 the meteorological measurements on board began with launching the 12UTC radiosonde. The weather conditions were perfect for the first balloon flight, with 60% relative humidity, a pressure of 1006.9 hPa (Appendix), 12.8°C (Figure 5.11), a wind direction of 343°, and round 10 m/s wind speed (Figure 5.3, 5.2). Due to the southerly (170°) course of the ship and its 7 m/s speed the apparent launching conditions were moderate and made it easy to control the balloon on deck before the start.

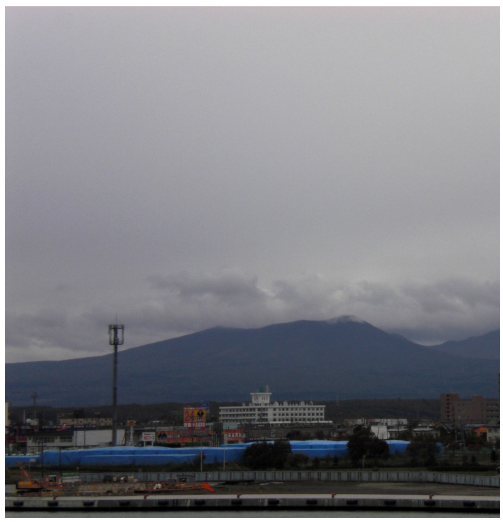

Figure 5.6: At start the weather conditions were moderate. Wind and drizzle impressed the view over the harbor of Tomakomai. (Picture was taken by Sebastian Wache)

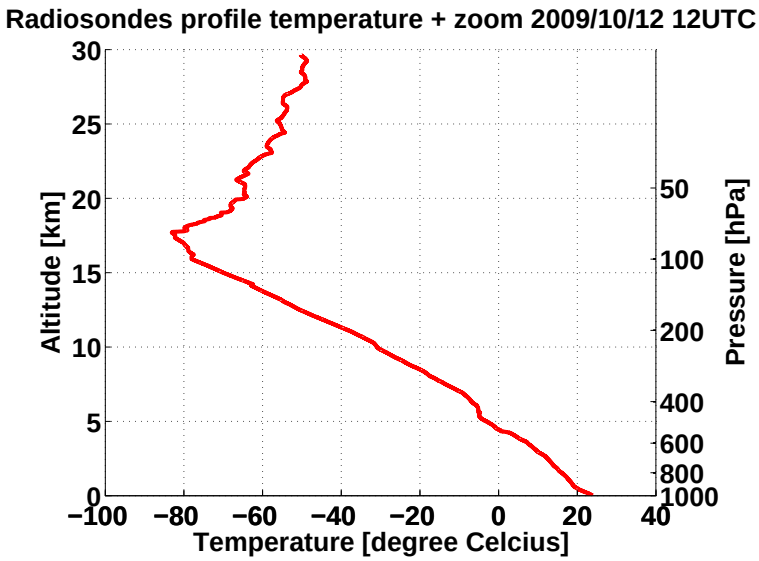

Figure 5.7: Radiosonde profile of air temperature (degree Celsius) from October, 12 2009 12UTC at 27°N and 145°E.

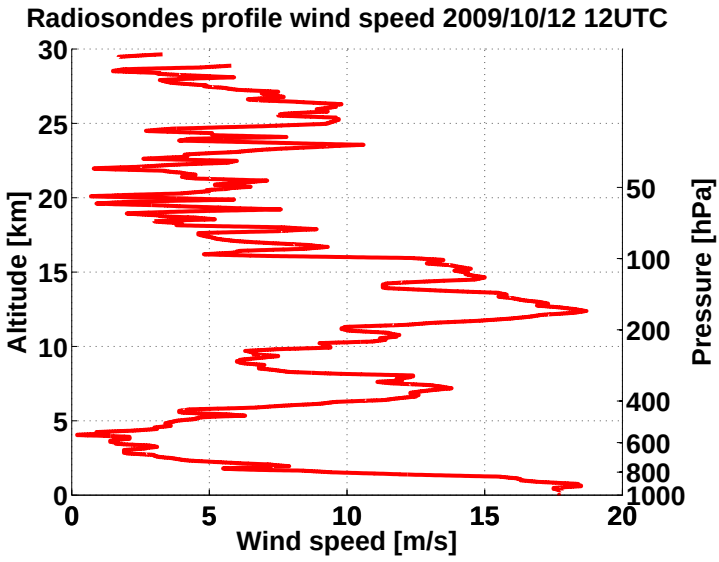

Figure 5.8: Radiosonde profile of wind speed from October 12, 2009 12UTC at 27°N and 145°E.

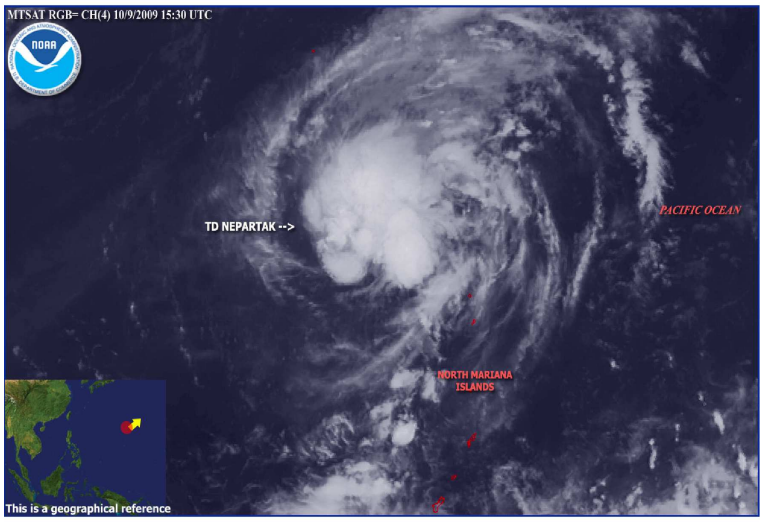

Figure 5.9: Source of data: A satellite picture of the tropical storm "Nepartak" at 20°N and 142°E on October 9, 2009, 12UTC, observed by the satellite "METOP". Source: http://www.osei.noaa.gov/Events/Tropical/W_Pacific/2009/TRCnepartak282_GJL.jpg

Until 33°N the wind was very variable, conditional on a ridge of high pressure which extended from China to Japan (Figure 5.10). Between 33°N and 25°N the wind became more steady from northeast (Figure 5.3). At the same time the wind speed increased continuously (Figure 5.2) and the pressure rapidly decreased (Appendix). These effects result from the tropical storm "Nepartak". Strong northeast winds blew on its Northern side. After a short course shift for a safer ship track the cruise passed "Nepartak" (Figure 5.9), closely on its Western and therefore, on the typical weaker side of a typhoon (Anthes, 1982). The wave heights were decreasing from more than 4 m to 2 m height. "Nepartak" was a tropical storm with a short lifetime of about four days. Its minimum pressure was 992 hPa and its maximum wind speed 90 km/h . An example temperature profile for October 12, 12UTC at 27°N and 145°E while the tropical storm "Nepartak" passed our ship cruise is shown in Figure 5.7. The typical vertical temperature structure of the atmosphere (discussed in Section 2.1) is well measured and illustrated. The tropopause lies at 84 hPa. The temperature decreases with increasing height until the tropopause is reached at 84 hPa. After crossing the tropopause and penetrating the stratosphere the temperature gradient reverses. Figure 5.8 shows the wind speed against the altitude of this radiosonde start. At the ground the wind speed was 17.7 m/s. It increases up to 18.5 m/s in round 500 m. The wind speed maximum of more than 20 m/s was measured by the ship measurements between radiosonde launchings dates. During lift up the wind speed alternates with a maxima at the ground, at round 7 km and at round 12 km altitude. At round 4.5 km and round 9 km it had wind speed minima. 19 m/s wind speed at the surface is produced by "Nepartak".

During the time of "Nepartak's" influence (between October 12 and 13) the cruise measurement interval was increased to an hourly frequency, to verify existing assumptions about correlations between higher wind speeds and increasing trace gases concentration by fluxes between the ocean and the air (Zhou et al., 2008). On October, 12 at 10 am UTC (20 pm LT) (27°N 145°E) the wind speed increased up to 20.4 m/s in maximum (Figure 5.2) accompanied by strong rain showers. After passing "Nepartak", the vessel turned back on its planned cruise track. The next main atmospheric regime were the subtropical calms between 25°N and 20°N. The wind speed decreased to very weak values from less than 1 m/s to max. 5 m/s. The wind direction varied from north to southeast (Figure 5.2, 5.3). In the calm zone weak winds were measured and almost no waves were seen. The wave height decreased from 2 m to nearly zero as well. More and more the cloud layer broke up and the temperature rose to 28°C (Figure 5.11). The curve progression reflects the typical temperature behavior from north to south in a good way. However, it was a short period of calm wind conditions and nice weather, which was used to calibrate some measurement techniques from other scientists (Figure 5.12).

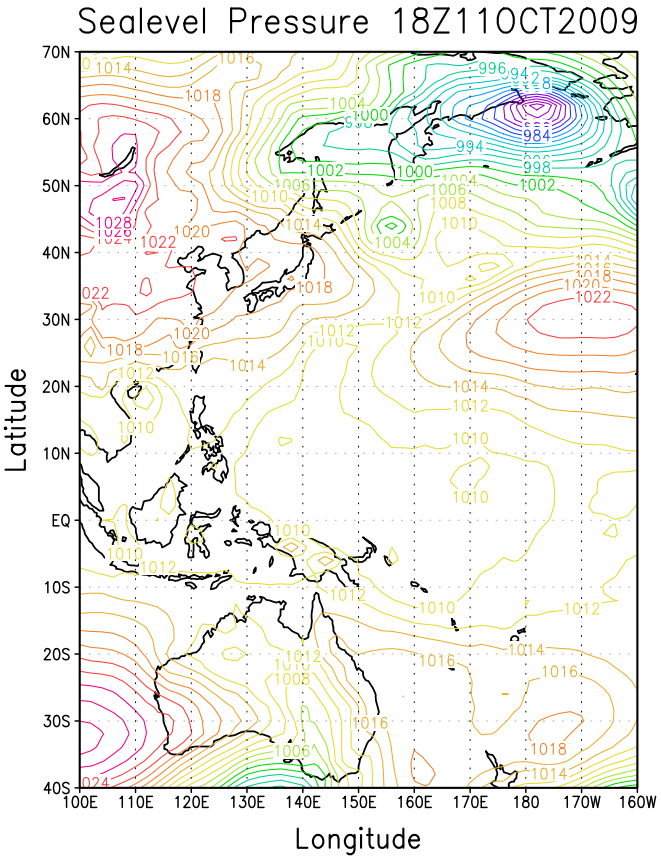

Figure 5.10: Sea level pressure distribution of the whole Western Pacific on October 12, 2009 00UTC (operational ECMWF data).

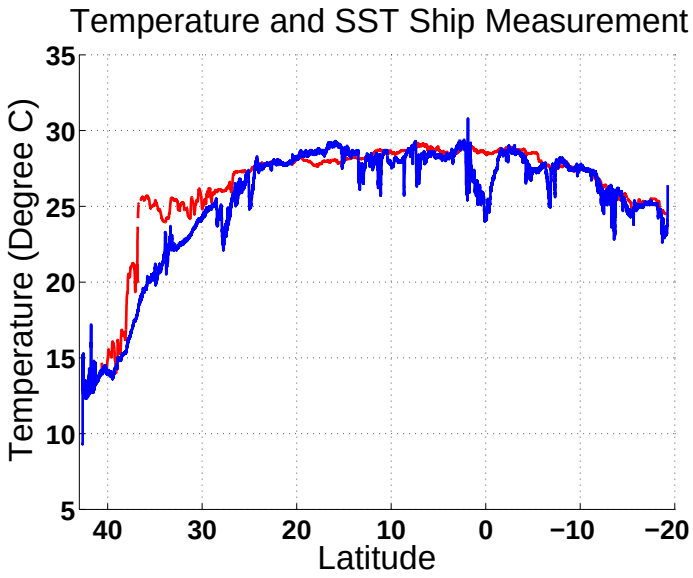

Figure 5.11: The blue curve shows the real measured air temperature and the red curve the offset corrected SST during the whole ship cruise.

Figure 5.12: Calm wind zone at 20°N 146°E on October 14, 2009, 00UTC. (Picture was taken by Sebastian Wache)

5.2.2 Tropics/ITCZ

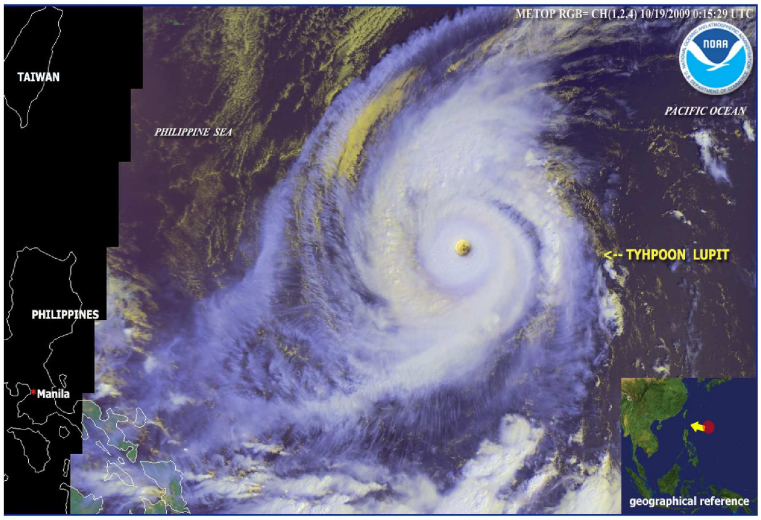

Figure 5.13: Super typhoon "Lupit" on October, 19 2009 at 12 UTC east of the Philippines. A very pronounced eye is given in the center of "Lupit", observed by the satellite "METOP"Source: http://www.osei.noaa.gov/Events/Tropical/W_Pacific/2009/TRClupit292_M2L.jpg

On October 15, at 15°N and 148°E the ship reached the ITCZ region. Rain showers occurred, the wave heights increased to round 2.5 m and the wind became stronger up to 9 m/s, reaching 14 m/s in its maximum. The thunderstorm tendency increased due to the crossing of the ITCZ. In addition the cruise passed the region where the future super typhoon "Lupit" was born (Figure 5.4). At this time it was already a tropical storm. Its pressure was round 1000 hPa. One day later it was classified into typhoon Category 1 (Table 2.6). Within 12 hour intervals the category of "Lupit" increased one step further. On October 18/19 "Lupit" reached its strongest phase. It became a super typhoon of Category 4. Figure 5.13 shows the distinct eye in the middle of the typhoon. Its track was straight ahead to the Philippines. After a dwell time over the North of the Philippines it moved to the Northeast. "Lupit" had a lifetime of 11.5 days and an averaged movement of 20.8 km/h. The TransBrom route did not intersect "Lupit's" pathway, but its influence was noticeable (Figure). The influence on the air samples by "Lupit" is investigated in Chapter 6.
The Figure (5.4) of the storm tracks shows the pathways from the start as a tropical depression up to the change to an extratropical depression. "Melor" and "Lupit" developed at similar latitudes (round 10°N). Just "Nepartak" developed further north

(round 17°N) than the other two, which could be the reason for it not developing into a typhoon. From October, 16 until 19 (15°N - 5°S) the ITCZ dominated the weather conditions (Figure 5.14). Showers, heavy in parts, developed from time to time and sheet lightning were registered. In the morning the temperatures climbed up near to to 30 °C (Figure 5.11). The relative humidity was constant between 70 % and 90 % (Appendix), reflected also by a temperature decrease. During the passage of "Melor" and while crossing the ITCZ the thermometer registered temperature minima. The explanation for this could be the heavy rain showers (high relative humidity) at that time. Coherent, in this region high convective clouds (cumulonimbus) were observed be the scientific crew. Figure 5.16 shows such deep convective clouds.
On October 18, 2009 at 18 UTC a radiosonde was launched in regions of the ITCZ (Section 2.2.1). Figure 5.15 shows the temperature on the left hand side and the dew point against the pressure. The dew point means the temperature of a volume of water vapor, which is isobaricly cooled to the point where the content of water vapor is saturated. The relative humidity has reached 100 %. The curve seems to have a typical behavior for lifting. At a second glance, it shows the up and down course of the balloon. The blue box marks a range which is shown on the right hand side of Figure 5.15 in a zoomed view. The pathway is not directly upward but moves randomly up and down. Before starting the sonde sheet lightning was visible at the horizon. Due to these facts the up and down curse of this sonde correspondes with convection processes. During ascend it reached a convective cloud system and became wet. It seems as if the balloon was frozen, heavier and sank. While it sank the attached ice melted partly, drained off the balloon and was lifted again. During the next lifting process the rest of the water on the balloon and new water from the convective precipitation froze again. It was a "vicious circle" without big chances of escape. However, after more than one hour the balloon escaped or the convection did appeared and it finally raised into the stratosphere.
The next main event was the equator crossing, which took place in the night between October, 18 and 19 (01:30 am LT). It showered abundantly and the temperatures decreased to 24°C (Figure 5.11) before increasing again up to round 28°C at 2°S.

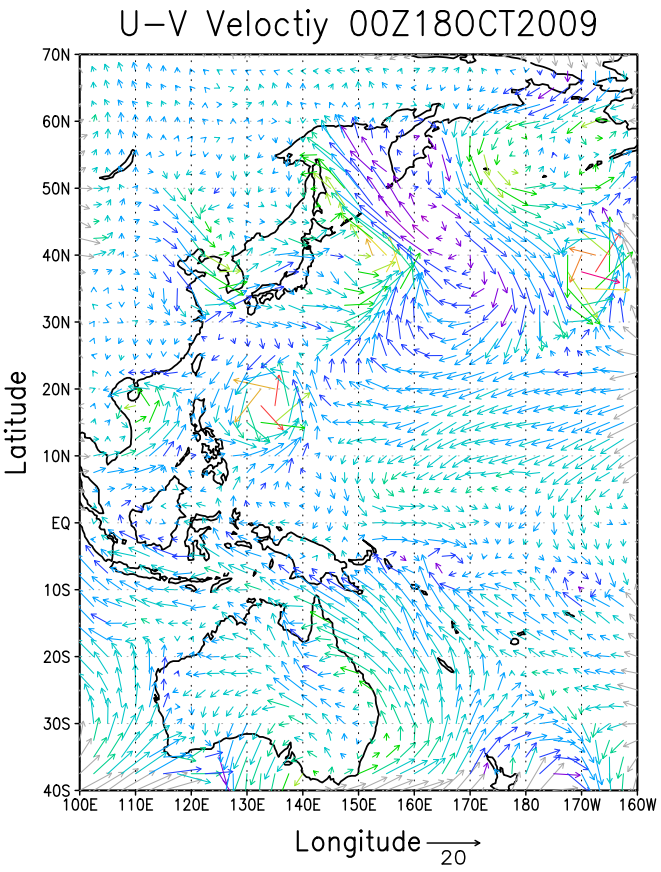

Figure 5.14: Wind distribution on October 18, 2009 00UTC. The ITCZ is found from round 15°N to 5°S. “Lupit“ and “Nepartak“ are well reflected, too (operational ECMWF data).

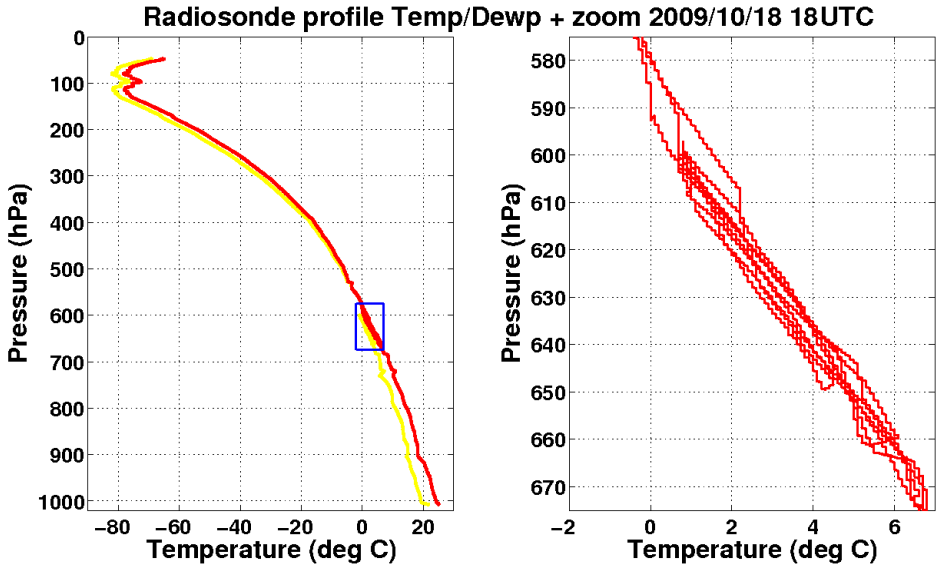

Figure 5.15: Radiosonde profile of air temperature and dew point temperature (degree Celsius) against pressure (hPa) from October 18, 2009 18 UTC at 0°S and 153°E. The zoom on the right hand shows the blue box of from the figure on the left hand side.

Figure 5.16: Cumulonimbus clouds in the ITCZ. (Picture was taken by Sebastian Wache)

5.2.3 SH extratropics/trade winds

After crossing the equator the ship was influenced by the ITCZ until around 5°S. After crossing this imaginary boundary the trade winds began to blow with increasing wind speed. While the course passed through the islands of Papua New Guinea (Figure 5.1) the wind direction changed to southeast and the wind speed increased steadily to 9 m/s (Figure 5.2, 5.3). This was a distinct sign of the strong southeast trade winds (Figure 5.17). On October 21, (12°S) the maximum in averaged wind speed with round 17 m/s was reached on the SH. The wave heights were at round 3 m and the sky was fully covered with clouds. With the ship coming closer to the coast, the wind speed reduced and it became sunnier (Figure 5.2). The temperature was constantly on a high level of around 25°C (Figure 5.11). In the morning on October 24, the Sonne reached the harbor of Townsville under high pressure (Figure 5.18 and an almost clear sky.

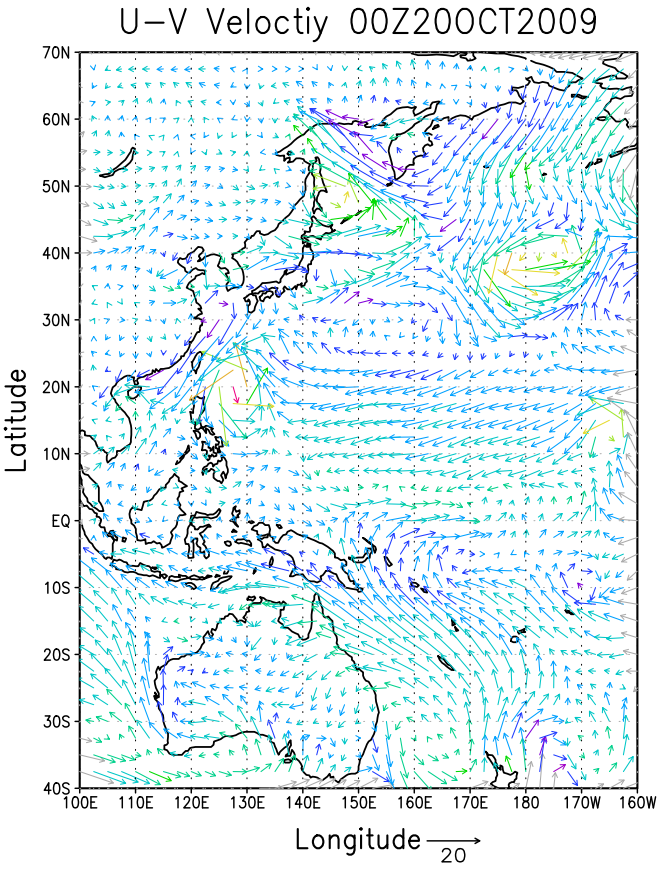

Figure 5.17: Wind distribution on October 20, 2009 00UTC. The strong trade winds are reflected from around 15°N to 21°S (operational ECMWF data).

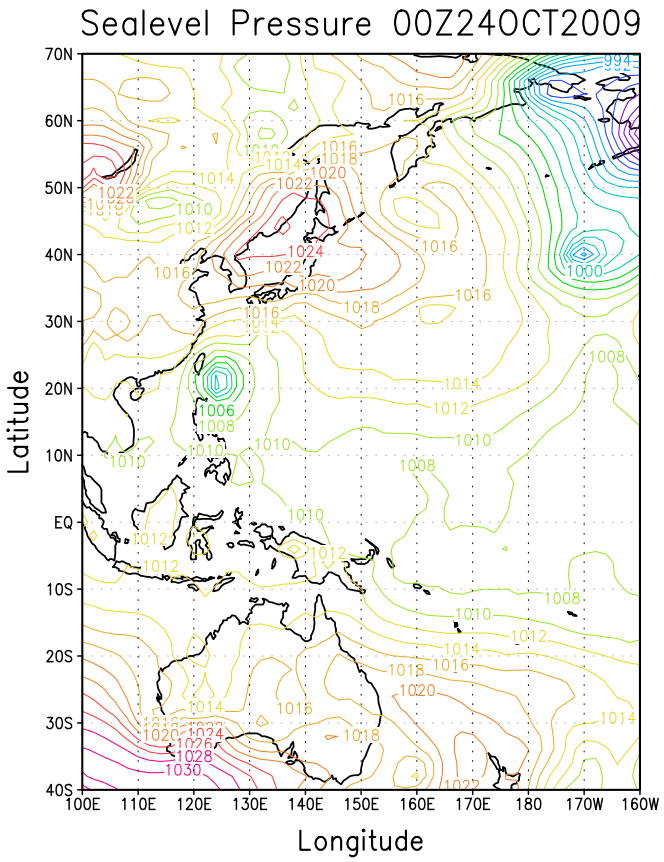

Figure 5.18: Sea level pressure distribution of the whole Western Pacific on October 24, 2009 00UTC (operational ECMWF data).

5.3 Data intercomparison (ship vs. opECMWF)

In order to compare ship measurements with assimilation data, opECMWF data were used and investigated. The opECMWF data have a resolution of a 0.25 x 0.25 grid. For a better checkup these data are interpolated by a Matlab program. Every time step the whole data matrix is interpolated to a 0.125 x 0.125 grid. Figure 5.19 shows the comparison between ship measurements and opECMWF data for wind direction. The blue curve is the wind direction measured by ship and the red curve are opECMWF data interpolated to the ship position. The y-axis is defined from -180° to 180°. The x-axis shows the complete cruise track from 42°N to 19°S. The behavior of the blue curve is discussed in more detail in Section 5.2. As expected the curve represents the typical meteorological wind regimes in a good way. The opECMWF data do not show any big differences. It seems like a mean of the real data set. Over the whole cruise the wind direction of the opECMWF data agrees almost perfectly to the measurements. The correlation between both data sets is 0.98. Hence both curves are highly correlated which is well seen in the smooth changes e.g. from 100° at 10°N back to 100° to the end of the cruise and the rapid changes of the direction especially at 19°N which are well represented by the opECMWF.

The same behavior can be seen in wind speed. Figure 5.20 shows the wind speed from ship measurements (blue curve) and from opECMWF data (red curve). As already seen for the wind direction the wind speed from the ship measurements is well represented in the opECMWF data. It should be mentioned that minima and especially maxima of measured wind speeds are underestimated in the operational data. During the storm event of "Nepartak" (28°N) wind speeds of 21 m/s were measured. During this time the opECMWF data shows just 14 m/s and hence, underestimates the in situ measurements by 6 m/s. It is a well known fact that storm or typhoon events cannot be resolved and are underestimated most of the time, which is reported by Molinari and Robasky (1992) in earlier investigations. Hence, the correlation with a value of 0.89 is less weaker than in the wind directions. One fundamental problem of assimilation data is that measurements over the ocean are very spare in comparison to mainland. Just ships, oil platforms or radio sondes of vessels can record weather data. On the other hand, the opECMWF data are very close to measured values, but do not match exactly. This can also be observed in the further course of the cruise. The next storm event ("Lupit" at 19°N) and also the southerly trade winds on the SH are underestimated. Overall for the complete course wind speed and wind direction from opECMWF data are in a good agreement with the observations. Thus one can draw conclusions about the well resolved weather situation and pressure systems. In this case just the intensity is underestimated.

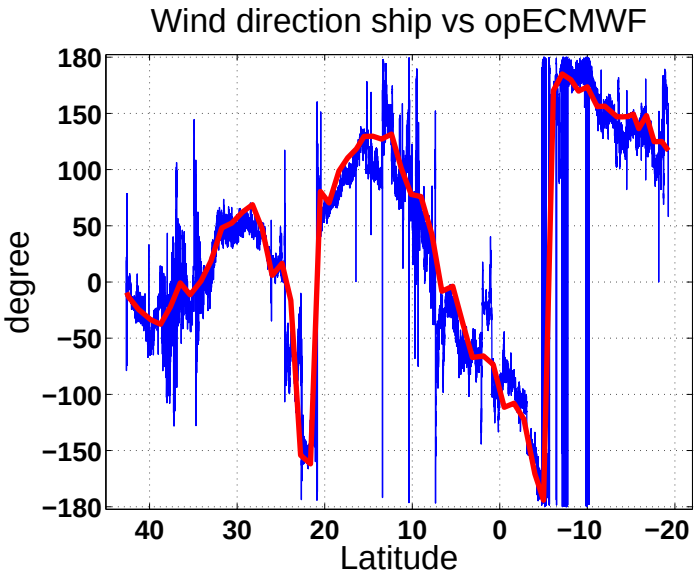

Figure 5.19: Wind direction of ship measurements (blue curve) against opECMWF data (red curve).

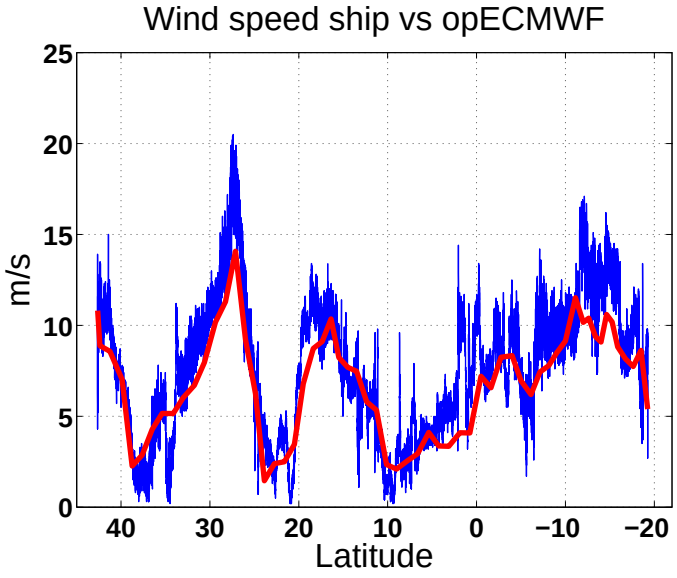

Figure 5.20: Wind speed based on ship measurements (blue curve) and based on opECMWF reanalysis data (red curve).

Chapter 6

Trajectory comparison

In this Chapter the results of ensemble trajectory calculations based on the HySplit model (Section 4.1) in comparison to ones based on the BADC model (Section 4.2) are analyzed. First three different case studies representative for the measured meteorological regimes (Section 5.2) are discussed. Section 6.2 shows a detailed comparison between results from both models by looking at daily trajectories and their different behavior.

6.1 Case studies

The following case studies illustrate the differences between HySplit and BADC trajectory model outputs. Shown are results for October 12, 17, and 22, 2009 which represents the three different cases of the different meteorological main regimes observed during the cruise.

6.1.1 Tropical storm passage 12.10.2009

On October 12, 2009 the tropical storm "Nepartak" crossed the cruise track (Figure 5.4), characterized by unstable weather conditions as discussed in Chapter 5. This instability is the main motivation for choosing this date and the intercomparison of the trajectory models. Since different data sets (Chapter 4) are used as input data for the trajectory models a discrepancy between the trajectories is expected. Due to the instability the discrepancy should be bigger than in more stable conditions.

Figure 6.1 shows the region from 0° to 85°N and 90°E to 160°W. The red line is the first part of the cruise track. The black lines are the HySplit trajectories and the blue lines mark the BADC trajectories. The green star labels the starting point of the backward trajectories. Both different models were started with 27 trajectories. Every trajectory starting point in HySplit differs automatically in height due to the

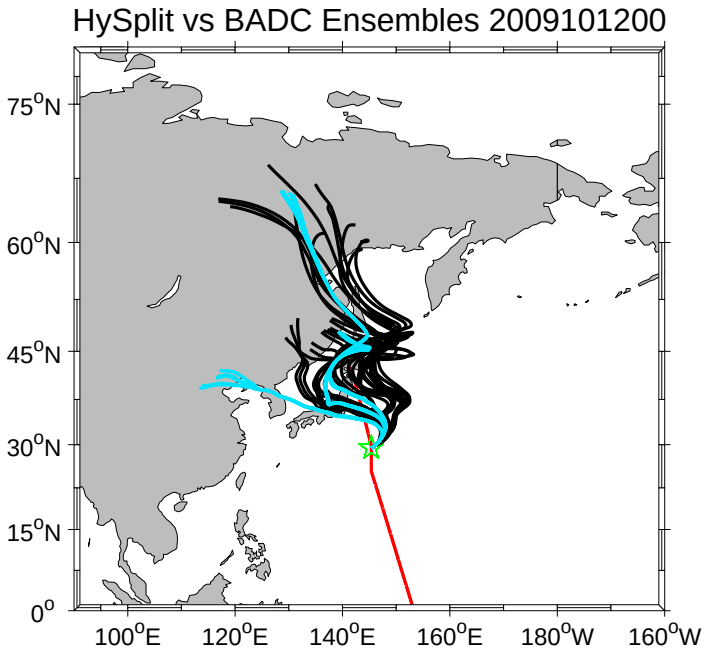

Figure 6.1: October 12, 2009. Ensemble of 27 trajectories each of HySplit (black lines) and BADC (blue lines)

presetting of this online tool. For the best possible intercomparison between both models the BADC trajectories are started at the same heights as the HySplit ones. Therefore, their pathways differs in a big range because of different wind speeds and directions in different heights. Hence, almost every trajectory follows its individual pathway. The more southerly trajectories are shorter than the northerlies. Almost all HySplits go over Japan's mainland. The shorter pathways end near China's coast and the longer ones reach even the Siberian part of Russia, which corresponds to 59 %, respectively 41 % of the ensemble. In contrast the BADC trajectories are split in three main groups, in which each group corresponds to 33 % of the ensemble. First, some of them follow the way to Siberia. The second group of trajectories have almost the same last part but come from the Russian coast. The third pathway comes from Korea and China and goes over the south of Japan's mainland. Thus the BADC trajectories have a similar behavior and overlay the HySplit trajectories directly. Just one group of pathways are more south than all others. However, almost all trajectories being higher than 45°N change their direction rapidly from a south eastern into a south western direction.

Because of the main turbulent influence on the general circulation system by the tropical storm "Nepartak", the difficulties of calculating this storm in the initial data sets and the different results obtained by different models, calculating the pathways of these

trajectories leads to such a big spread. By looking at the major pathway it can be seen that at 47°N trajectories switch their direction by over 90°. At this point the fully grown tropical storm "Nepartak" begins to influence pathways, likewise in both models, which leads to large spread. Its dimension reaches vertically from the surface to the tropopause and influences every air mass regardless of different height levels.

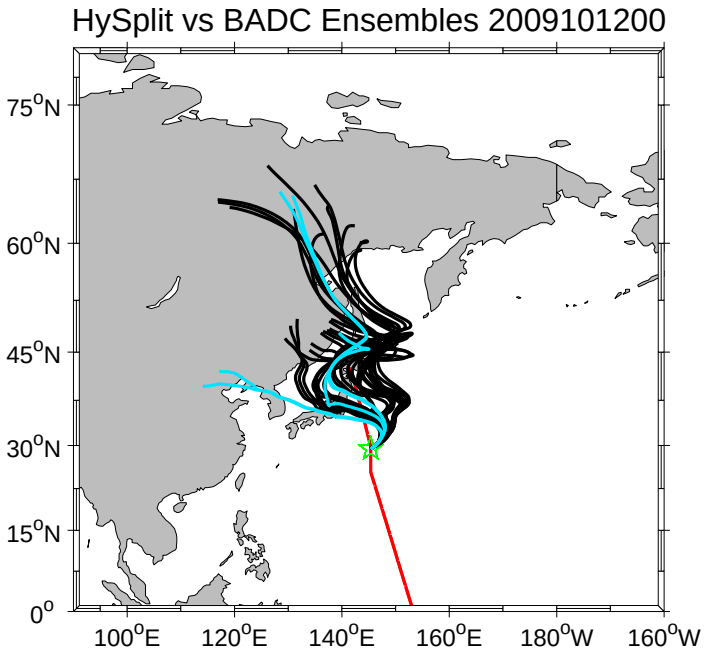

Figure 6.2: October 12, 2009. Ensemble of 27 trajectories of HySplit (black lines) and 5 BADC (blue lines) trajectories

To simplify the trajectory calculation and decrease the processing time the number of BADC trajectories are reduced from 27 to 5. These 5 trajectories are chosen from the top, the middle and the below of the HySplit range. Hence, it is investigate if the 5 BADCs height points can represent all 27 height points and how big is the difference between two different models.

Therefore, the second step for intercomparison of both models is to choose 5 samples of different heights in the HySplit raw data set and to use them as reference heights in BADC. Samples of highest, middle and lowest pressure are chosen for a good representation of all 27 trajectories. Figure 6.2 shows the result of that calculation. Shown is the same zoom into the region as in Figure 6.1. Overall Figure 6.2 looks very similar to the one including the 27 trajectories. The three different pathways can be seen as well and thus, there is no big difference visible. Hence, the 5 samples are a good representation for the 27 trajectories. To verify this conclusion, two more cases will be shown further on.

6.1.2 ITCZ 17.10.2009

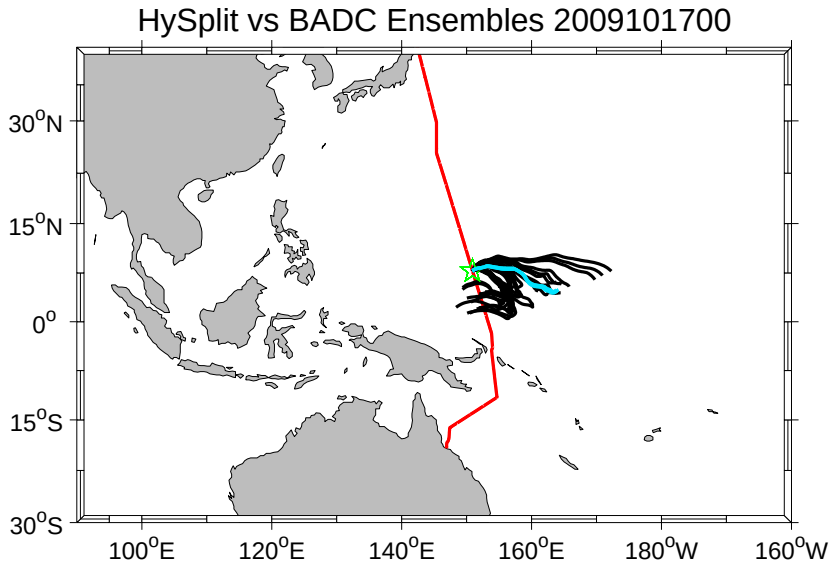

Figure 6.3: October 17, 2009. Ensemble of 27 trajectories of HySplit (black lines) and 5 BADC (blue lines) trajectories

Representative for the second meteorological regime, the ITCZ, October 17 is chosen as a starting point for the trajectories. Figure 6.3 displays the latitudes from 40°N to 30°S and the longitudes from 90°E to 160°W. Since in the first case study 5 trajectories have been shown to be representative for all 27 BADC trajectories. This thesis focuses on analysis of the following case studies on 5 BADC trajectories started on varying pressure levels. This case shows also a wide spread of the HySplit trajectories, which is likely related to the ITCZ and its unsteady conditions. The pathways vary from coming from the West (37 %) to coming from the East (63 %). The BADC lines concentrates just in the middle of the HySplit spread and come just from the East (100 %). Convective systems develop very often in the ITCZ due to converging of air masses. Air masses transported eastwards seem to switch their direction very fast because of such a possible convective system. Both models seem to include weak winds due to the mostly short range of the trajectories.

6.1.3 Southerly trade winds 22.10.2009

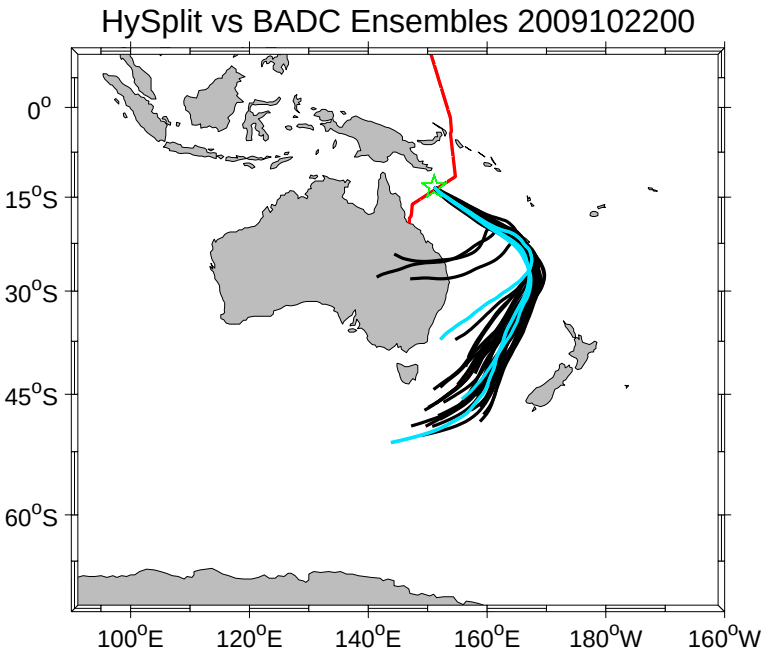

Figure 6.4: October 22, 2009. Ensemble of 27 trajectories of HySplit (black lines) and 5 BADC (blue lines) trajectories

The third trajectory intercomparison deals with the third main meteorological regime, the trade wind regime. This sector of the cruise is mainly influenced by strong southeast trade winds. The strong trade winds can be seen in Figure 6.4 by the straight southeast direction the trajectories follow between 13°S - 29°S. This Figure includes 5 BADC and 27 HySplit trajectories as the cases before. The HySplit trajectories are very close together and become tighter under the influence of the strong trade winds. Just three of 27 trajectories, which corresponds to 11 %, are separated from the rest and are located directly over Australia. They fit with the other 24 trajectories (89 %) after three days and follow the same way in the last part. 60 % of the BADC trajectories follow the same way like the main track of the HySplit bunch. 40 % come from western regions and get into the bundle of all trajectories after 2 days.

HySplit has mostly a larger spread in its outputs. The BADC trajectories mostly concentrates in certain pathways and do not differ such like the HySplits. However, HySplits larger range can give a better conclusion for the gas measurements. For a further verification in the following Section (6.2) single trajectories of the main measurement dates are compared.

6.2 HySplit vs. BADC

In the previous Section HySplit and BADC ensembles are compared. It seems as if there are no big differences as between the models in various weather situations BADC trajectories (red lines) mostly follow the main way of the HySplit ensembles (blue lines). Hence, the behavior of both models are almost the same. To be sure about this behavior over the whole cruise just one trajectory per day is started. Thereby both models were started in almost the same height. Because of different input masks (Chapter 4) and various needed initial conditions HySplit trajectories are started in 500 m and BADC's in 950 hPa which is the lowest starting opinion in BADC. The starting heights of both models corresponds with each other based on the U.S. Standard Atmosphere (U.S. Standard Atmosphere, 1976). Thus, both models lie within the boundary layer and big differences of pathways may be expected. The results of these calculation can be seen in Figures 6.5 and 6.6, which are also the dates of air parcels measurements. The Figures show trajectories of HySplit and BADC (one per day) on the complete TransBrom-Sonne cruise. Blue lines are the HySplit and red lines the BADC trajectories. The green star marks the starting point lying on the cruise track. Apparently, the three in Chapter 5 discussed meteorological regimes are well reflected. The transitions between different regimes lie at 25°N and 2°S. Until 25°N the air parcels are mainly influenced by "Melor" and "Nepartak". The main variation between both models is the length in this part of the cruise. The BADC trajectories are longer and reach the northeast of Russia. In contrast the HySplit trajectories end at China's coast. Just two of them reach China's inland. Both models show a rapid direction change. From start to this change there is a wide spread of 8° between them. The BADCs go more over Japan's mainland. The HySplits choose the way over the Western North Pacific. In the second part from 25°N to 2°S both models behave almost identical. Just one trajectory of HySplit has a longer path into the East. From coming from the East to be steady in the ITCZ region near the equator almost all trajectories of both models show the same ways and overlay each other. From 2°S to the end of the cruise at 19°S it seems that the pathways concentrate in one point at 25°S and differ in the further way. Hence, the BADCs show a larger spread, while one trajectory comes from Australia's mainland and the most eastern one goes over the middle of Pacific between Australia and New Zealand. The HySplits lie amidst the BADCs. In this part of the cruise both models also show the same behavior and coats the same regions.

In Figure 6.6, shown are all 12UTC trajectories, are no big differences to the 00UTC trajectories. In the first part the BADCs reach even further the North especially the northwest of Russia. The more important last part of the pathways is quite the same. In the second regime big variations of pathways are not visible. Both models show a good agreement with each other. Also in the third regime big differences are not

identifiable. Just in the 00UTC trajectories show a little more differences in the spread than in the 12UTC trajectories.
Thus, it is, additional to Section 6.1, another verification that both models behave very similar. Due to this fact that almost all HySplit and BADC trajectories follow almost the same pathways and show no big differences, despite lying within the boundary layer, in following Chapter 7 only HySplit trajectories are used to investigate the source regions. Another reason is that also in other scientific papers e.g. (Quack et al., 2007; Carpenter et al., 2007) HySplit trajectories are used. All advantages and disadvantages of both models cannot be given in detail in this thesis without more examine these models.

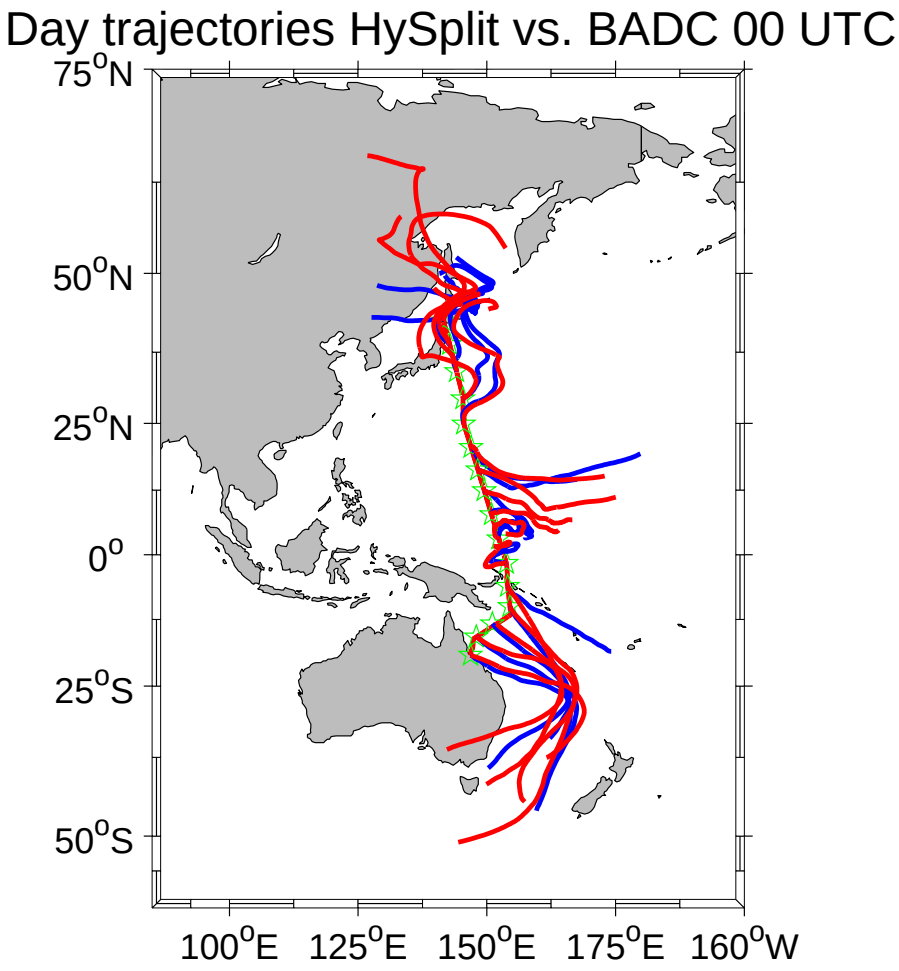

Figure 6.5: HySplit (blue) versus BADC (red) trajectories. One trajectory per day at 00 UTC.

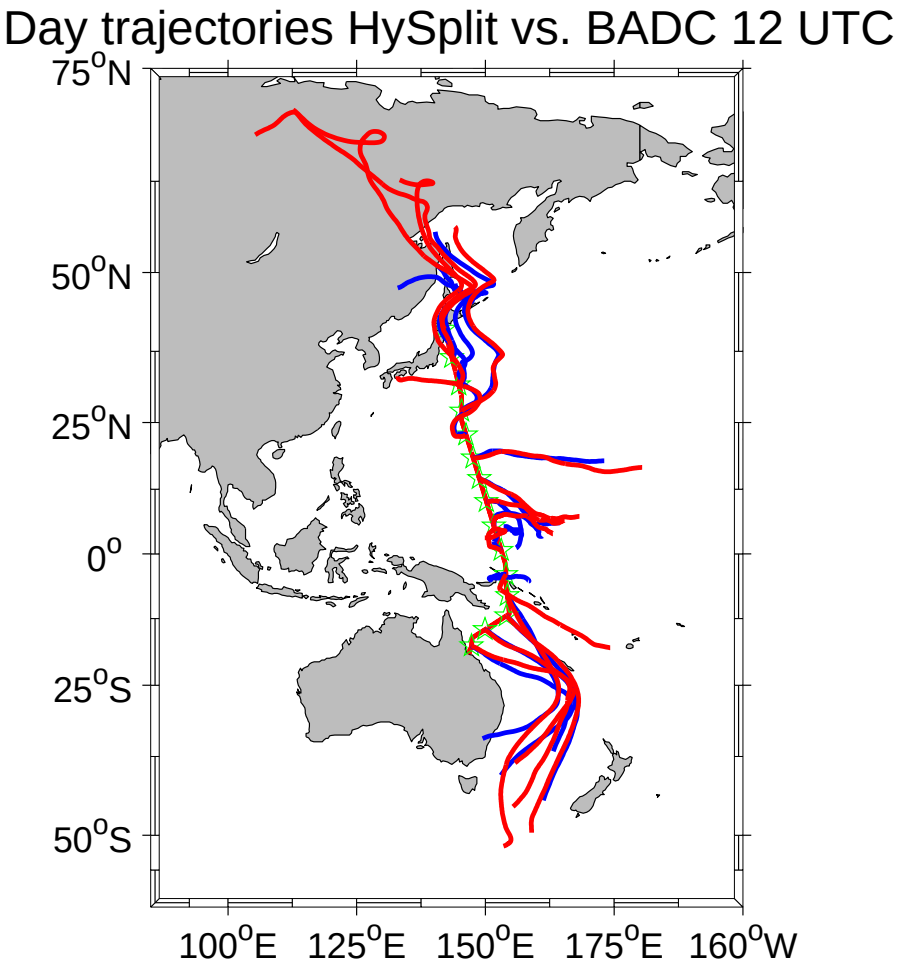

Figure 6.6: HySplit (blue) versus BADC (red) trajectories. One trajectory per day at 12 UTC.

Chapter 7

Analysis of air masses

In the following Chapter HySplit trajectories are used to investigate the source regions of atmospheric bromoform, methyl iodide and methane. Results from air parcel measurements during the TransBrom-Sonne campaign and from trajectory calculation will be shown. The definitions of boxes (Section 4.3) are used and evaluated. Every regime Figure shows one example trajectory which represents all trajectories of each regime.

7.1 Case studies

7.1.1 Bromoform

Figure 7.1 shows the atmospheric bromoform measurements (red line) and wind speed (blue line) during the TransBrom-Sonne cruise. The atmospheric sampling started a little bit later than the wind measurements. The canister samples were analyzed for various trace gases form the group of Elliot Atlas (Rosenstiel School of Marine and Atmospheric Sciences, Miami). Bromoform is decreasing from 2 ppt at the beginning of the cruise (40°N) to 0.4 ppt at around 19°N. Earlier investigations show that atmospheric bromoform concentrations are higher in coastal source regions (Quack and Wallace, 2003). Thus, decreasing bromoform concentration can be expected by an increasing distance to Japan's coastal region. At 28°N the concentration shows a peak little after the maximum of the passage of the tropical storm "Nepartak" . Such storms can lead to entrances of distant air masses and can have an impact on the atmospheric concentration by introducing coastal influenced air including possible strong sources. After this storm event the concentrations decrease further. From 19°N to 4°S it varies around 0.5 ppt. During this time the cruise crossed the ITCZ and entered mostly open ocean regions. The evaporation and, hence the salinity (not shown here) becomes higher, which doesn't increase the concentrations. The high salinity makes this regions hostile to life. Hence, low phytoplankton concentrations (measured inboard, not shown

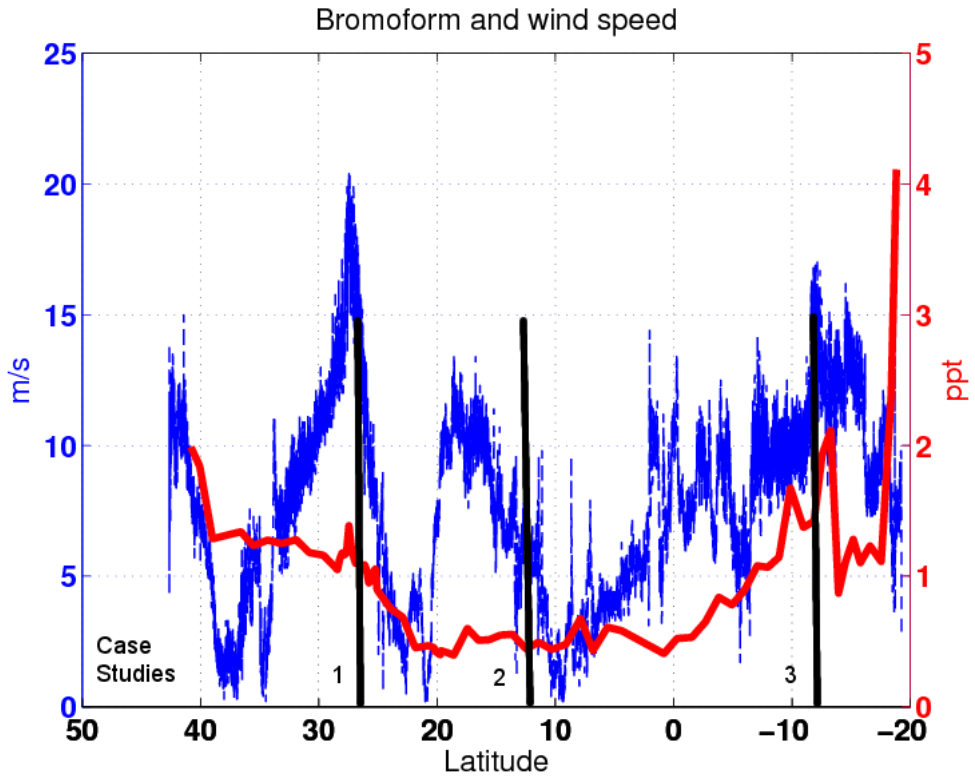

Figure 7.1: Atmospheric bromoform concentrations (ppt, red line) and true wind speed (m/s, blue dashed line) during the TransBrom-Sonne cruise.

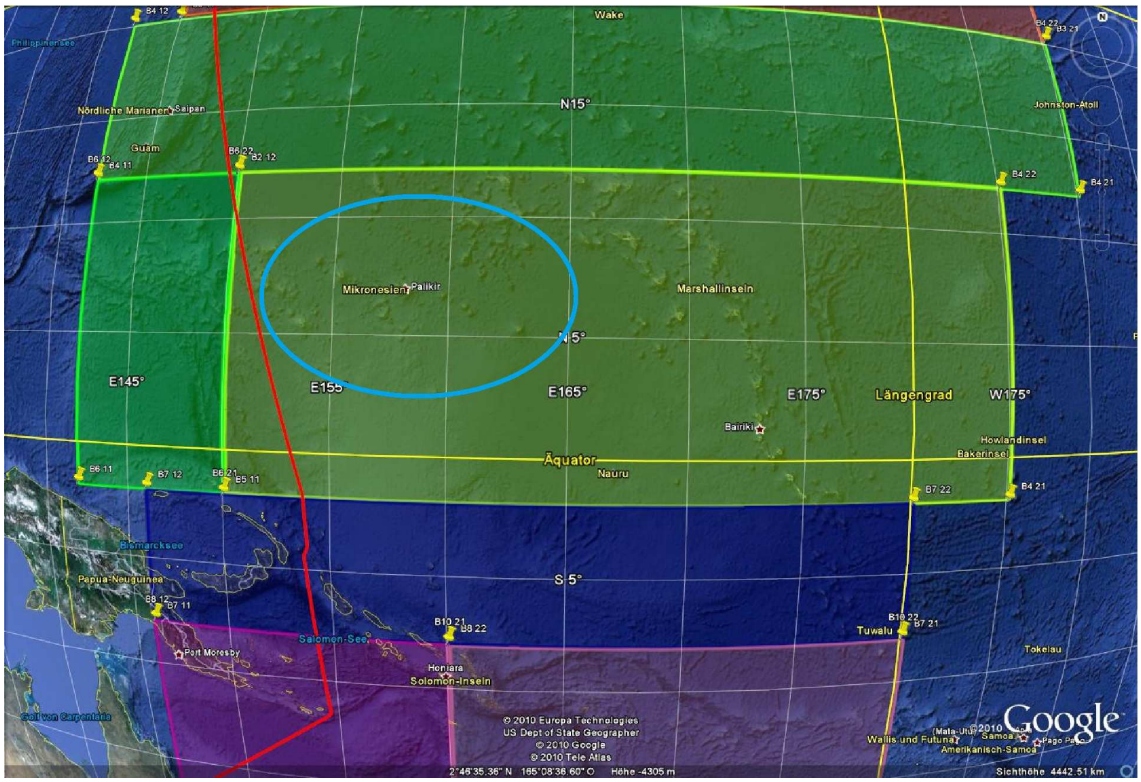

Figure 7.2: Google Earth satellite picture including the different boxes. The focus lies on box 5 and its islands of the Federated States of Micronesia (blue cirlce).

in this thesis) are correlated to small bromoform amounts. After passing the equator the concentration increases to 2 ppt at 14°S and to over 4 ppt at 19°S. Between both SH maxima the values decrease to 1 ppt. The strong southerly trade winds transport distant air masses with low amounts of bromoform (1 ppt) into the region. The maxima coincide with the approach to Papua New Guinean and Australian coastal regions, and could be caused by coastal emissions. During this time the ship also crossed the Coral Sea (8°S - 19°S), possibly including sources (e.g. high amounts of aquatic fauna), which may also have lead to the high concentrations. The wind speed, was discussed in detail in Chapter 5.2, correlate with wind speed (Zhou et al., 2008). During TransBrom Sonne however there is a weak correlation visible between both curves. The correlation coefficient is 0.23. In order to identify the atmospheric source regions of the enhanced atmospheric bromoform concentrations backward trajectories are analyzed.

7.1.1.1 Case Study: 2009-10-12 12 UTC

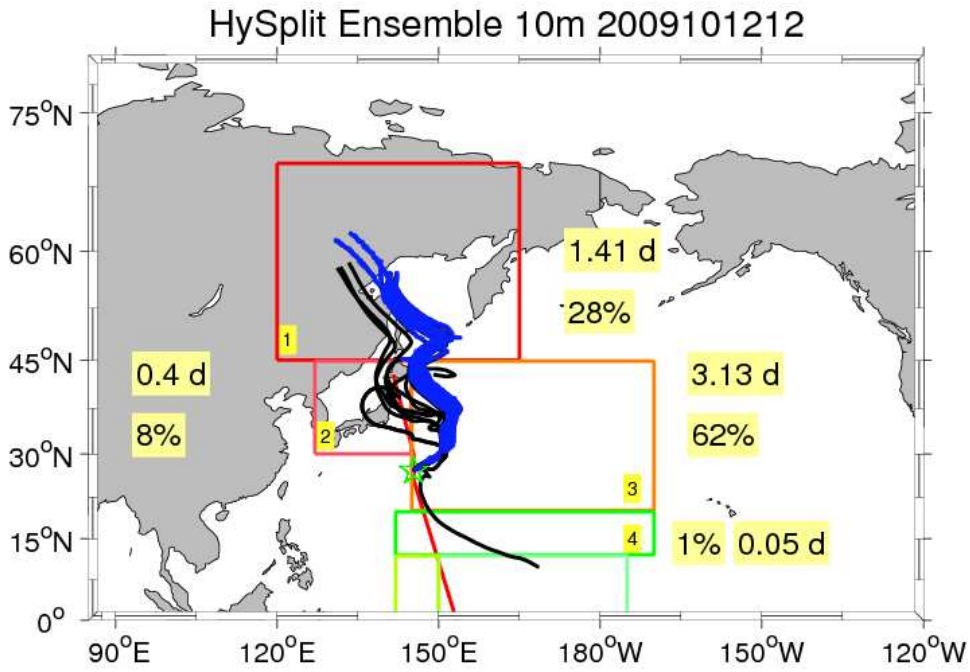

Figure 7.3: Case study trajectory calculations started at 10m height on October 12, 2009, 12 UTC. The bluish trajectories are the highest.

The high concentration of bromoform at the beginning of measurements can be associated with the proximity to Japan and the high wind speeds during the passage of "Melor". Figure 7.3 shows HySplit trajectories (10 m) during the storm event of "Nepartak" on October 12, 12UTC, which are started 5 days backward. Most of the trajectories come from box 1 and go into box 3. Based on a 5 day backward calculation 62 % of all trajectory points can be found in box 3, which stays to 3 out of 5 days. Box 1 shows the second highest residence time and percentage with 1.4 days and 28 %. Just 8 % crossed box 2 and 1 % is in box 4. Because of rounding errors within the program (Matlab), the total only amounts to 99 %. Hence, the air masses during the passage of "Nepartak" are mostly influenced by box 3 (62 %) and box 1 (28 %). The trajectory ensemble run is also shown in the figure. Only one trajectory has a pathway from southerly direction. All the others come from north-northwest. By coming this way, they crossed Japan's northern mainland and especially Japan's and Russia's coasts. Thus, the air masses being transported to the ship from those regions include anthropogenic sources (e.g. coastal power stations), which have lead to the slightly elevated concentrations of 1.2 ppt at 28°N. "Nepartak" and ex-super typhoon "Melor" suck air masses from large areas, including source regions, into the storms (Section 2.6). This

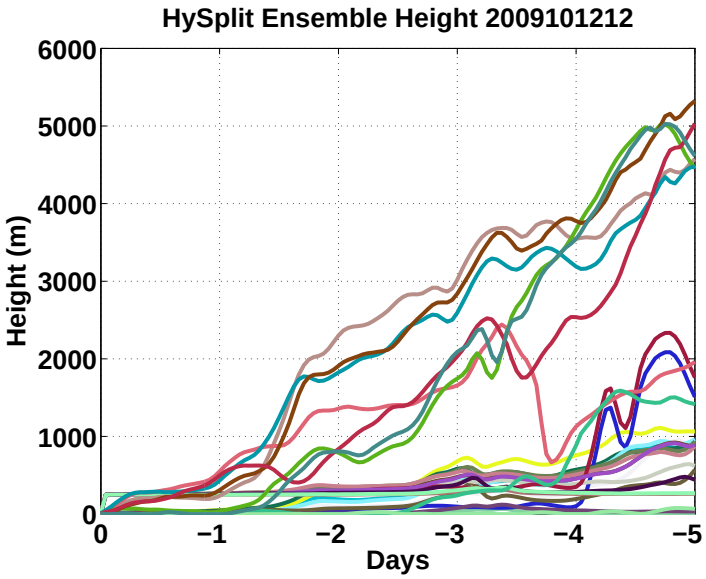

Figure 7.4: Evolution of height in HySplit trajectories during the 5 days backward on October 12, 2009, 12 UTC.

can explain the higher concentrations of bromoform at the beginning of the cruise. The evolution of trajectory heights in the HySplit model is shown in Figure 7.4. A split of the air mass origins into two levels is visible. The first part of the air masses comes from a height of around 5000 m (bluish colored trajectories in Figure 7.3). The second more interesting part shows only a small gradient in height. The entire 5 days the air masses stay in a height between surface and 1000 m, which lies within the boundary layer and underlies turbulence (Section 2.1.1.1). This implies strong mixing and has a high probability that the air masses are influenced by coastal ground sources of Japan and East Russia. But even the air masses of the higher level penetrate the boundary layer after 3 days, thus being influenced by ground emissions as well.

7.1.1.2 Case Study: 2009-10-16 00 UTC

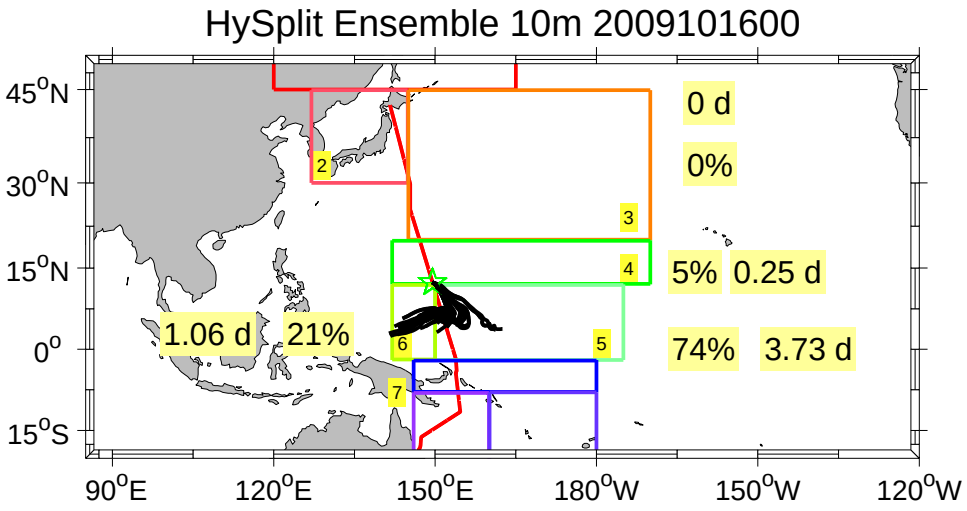

Figure 7.5: Case study trajectory calculations started at 10m height on October 16, 2009, 00 UTC.

The bromoform concentration decreases until 22°N and stays almost constant (0.5 ppt) until the ship reaches 4°S. During this time the trajectories mostly come from the open ocean, which can be seen in Figure 7.5 (October 16, 00UTC). 74 % of all trajectory points lie in box 5 for 3.73 days. 21 % of the trajectory points crossed box 6. Both boxes include open ocean sources, while box 5 also includes islands of the Federated States of Micronesia (Figure 7.2). The low concentrations of bromoform between 19°N and 4°S reflect the open ocean conditions. Despite the low altitude pathways of the trajectory ensembles (only up to 400 m), meaning high mixing within the boundary layer, the bromoform concentration is low (Figure 7.6). At 9°N a slightly higher mixing ratio of bromoform occurs. This leads to the conclusion that the low trajectories overcoat islands with coastal sources or an open ocean source (e.g., bromoform producing phytoplankton)(Figure 7.2). The air masses between the surface and 400m underlie the characteristics of a boundary layer. Hence, the low bromoform concentration despite turbulent conditions must be explained by the lack of bromoform source in the open blue ocean.

From 4°S to 18°S bromoform concentrations increases rapidly. Between 12°S and the arrival in Townsville two high maxima and a lower concentration inbetween are visible. The maxima with 2.1 ppt and 4.1 ppt are higher than the concentrations in the NH.

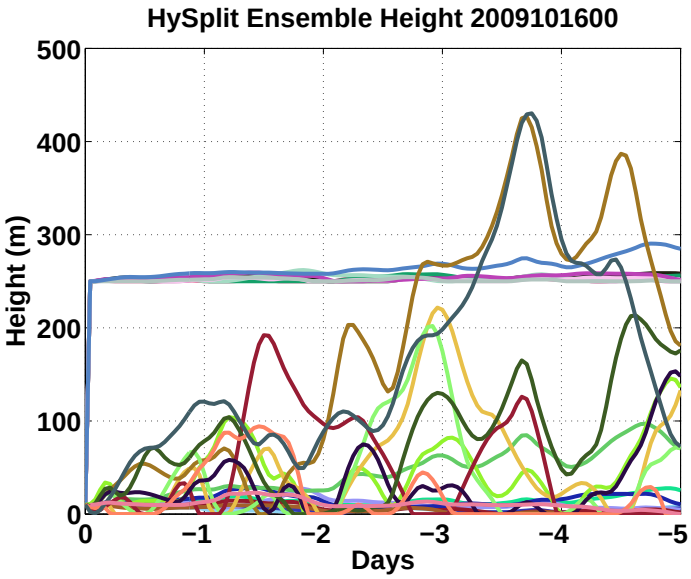

Figure 7.6: Evolution of height in HySplit trajectories during the 5 days backward on October 16, 2009, 00 UTC.

The bromoform concentration increases with the wind speed. The trajectories will be used for a better distinction between the two maxima.

7.1.1.3 Case Study: 2009-10-21 12 UTC

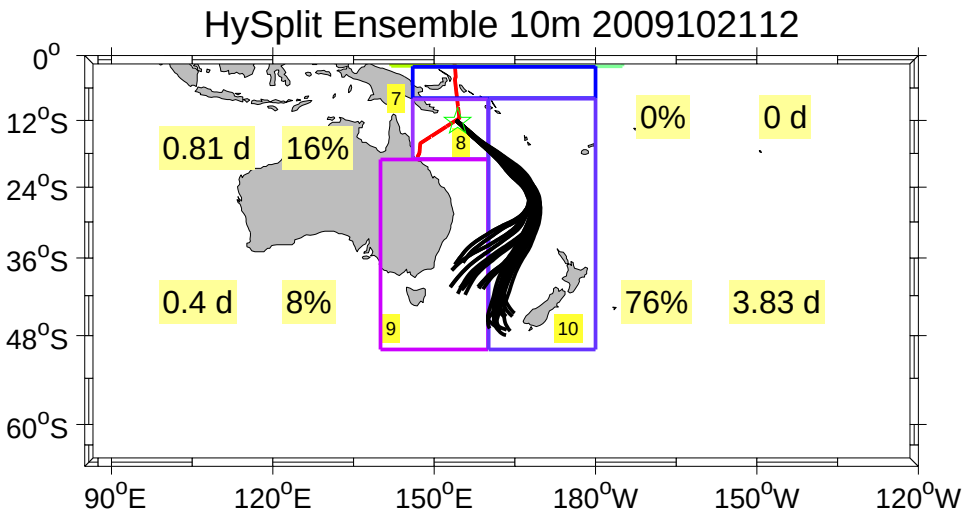

Figure 7.7: Case study trajectory calculations started at 10m height on October 21, 2009, 12 UTC.

Figure 7.7 shows the 5 day backward trajectory of October 21, 2009 12UTC, one day before measuring the first high maximum. All trajectories show similar pathways during the last part of the cruise (not shown here). The calculation starts within box 7 and 8. It is visible that the air masses come straight from box 10. The air mass origin is splitted into two parts (box 9 and 10) between New Zealand and Australia. After 1 day the pathways end to vary slightly and get bundled. 76 % of the points lie in box 10 for a duration of 3.83 days, 16 % in box 8 and 8 % in box 9. Hence, the Great Barrier Reef and the coastal region of Australia in box 8 and the Coral Sea in box 10 may be responsible for the generally high concentration of bromoform in the SH. The decrease between both maximum bromoform concentrations may be caused by a lack of bromoform sources or by a slightly change of the trajectory pathways. Local sources within the boundary layer including strong mixing can also lead to temporal variability of the atmospheric concentration. The correlation coefficient between wind speed and bromoform is just 0.20, implying that the wind speed is not the factor for the varying atmospheric concentrations. The height of the trajectory ensembles is very low(¡1000 m) and hence, they lie within the boundary layer (Figure 7.8). Only one trajectory comes from an altitude of 1400 m. Hence, a direct influence of the surface and their sources on the measured gases has a high probability. However, it is possible that air parcels in higher levels than the boundary layer follow more landward pathways and may include higher concentrations of bromoform from coastal regions, leading to

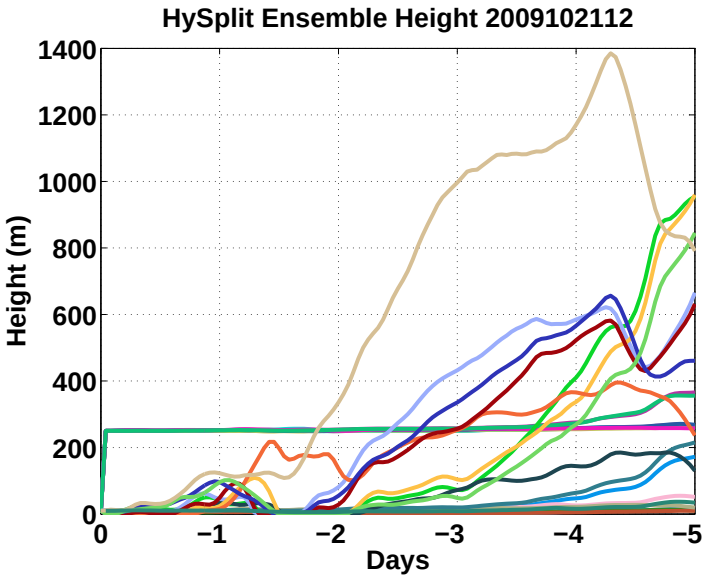

Figure 7.8: Evolution of height in HySplit trajectories during the 5 days backward on October 21, 2009, 12 UTC.

elevated concentrations on the ship. Due to bromoform's lifetime of two to three weeks it is likely that air at the ship includes air masses from different heights, hence, different concentrations of gases.

7.1.2 Methyl iodide

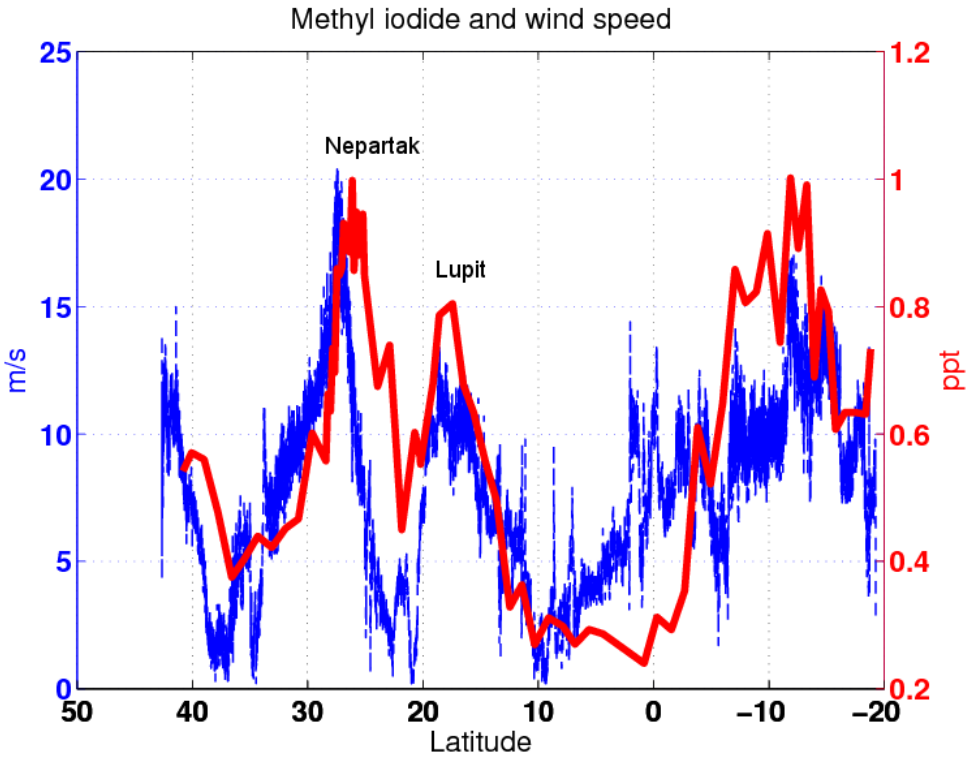

Figure 7.9: Atmospheric methyl iodide concentrations (ppt, red line) and true wind speed (m/s, blue dashed line) during the TransBrom-Sonne cruise.

Figure 7.9 shows the measurements of the next interesting VSLS, methyl iodide. Correlation between wind speed and atmospheric methyl iodide are investigated by Wanninkhof et al. (1985); Smethie et al. (1985); Liss and Merlivat (1986); Tsai and Liu (2003). North of 20°N the concentration of methyl iodide follows the wind speed with a little temporal offset. During the "Nepartak" passage methyl iodide and wind speed increase and decreases simultaneously as well but with a short delay in the methyl iodide concentration. However during other parts of the cruise the curves show a good agreement without a shift. During the tropical storm passage of "Lupit" 18°N the minimum and maximum of wind speed occurs at the same time as the minimum and maximum of the methyl iodide concentration. An interesting behavior takes place between 10°N and 0°. Although, the wind speed increases again after the minimum of wind speed at 10°N, the methyl iodide concentrations do not increase simultaneously, despite high wind speed have been the accelerator for high methyl iodide concentrations the days before. The trajectory altitudes generally are below 200 m and can interact with the surface respectively the open ocean. The low trajectories and the circulation of

the air (Figure 7.5) over the same region could be a good basis for high concentrations of methyl iodide in air samples. The low concentrations show that sources are missing. Being only over open ocean and especially regions with high evaporation rates, the higher salinity prevents high concentrations of phytoplankton (Qasim et al., 1972),), a natural source for methyl iodide. The atmospheric methyl iodide concentrations in this region do not fluctuate as much as those of bromoform. The concentrations increase after 4°S. With a rapid growth up to 1 ppt (12°S - 14°S) the curve turns back to the correlation with the wind speed. The overall correlation coefficient is about 0.56 and higher than the coefficient of bromoform. A correlation between wind speed and the atmospheric concentration of bromoform and methyl iodide can only exists if a marine source is available. This matches with earlier investigations from other trace gases by Wanninkhof et al. (1985); Smethie et al. (1985); Liss and Merlivat (1986); Tsai and Liu (2003).

The flux of gases between the mixed layer in the ocean and the air increases during the built up of waves and the acceleration of other air-sea exchange processes (e.g. bubble formation, disturbance of surface film) during the passage of a storm. It looks like, that it takes time before the atmospheric concentration of methyl iodide, produced by phytoplankton (Moore and Tokarczyk, 1993; Manley and dela Cuesta, 1997) and photochemical processes in the ocean, is built up in the air masses of the storm. This could be one possible explanation for the delay between wind and methyl iodide maxima. High concentration (1 ppt) is reached again at 12°S, similar to bromoform. During this part of the cruise the trajectories are mostly influenced by the Great Barrier Reef andits possible sources. It can be highlighted that methyl iodide is well correlated with the wind speed, but it is important to know if sources for producing methyl iodide concentration in the atmosphere exist in this regions.

7.1.3 Methane

Methane shows a total different behavior compared to the first two trace gases (Figure 7.10). The course of this curve verifies the global distribution of methane. Because of being a more anthropogenic gas the concentration of methane in the NH is higher than in the SH (between 1.7 and 1.8 ppmv) (Blake, 2010). In the NH there are more anthropogenic methane sources (Section 3.2.1). Hence, the higher concentrations at the beginning of the cruise can be related to elevated anthropogenic sources. In that case the reason for the break at 15°N is the barrier of the ITCZ. Strong winds from the NH and SH converge in this region and the air masses are pushed upward. While the ITCZ is shifted more towards the NH during October, the concentrations of methane are lower in this region compared to mean boreal values, since the air is mixed with SH air masses. Considering the graph without the peak at 20°N the curve would decrease further from 22°N. This is exactly the point where the wind direction and hence, the

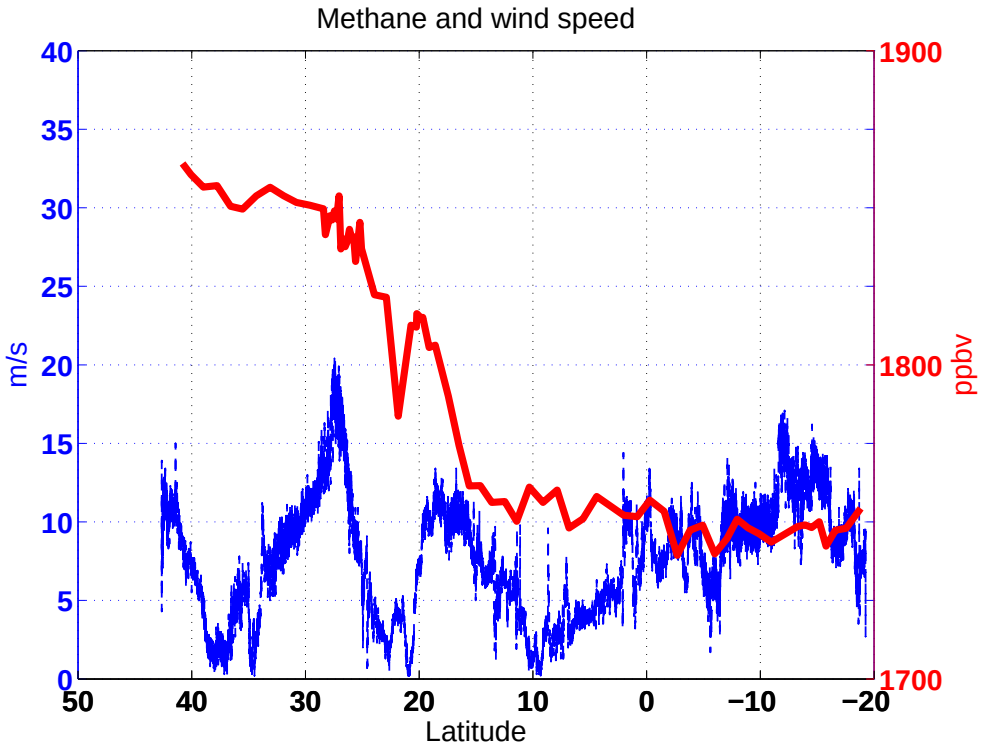

Figure 7.10: Atmospheric methane concentrations (ppb, red line) and true wind speed (m/s, blue dashed line) during the TransBrom-Sonne cruise

trajectories switch from northerly to more southerly winds. At 15°N methane stays almost constant at 1750 ppt. It is an obvious sign for SH (less sources of anthropogenic gases) influence and the typical behavior between both hemispheres. The concentration of a long-lived anthropogenic trace gas highlights the different origin of VSLS coming from natural or anthropogenic sources.

7.2 Overview

In the following Section the results of the HySplit trajectory calculations are evaluated. The evaluation is split into two parts. First the meteorological and following the source regimes are investigated. The meteorological regimes are divided based on the wind speed and wind direction measurements of the cruise. The source regimes are divided based on the results of the bromoform concentrations during the cruise.

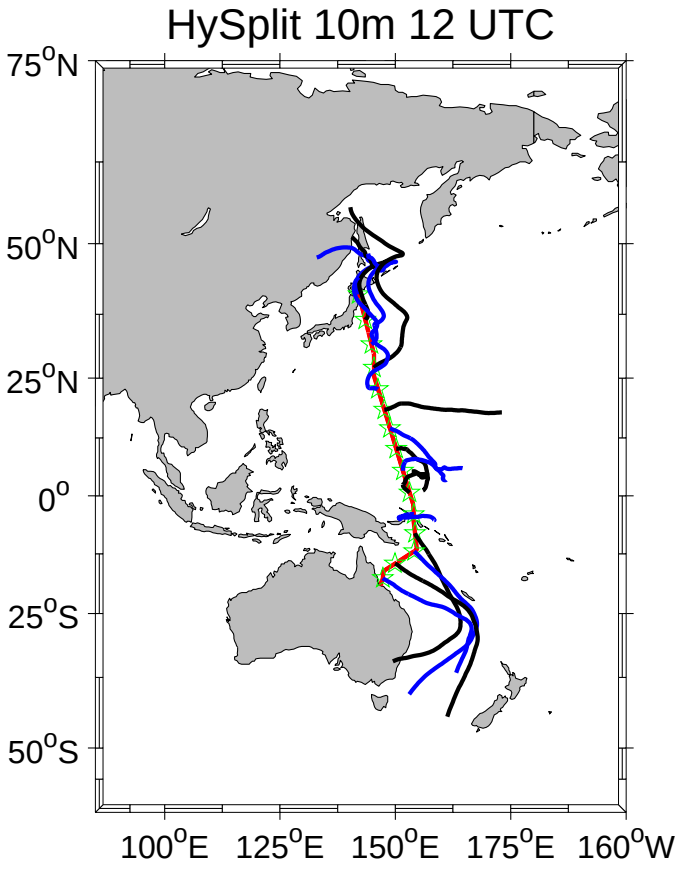

Figure 7.11: One trajectory per day at 12 UTC is shown for the whole cruise. They are alternating between black and blue for a better visualization.

7.2.1 Meteorological regimes

Before coming to the evaluation of the air masses and their sources in relationship to the boxes, the main regimes will be introduced. The main measured meteorological regimes as mentioned in Chapter 5 are separated into three parts. In the first part the wind is more northerly. In the second part the air comes easterly and in the last part of the cruise the air is dominated by southerly trade winds. This is reflected by the trajectory calculations (Figure 7.11). Until 23°N the trajectories come from the north influenced mainly by Japan's and Russia's mainland. From 23°N the direction switches into an easterly, later east-southerly. At the equator the trajectories circle around about but the last part of them comes from the east as well. At 4°S, the location of the ITCZ, another switch of the direction happens and they come from the south.

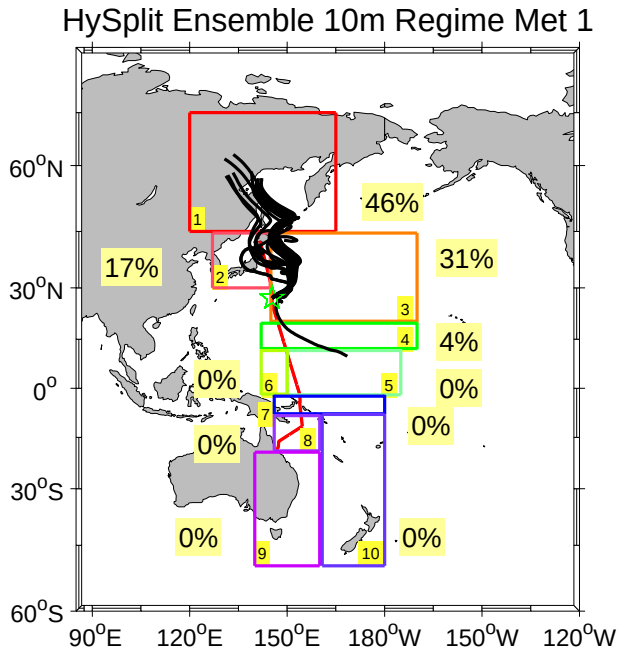

Figure 7.12: Percentage distribution of the meteorological regime 1 including an example trajectory.

7.2.1.1 Meteorological Regime 1

The first meteorological regime is defined from the beginning of the cruise (October 9, 2009, 42°N) until the turn over date (October 13 18 UTC, 23°N) of the air mass origin. With the definition of boxes it is investigated how many percent of all 121, including the starting point, trajectory points (one per hour) of a 27 ensemble (5 day backward) lie in such a box and can be influenced by different source regions. The trajectories are started at 10 m height. In the meteorological regime 1 46 % of all points lie in box 1, 17 % in box 2, and 31 % in box 3 (Figure 7.12). Just 4 % lie in box 4. Between box 3 and 4 there is the region of changing the wind direction. At this point the meteorological regime 1 ends because the air mass origin switches from coming from the north into coming from the south. Here, the calculation for the first meteorological regime stops to keep the influence of southerly air masses in this regime low. At the beginning of the cruise bromoform, methyl iodide, and methane measurements show high concentrations, which can now be verified by the trajectories and the percentage of boxes. The highest values can be found in box 1. The air masses have their longest residence time in box 1 which includes coastal regions being interesting for bromoform and methyl iodide as well as mainland being more important for methane.

7.2.1.2 Meteorological Regime 2

The second meteorological regime is the region dominated by the ITCZ. The separation of trajectory calculation is done between October 14 to October 19 (06 UTC) where the air masses tend to be influenced more by the trade winds (Figure 7.13). Therefore, boxes 4 till 7 are the important ones. Hence, boxes 5 jutes out with 69 %. Box 4 has 19 % and number 6 and 7 are almost negligible with 6 % and 3 %. Easterlies lead to such a result of box 6 and 7. Almost all trajectory points of meteorological regime 2 are included in box 5. Due to a slow change of the trajectory origin box 4 gets a non marginally part of the percentage.

7.2.1.3 Meteorological Regime 3

The last part of the meteorological regime is that part including the strong trade and southerly winds (Figure 7.14). From October 19 (12 UTC, 4°S) until the end of the cruise boxes 8, 9, and 10 play a main role in the calculation. Especially box 10 jutes out in this case with 61 %. Boxes 8 and 9 has the same percentage of 16 %. With a small value of 7 % box 7 plays a weak role in this evaluation. Almost all trajectories during this part of the cruise nearly show the same pathways. The pathways have a very long range. As they come under the influence of the strong trade winds at round about 30°S their residence time in box 8 during the last parts of pathways are very short.

7.2.1.4 Overall Meteorological Regimes

If all trajectory points for all three case studies are considered a similar result as the meteorological classification is given (Figure 7.15). Three example trajectories are overlayed over these results(Figures 7.12, 7.13, 7.14). Overall boxes 5, 10 and 1 are predominant for the trace gas concentrations measured on board with 25 %, 19 % and 15 % part of the whole cruise trajectories.

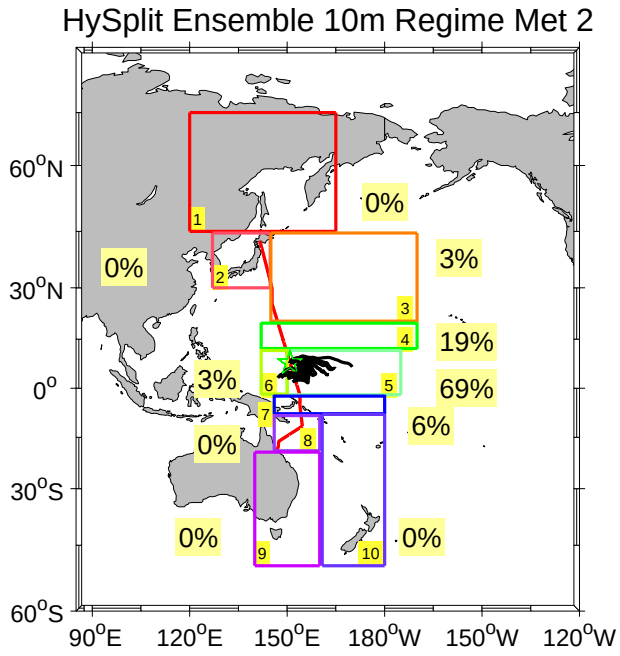

Figure 7.13: Percentage distribution of the meteorological regime 2 including an example trajectory.

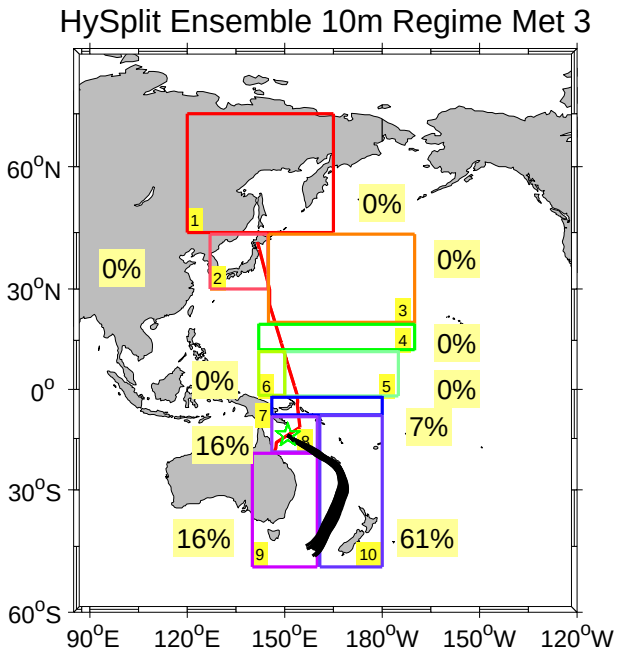

Figure 7.14: Percentage distribution of the meteorological regime 3 including an example trajectory.

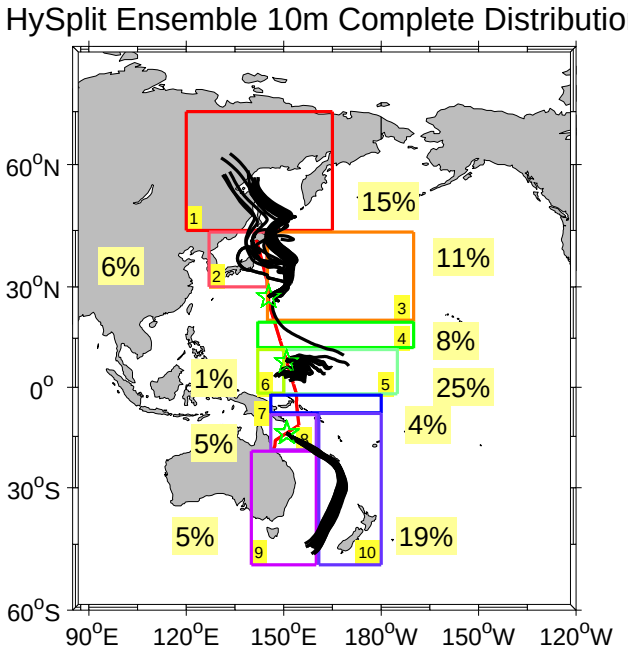

Figure 7.15: Percentage distribution of the complete cruise including example trajectories for the three different meteorological regimes.

7.2.2 Source regimes

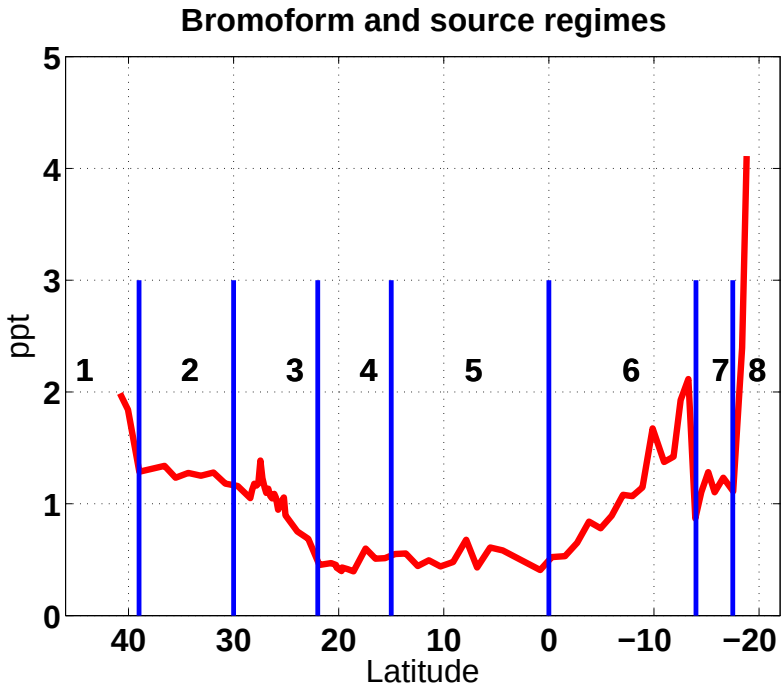

Figure 7.16: The red curve shows the bromoform concentration measured during the cruise. It is classified into 8 different regimes based on the course of the curve.

Source regimes are subjectively classified, based on variations in the atmospheric bromoform concentrations on the ship. Due to the curve progression it is separated into 8 regimes (Figure 7.16). The boxes (1-10), which are used for categorizing the source regions, are the same as in the meteorological separation before.

7.2.2.1 Source Regime 1

Regime 1 starts from 42°N to 39°N (October 9, 00UTC - October 10, 00UTC) (Figure 7.17). In source regime 1 box 1 dominates the results very clearly with 74 %. Box 2 has 17 % and box 3 7 %. In relationship to the results of bromoform and its relative high concentration of 2 ppt, it is important to follow the trajectory pathway. Therefore, for every regime an example trajectory is included in each Figure, which represents the other trajectories in this regime as well. In source regime 1 the pathways are almost completely mainland and coastal influenced, which corresponds to the first part of bromoform. Almost three quarters of the trajectory way points are included in box 1 and hence, they are mostly influenced by coastal and landmass regions. The percentage of box 2 refers to the starting points of the trajectories, but these lie in coastal regions

as well. Especially coastal regions are interesting for bromoform and methyl iodide. The land mass regions are more important for methane which corresponds to the highest concentration at the beginning of the cruise. The trajectory altitudes show an increasing behavior from the beginning until the end of this regime. First almost all trajectories come from round about 600 m and fluctuate very strong until the measurement point at 10 m after 5 days. Later the trajectories come from higher levels between 1000 and 2000 m (not shown here). This fact fits to the decreasing behavior of the gas concentrations due to less influence of the surface and their source regions.

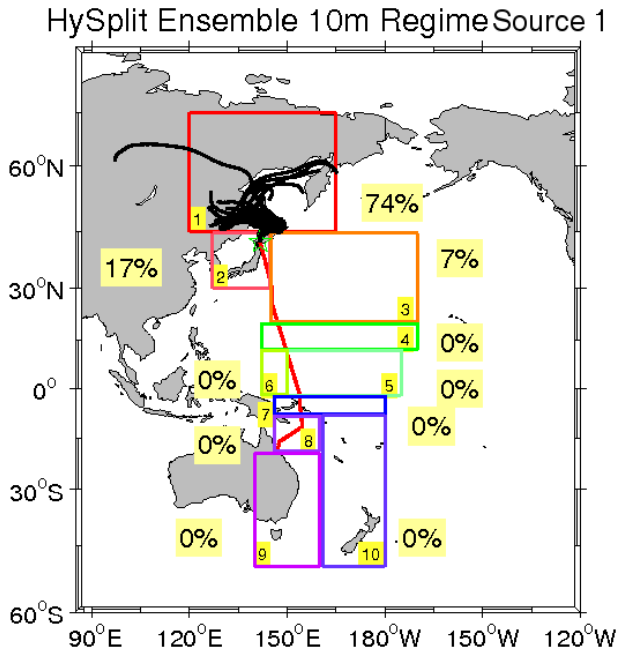

Figure 7.17: Percentage distribution of the source regime 1 including an example trajectory.

7.2.2.2 Source Regime 2

The source regime 2 extends from 39°N until 30°N (October 10, 00UTC - October 11, 18UTC). In this part bromoform shows no fluctuating behavior with values between 1.2 and 1 ppt. The box distribution is similar to the first regime but the percentage of box 1 is less with 54 % (Figure 7.18). Box 3 (18 %) and especially box 2 (28 %) include more trajectory points than before . The weak concentration and weaker fluctuating of bromoform can be explained by the over coating of Japan in the earlier parts of the trajectories. Due to less influence of box 1 and therefore, more ocean regions and being further away from the ex-typhoon of “Melor“ the concentration decreases.

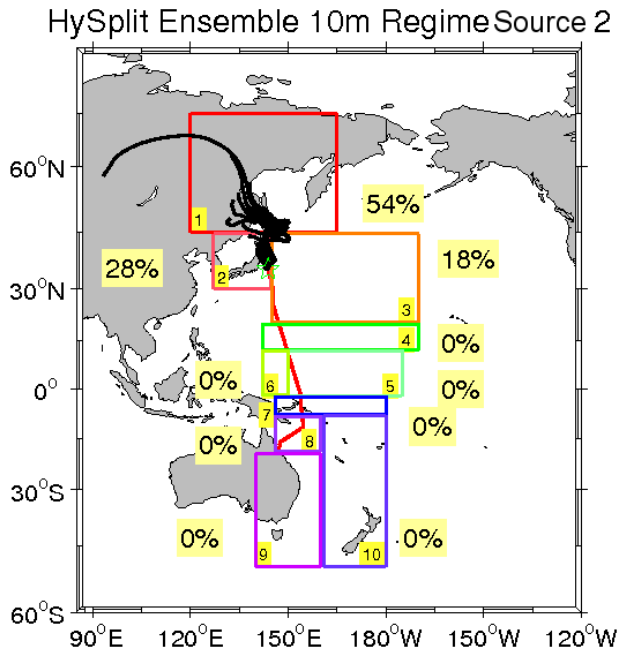

Figure 7.18: Percentage distribution of the source regime 2 including an example trajectory.

For trajectories starting on October 10, 00UTC the trajectory altitudes lie between 1000 and 3000 m and decrease to 500 m abd 2000 m (not shown here). Therefore, the interaction between the open ocean and the air increases and the influence of anthropogenic sources decreases.

7.2.2.3 Source Regime 3

In contrast the third regime (October 11, 18UTC - October 13, 06UTC), extends from 30°N to 24°N, (Figure 7.19), showing a switch from a predominance of box 1 (31 %) to an overweight of box 3 (60 %). Box 2 is less than before with just 7 %. The example trajectory shows that the pathways are more concentrated to boxes 3 and 1. The residence time is longer in box 3 than in box 1. The distribution has shifted more towards box 3 and the open ocean. However, an important influence comes from Japan, its coast and from the mainland of Russia as well. In this regime especially the tropical storm “Nepartak“ which crossed the cruise in the night of October 12 plays an important role (see section 7.1.1, 7.1.2)

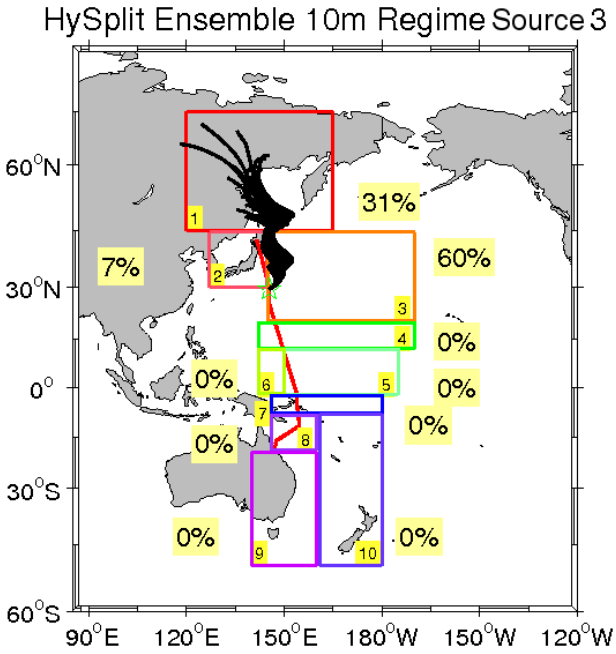

Figure 7.19: Percentage distribution of the source regime 3 including an example trajectory.

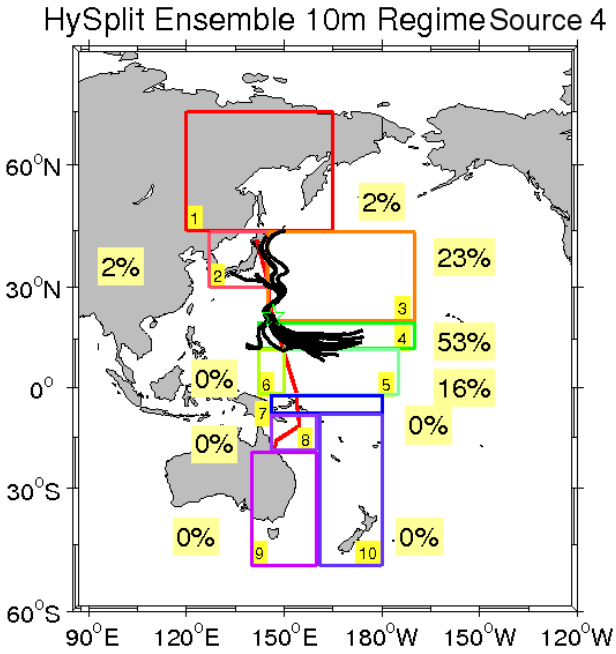

Figure 7.20: Percentage distribution of the source regime 4 including an example trajectory.

7.2.2.4 Source Regime 4

The fourth source regime (24°N to 15°N) shows another interesting behavior (Figure 7.20), also due to the third storm event of the tropical storm "Lupit". It is the time (October 13, 06UTC - October 15, 06UTC) when the wind direction and hence, the air mass origin changes in more easterly. The rest of the northerly coming air masses are shown in box 1 (2 %), 2 (2 %) and 3 (23 %). Box 3 has a relative high percentage because the starting points of the trajectories almost lie all within the box and some of the pathways follow the way north. But, most of the pathways go in southerly and later in easterly direction. There box 4 has the highest percentage (53 %) and box 5 enters the distribution with 16 %. It is obviously that box 4 and their neighbour boxes have the highest percentage. Box 1 and 2 are too far away from the dominant box. One important event during the trajectory calculation is the storm event of "Lupit" which is explored in more detail in the sections 7.1.1, 7.1.2. It develops more and more into a typhoon on the Westside of the cruise track. Hence, its influence can play an essential role in air mass flow and its flow direction from east to west.

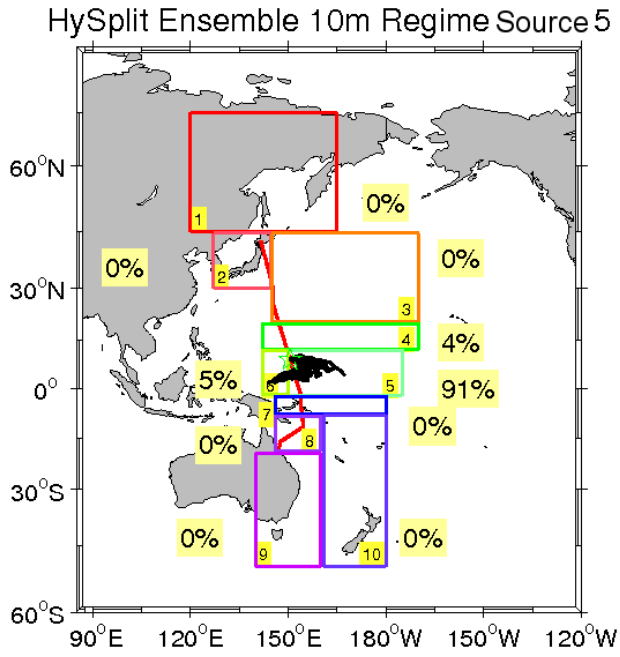

Figure 7.21: Percentage distribution of the source regime 5 including an example trajectory.

7.2.2.5 Source Regime 5

The fifth regime is predominated by box 5 (Figure 7.21). This calculation section reaches from 15°N to the equator (October 15, 06UTC - October 18, 12UTC). The percentage distribution between the boxes is one sided. Box 5 predominates the results with 91 %. Just 5 % of box 6 and 4 % of box 4 fill the rest to 100 %. Consequently, most of the trajectories are influenced by box 5 and their characteristics. All three gases show a behavior without big peaks during this part of measurements.

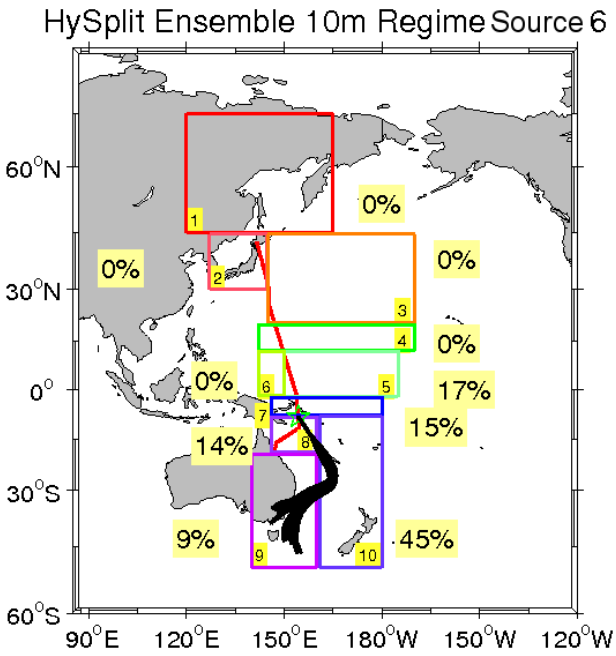

Figure 7.22: Percentage distribution of the source regime 6 including an example trajectory.

7.2.2.6 Source Regime 6

The sixth source regime (October 18, 12UTC - October 22, 06UTC) reaches from the equator to 14°S. In this regime the change between the meteorological regime 2 and 3 takes place. It can be seen that the percentage is distributed from box 5 to box 10 (Figure 7.22). Some of the trajectory points lie in box 5 (17 %) but most of them are scattered between the boxes 7 to 10, the boxes of the third meteorological regime. Box 7 has 15 %, box 8 14 %, box 9 just 9 %, and box 10 even 45 %. During this part of the cruise the origin of air masses change from alternating in small scales near the equator and the regions of the Federated States of Micronesia to the trade and southerly winds influenced from the Great Barrier Reef and the south of Australia coming origin.

7.2.2.7 Source Regime 7

The regime before the last regime is number 7 reaching from 14°S to 17°S (October 22, 06UTC - October 23, 12UTC). The distribution is separated into almost 2/3 in box 10 (68 %) and 1/3 in box 8 and 9 (16 % each) (Figure 7.23). The other boxes 7 do not play a role. The ship cruise goes through box 8 and the air masses follow the same way like in the sixth source regime. Just at the beginning of the calculations there is a little shifted towards New Zealand. The decrease in bromoform can not explained by a substantially difference in the trajectory pathways. Hence other factors such as a lack of marine sources may play a role, as the trajectories seem to be more dominated by the boundary layer.

7.2.2.8 Source Regime 8

The eighth and last source regime can be the reason for the increasing in the bromoform concentrations. It describes the latitudes from 17°S to 19°S (October 23, 12UTC - October 24, 00UTC). The percentage distribution shows a small part of box 8 (5 %) and two bigger parts of box 9 (36 %) and of box 10 (59 %).
The residence time is almost completely concentrated in box 9 and 10 (not shown here). This regime is influcenced by the closeness to the coast of Australia, including the Great Barrier Reef. These are the main indicators for the rapid increase in the last part of the methyl iodide and bromoform curves. Actually methane indicates a small increase, due to the influence of the Australien coast and the possible appearance of anthropogenic sources. Bromoform shows the highest concentration of the whole cruise by over 4 ppt in this case. The near to the coast and the warmer waters with its possible amounts of organic life can be the reason for this peak. Additionally the splitting into two parts of the trajectory altitudes play an essential role (not shown here). The lower part stays in a height of below 100 m the whole 5 days backward. The higher part varies between 500 m and 2000 m. More trajectories stay within the boundary layer and can account for this high concentrations at the end of this ship cruise.

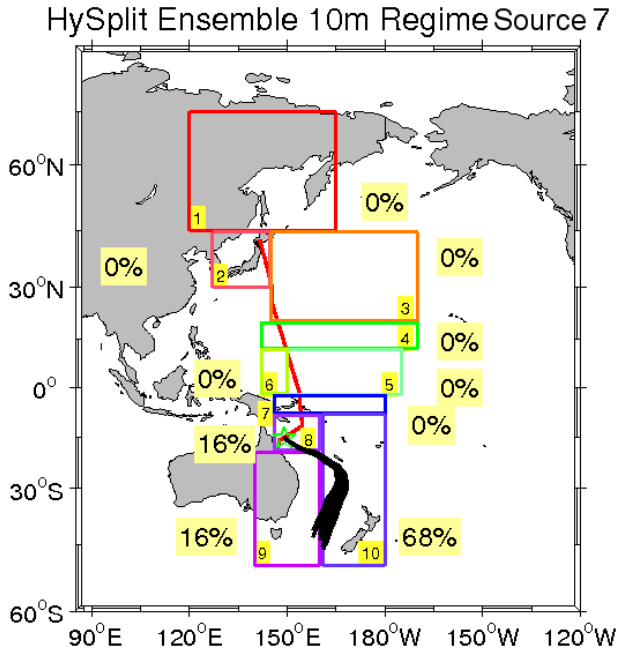

Figure 7.23: Percentage distribution of the source regime 7 including an example trajectory.

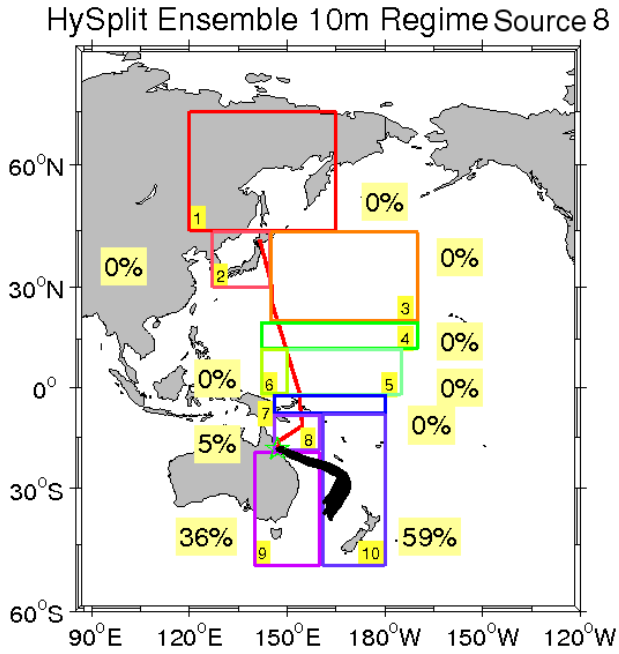

Figure 7.24: Percentage distribution of the source regime 8 including an example trajectory.

Chapter 8

Discussion

Trajectories are helpful tools to verify origins of measured air masses. The main differences of all trajectory models are the meteorological input data, which leads to different results (Harris et al., 2005). The main problem is the interpolation within regions of few measurements. Open oceans are more fragile than mainland. To overcome this problem, we carried out regularly radiosonde measurements which we distributed to the WMO measurement data base. These data were used for the meteorological assimilations such es ECMWF. The cruise crossed the Western Pacific and hence, the used data show some differences (Section 5.3). Overall the curve of the wind speed and direction of the opECMWF data show a good agreement to the measured values. However, the opECMWF data underestimate the wind speeds especially during strong wind events, what agrees with the earlier results of (Molinari and Robasky, 1992). It can be usefull to check different models of e.g. NCEP, MetOffice including assimilation data if they show similar behaviors and compare it with each other. A comparison between NCEP-GADS and opECMWF gives a hint how variable and reliable the results of different models are (Chapter 6). Both trajectory calculations behave similar with each other. However the BADC trajectories are longer than the HySplit trajectories due to higher wind speeds in the opECMWF data. The wind directions are well reflected in comparison with the measured values onboard. Due to faster calculation, easier handling and good overall agreement between the two models the HySplit model is used for the source region analysis.

The HySplit pathways and their residence times in the defined boxes help to analyse the measured concentrations of the three gases (Chapter 7). But the trajectories can just give a hint due to the complexity of the combined chemical and transport processes along the pathway. Chemical processes are not included in the trajectory calculations, which could better explain the observed concentrations. More investigations about the processes within tropical storms respectively typhoons, which are conducted e.g. by Cram et al. (2007), can be useful. The microscale interaction between the surface and the air is also too complex for being included in such trajectory models.

Overall this method of origin investigations by using trajectories is a good basic for further and more detailed studies.

Chapter 9

Conclusion and Outlook

In this thesis the origin of trace gases measured in the marine boundary layer in the tropical West Pacific is investigated. After an introducing of the current scientific state, the important meteorological and chemical processes, and the weather phenomena during the TransBrom-Sonne cruise are described and investigated in more detail (Chapter 5). The cruise passed three different meteorological regimes. Tropical storms and typhoons escorted the cruise in the NH and influenced the measurements. Also the region of the ITCZ and the strong trade winds in the SH played an important role. The effect of convective systems within the ITCZ is detected in radio sonde measurements. A comparison between ship measurements of wind speed respectively wind direction and high resoluted opECMWF data fits qualitatively well with correlations of 0.89 respectively 0.98. In which the maxima in wind speed are slightly underestimated by the opECWMF, especially during typhoon or tropical storm events.
Before analysing the air mass origin a comparison between HySplit and BADC trajectory calculations is carried out. Case studies (one for each meteorological regime) are chosen to investigate the trajectory behavior during different weather situations. The pathways of both models are very similar, however, the BADC trajectories are more bundled than the HySplit trajectories. In the one to one comparison the BADC trajectories show a longer reach over the whole cruise, which is due to by stronger winds of the meteorological input data (opECMWF data). Altogether, directions of the trajectories agree very well between the BADC and the HySplit models.

The next step is to use case studies to explain the atmospheric concentrations of three different trace gases (bromoform, methyl iodide, and methane) (Chapter 6). The residence time of air mass per boxe gives insights on trace gas variations and their part and possible source regions. Box 5, 10 and 1 are the boxes with the highest percentages over the whole cruise. In good agreement with the first meteorological regimes box 1 represents the sources of mainland and coastal regions with 15 % overall percentage. The eastern part of Russia, Japan and their coasts fits to the relatively high concentra-

tions of all three trace gases. Box 5 (25 %) lying in the second meteorological regime represents the open blue ocean. The long overall residence time in this box is caused by the ITCZ, with weak cirrculating winds. There all three trace gases get into an almost constant phase with low concentrations, which matches with the relatively weak wind speeds and the open ocean origin of the air masses. In the third meteorological regime box 10 dominates with 19 %. In this box the South Pacific and especially the coast of Australia (Great Barrier Reef) play an essential role for the origin of their air masses and hence for the high trace gas concentrations. The different characteristics of the three shown trace gases along the cruise resembles the identified atmospheric regimes (Chapter 7). Methyl iodide is well correlated with the wind speed over almost the whole cruise with a correlation coefficient of 0.56. Hence, it is an additional observation to the results of Wanninkhof et al. (1985); Smethie et al. (1985); Liss and Merlivat (1986); Tsai and Liu (2003). They reported a correlation between methyl iodide concentrations and wind speed. Bromoform and methane show a weak correlation coefficient of 0.20 respectively 0.23, hence, weak correlations with wind speed. Along the cruise methane shows the typical meridional behavior with a gradient from the NH to the SH. The concentrations decrease with decreasing latitudes (NOAA, 2010).

Within the scope of this study the transport of trace gases is investigated by using two different trajectory models. Using other trajectory models, which include chemical precesses, are usefull to verify these results and give more details. Additionally further trace gases of the air parcels should be examined to check their origins and connect it with the results of this thesis. Furthermore investigations of the Western Pacific regions and a precise determination of their sources can give more information in relationship to the trace gases concentrations worldwide.

List of Figures

List of Tables

Appendix A

Addition to Chapter 5

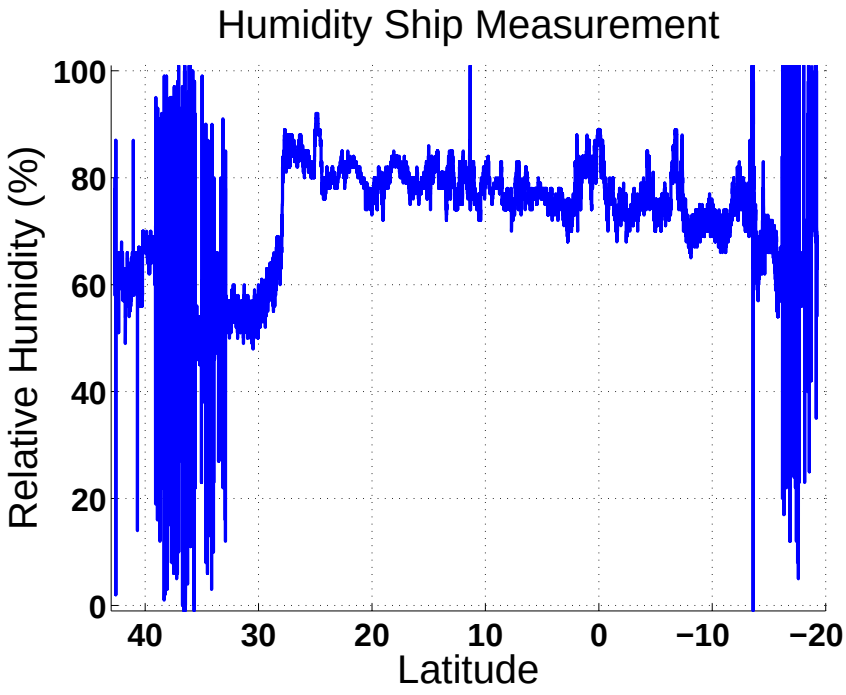

Figure A.1: The blue curve shows the real measured humidity during the whole track of the TransBrom-Sonne campaign from October 9 to 24, 2009.

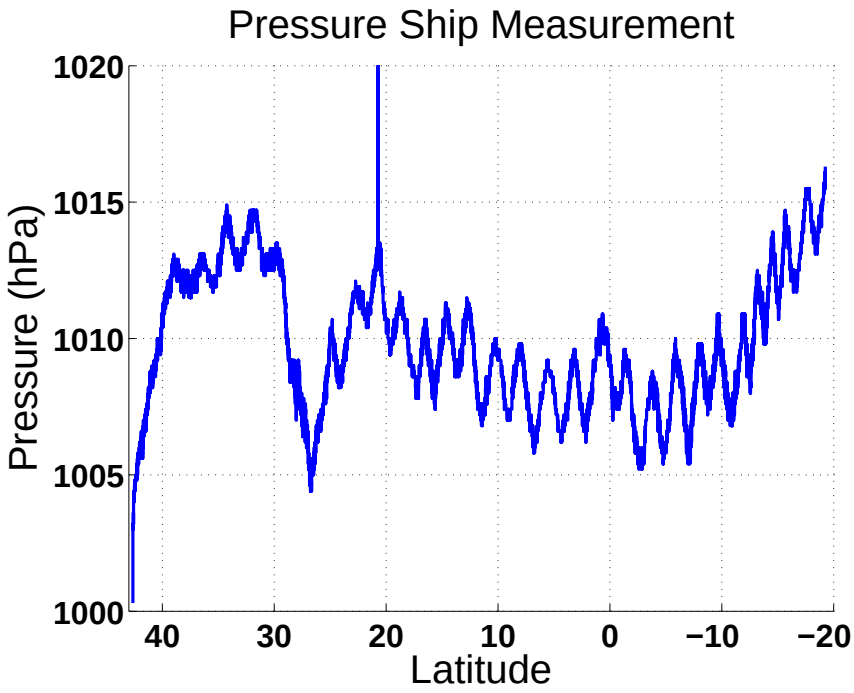

Figure A.2: The blue curve shows the real measured pressure during the whole track of the TransBrom-Sonne campaign from October 9 to 24, 2009.

Bibliography

Andreae, M. O., E. Atlas, G. W. Harris, G. Helas, A. de Kock, R. Koppmann, W. Maenhaut, S. Mano, W. H. Pollock, J. Rudolph, D. Scharffe, G. Schebeske, and M. Welling, 1996: Methyl halide emissions from savanna fires in southern africa. *Journal of Geophysical Research-Atmospheres*, **101**, 23603–23613.

Anthes, R. A., 1982: *Tropical Cyclones: Their Evolution, Structure and Effects*. American Meteorological Society.

Bjerknes, J., 1966: A possible response of the atmospheric hadley circulation to anomalies of ocean temperature. pp. 820–829.

Bjerknes, J., 1969: Atmospheric teleconnections from the equatorial pacific. pp. 163–172.

Blake, D., 2010: Methane, nonmethane hydrocarbons, alkyl nitrates, and chlorinated carbon compounds including 3 chlorofluorocarbons (cfc-11, cfc-12, and cfc-113) in whole-air samples.

Blake, N. J., D. R. Blake, A. L. Swanson, E. Atlas, F. Flocke, and F. S. Rowland, 2003: Latitudinal, vertical, and seasonal variations of c-1-c-4 alkyl nitrates in the troposphere over the pacific ocean during pem-tropics a and b: Oceanic and continental sources. p. 108.

Blake et al., 1999: Aircraft measurements of the latitudinal, vertical, and seasonal variations of nmhcs, methyl nitrate, methyl halides, and dms during the first aerosol characterization experiment (ace 1). *J. Geophys. Res.*, **104**, 21,803 – 21,818.

Butler, J. H., D. B. King, J. M. Lobert, S. A. Montzka, S. A. Yvon-Lewis, B. D. Hall, N. J. Warwick, D. J. Mondeel, M. Aydin, and J. W. Elkins, 2007: Oceanic distributions and emissions of short-lived halocarbons. *Global Biogeochem. Cycles*, **21**, GB1023.

Carpenter, D. J. W., L. J., J. R. Hopkins, R. M. Dunk, C. E. Jones, K. E. Hornsby, and J. B. McQuaid, 2007: Bromoform in tropical atlantic air from 25Â°n to 25Â°s. *eophys. Res. Lett.*, **34**, L11810, doi:10.1029/2007GL029893.

Chameides, W. L. and D. D. Davis, 1980: Iodine: Its possible role in tropospheric photochemistry. *J. Geophys. Res.*, **85**, 7383 – 7398.

Cram, T. A., J. Persing, M. T. Montgomery, and S. A. Braun, 2007: A lagrangian trajectory view on transport and mixing processes between the eye, eyewall, and environment using a high-resolution simulation of hurricane bonnie (1998). *J. Atmos. Sci.*, **64**(1835-1856).

Davis, D., J. Crawford, S. Liu, S. McKeen, A. Bandy, D. Thornton, F. Rowland, and D. Blake, 1996: Potential impact of iodine on tropospheric levels of ozone and other critical oxidants. *J. Geophys. Res.*, **101**, 2135 – 2147.

Deutscher Wetterdienst, 1987: *Allgemeine Meteorologie*. Deutscher Wetterdienst, 3rd edition.

Dimmer, C. H., P. G. Simmonds, G. Nickless, and M. R. Bassford, 2001: Biogenic fluxes of halomethanes from irish peatland ecosystems. *Atmospheric Environment,*, pp. 321–330.

Dlugokencky, E. J., K. A. Masarie, P. M. Lang, and P. P. Tans, 1998: Continuing decline in the growth rate of the atmospheric methane burden. *Nature*, **393 (6684)**, 447–450.

Dorf, M., J. H. Butler, A. Butz, C. Camy-Peyret, M. P. Chipperfield, L. Kritten, S. A. Montzka, B. Simmes, F. Weidner, and K. Pfeilsticker, 2006: Long-term observations of stratospheric bromine reveal slow down in growth. *Geophys. Res. Lett.*, **32**(L24803, doi:10.1029/2006GL027714).

Draxler, R. R. and G. D. Hess, 2004: Description of the hysplit 4 modeling system. *NOAA Technical Memorandum*, pp. ERL, ARL–224.

Etling, D., 2008: *Theoretische Meteorologie Eine Einfuehrung*. Springer Verlag.

Flohn, H., 1950a: Studien zur allgemeinen Zirkulation der Atmosphäre. p. 50 pages.

Frauen, C., 2010: Enso mechanismen und wechselwirkungen in einem hybrid-gekoppelten “recharge oscillator“modell. *Leibniz - Institut für Meereswissenschaften Kiel*.

Fujiwara, M., 2007: *http://sower.ees.hokudai.ac.jp/snowwhite/sys/tmax/ozonesonde.preparation.doc*.

Fujiwhara, S., 1923: On the growth and decay of vortical systems. pp. 75–104.

Fujiwhara, S., 1931: Short note on the behavoir of two vortices. pp. 106–110.

Globalview CH4, 2005: Cooperative atmospheric data integration project - methane. *CD-ROM, NOAA CMDL, Boulder, Colo.*, pp. Available via anonymous FTP to ftp.cmdl.noaa.gov, Path: ccg/ch4/–GLOBALVIEW.

Gray, W., 1979: Hurricanes: Their formation, structure and likely role in the tropical circulation. meteorology over the tropical oceans. *Royal Meteorological Society, Bracknall, England*.

Haeckel, H., 2005: *Meteorologie*. Ulmer UTB, 5th edition.

Harris, J. M., R. R. Draxler, and S. J. Oltmans, 2005: Trajectory model sensitivity to differences in input data and vertical transport method. *J. Geophys. Res*, **110**(D14109, doi:10.1029/2004JD005750.).

IPCC, 2001: (Intergovernmental Panel on Climate Change), Climate Change 2001: The Scientific Basis: Contribution of Working Group I to the Third Assessment Report of the Intergovernmental Panel on Climate Change. *edited by J.T. Houghton, Y. Ding, D.J. Griggs, M. Noguer, P.J. van der Linden, X. Dai, K. Maskell, and C.A. Johnson*, pp. 881 pp., Cambridge University Press, Cambridge, U.K.

Koennen, G. P., P. D. Jones, M. H. Kaltofen, and R. J. Allan, 1998: Pre-1866 extensions of the southern oscillation index using early indonesian and thahitian meteorological readings.

Latif et al., 2007: Tropical sst and hurrican development. *Geophysical Research Letters*.

Lee-Taylor, J. and K. R. Redeker, 2005: Reevaluation of global emissions from rice paddies of methyl iodide and other species,. *Geophysical Research Letters*, **32**.

Li, H.-J., Y. Yokouchi, H. Akimoto, and Y. Narita, 2001: Distribution of methyl chloride, methyl bromide, and methyl iodide in the marine boundary layer air over the western pacific and southeastern indian ocean. *Geochemical Journal*, **35**, pp. 137–144.

Liss, P. S. and L. Merlivat, 1986: Air-sea exchange rates: Introduction and synthesis, in: Buat-mĂ©nard, p. (eds.), the role of air-sea exchange in geochemical cycling. *D. Reidel Publishing Company, Dordrecht, Boston, Lancaster, Tokyo*, pp. 113–127.

Liu, C. and E. J. Zipser, 2005: Global distribution of convection penetrating the tropical tropopause. *J. Geophys. Res*, **110**, D23104, doi:10.1029/2005JD006063.

Lovelock, J. E., R. J. Maggs, and R. J. Wade, 1973: Halogenated hydrocarbons in and over the atlantic. *Nature*, **241**, 194 – 196.

MacFarling-Meure, C., 2004: The variation of atmospheric carbon dioxide, methane and nitrous oxide during the holocene from ice core analysis. *Ph.D. thesis, University of Melbourne, Australia*.

Manley, S. L. and J. L. dela Cuesta, 1997: Methyl iodide production from marine phytoplankton cultures. *Limnol. Oceanogr.*, **42**, 142–147.

McFiggans, G., J. M. C. Plane, B. J. Allan, L. J. Carpenter, H. Coe, and C. O'Dowd, 2000: A modeling study of iodine chemistry in the marine boundary layer. *J. Geophys. Res.*, **105**, 14,371 – 14,386.

Molinari, J. and F. Robasky, 1992: Use of ecmwf operational analyses for studies of the tropical cyclone environment. *Meteor. Atmos. Phys.*, **47**, 127–144.

Moore, R. M. and R. Tokarczyk, 1993: Volatile biogenic halocarbons in the northwest atlantic. *Global Biogeochem. Cycles*, **7**, 195–210.

NASA, 2006: Nasa. http://www.nasa.gov/vision/earth/lookingatearth/ozonerecord.html.

NOAA, 2010: Global methane distribution. http://www.esrl.noaa.gov.

O'Dowd, C. D., J. L. Jimenez, R. Bahreini, R. C. Flagan, J. H. Seinfeld, K. Hameri, L. Pirjola, M. Kulmala, S. G. Jennings, and T. Hoffmann, 2002: Marine aerosol formation from biogenic iodine emissions. *Nature*, (417), 632 – 636.

Petterssen, S., 1950: Some aspects of the general circulation of the atmosphere. pp. 120–155.

Pidwirny, M., 2010: Understanding physical geography, 1st edition. http://www.physicalgeography.net/understanding/contents.html.

Qasim, S., P. Bhattathiri, and V. Devassy, 1972: The influence of salinity on the rate of photosynthesis and abundance of some tropical phytoplankton. *Marine biology*, **12**, pp. 200–206.

Quack, B., E. Atlas, G. Petrick, V. Stroud, S. Schauffler, and D. W. R. Wallace, 2004: Oceanic bromoform sources for the tropical atmosphere. *Geophysical Research Letters*, **31**.

Quack, B., E. Atlas, G. Petrick, and D. W. R. Wallace, 2007: Bromoform and dibromomethane above the mauritanian upwelling: Atmospheric distributions and oceanic emissions. *Geophysical Research Letters*, **112**, D09312, doi:10.1029/2006JD007614.

Quack, B. and D. Wallace, 2003: Air-sea flux of bromoform: Controls, rates, and implications.

Rasmussen, R. A., M. A. K. Khalil, R. Gunawardena, and S. D. Hoyt, 1982: Atmospheric methyl iodide. *J. Geophys. Res.*, **87**, 3086 – 3090.

Richter, U. and D. W. R. Wallace, 2004: Production of methyl iodide in the tropical atlantic ocean. *Geophys. Res. Lett.*, **34**.

Roe, J. M. and W. H. Jasperson, 1981: A temperature lapse rate definition of the tropopause based on ozone. *WMO*.

Salawitch, R., D. Weisenstein, L. Kovalenko, C. Sioris, P. Wennberg, K. Chance, M. Ko, and C. McLinden, 2005: Sensitivity of ozone to bromine in the lower stratosphere. *Geophys. Res. Lett.*, **32(5)**(L05811, doi: 10.1029/2004GL021504, 2005.).

Smethie, W., T. Takahashi, D. Chipman, and J. Ledwell, 1985: Gas exchange and $co/_2$ flux in the tropical atlantic ocean from ^{222}rn and $_pco/_2$ measurements. *J. Geophys. Res.*, **90,C4**(7005-7022).

Solomon, S., R. R. Garcia, and A. R. Ravishankara, 1994: On the role of iodine in ozone depletion. *J. Geophys. Res.*, **99**, 20,491–20,499.

Spahni et al., 2005: Atmospheric methane and nitrous oxide of the late pleistocene from antarctic ice cores. *Science*, **310 (5752)**, 1317–1321.

Troup, A., 1965: The southern oscillation.

Tsai, W.-T. and K.-K. Liu, 2003: An assessment of the effect of sea surface surfactant on global atmosphere-ocean $co/_2$ flux. *J. Geophys. Res.*, **108,C4**(24-1 - 24-6).

U.S. Standard Atmosphere, 1976: (nasa-tm-x-74335) national oceanic and atmospheric administration,.

Walker, G. T., 1923: Correlation in seasonal variation of weather viii: A preliminary study of world weather. pp. 75–131.

Walker, G. T., 1924: Correlation in seasonal variation of weather ix: A further study of world weather. pp. 225–232.

Wanninkhof, R., J. Ledwell, and W. Broecker, 1985: Gas exchange-wind speed relation measured with sulfur hexafluoride on a lake. *Science*, **227**(869-875).

Warwick, N. J., A. Pyle, G. D. Carver, X. Yang, N. H. Savage, F. M. O'Connor, and R. A. Cox, 2006: Global modeling of biogenic bromocarbons. *J. Geophys. Res.*, **111**(D24305, doi:10.1029/2006JD007264).

WMO, 1993: *Tropical Cyclone Programme, Report No. TCP-31,*. World Meteorological Organization, Geneva, Switzerland, wmo/td - no. 560 edition.

WMO, 2007b: *Scientific Assessment of Ozone Depletion*. World Meteorological Organization, Geneva, Switzerland.

Yokouchi, Y., K. Osada, M. Wada, F. Hasebe, M. Agama, R. Murakami, H. Mukai, Y. Nojiri, Y. Inuzuka, D. Toom-Sauntry, and P. Fraser, 2008: Global distribution and seasonal concentration change of methyl iodide in the atmosphere. *J. Geophys. Res.*, **113**, D18311.

Zafiriou, O. C., 1974: Photochemistry of halogens in the marine atmosphere. *J. Geophys. Res.*, **79**(2730-2732), doi:10.1029/JC079i018p02730.

Zhou, Y., H. Mao, R. S. Russo, D. R. Blake, O. W. Wingenter, K. B. Haase, J. Ambrose, R. K. Varner, R. Talbot, and B. C. Sive, 2008: Bromoform and dibromomethane measurements in the seacoast region of New Hamsphire, 2002-2004. pp. D08305, doi:1029/2007JD009103.

Acknowledgments

In erster Linie möchte ich mich bei Prof. Dr. Kirstin Krüger für die Vergabe des Themas, die gute Betreuung, die Möglichkeit der Teilnahme an der TransBrom-Sonne Kampagne und für die anschließende Korrektur der Arbeit bedanken. Desweiteren möchte ich mich bei Dr. Birgit Quack ebenfalls für die Möglichkeit der Teilnahme an der Kampagne und für die Zweitkorrektur bedanken.
Außerdem danke ich dem WGL Projekt und dem BMBF für die Finanzierung der Fahrt, sowie dem TransBrom-Team und der Sonne-Crew für die gute Zusammenarbeit und Elliot Atlas für das zur Verfügung stellen der Luftmessungen.
Ebenso danke ich der gesamten Arbeitsgruppe Krüger für die ständige Bereitschaft, Hilfestellung zu leisten (speziell in Matlabfragen und bei den Korrekturen) und den Anregungen während der Gruppensitzungen.

Micha, Viky und Alex möchte ich ebenfalls für die Hilfe bei Programmierproblemen, das Korrekturlesen von Kapiteln und vor allem für die netten und oft sehr lustigen (Mittags-/Kaffe-)Pausen danken.
Mein Dank gilt vor allem auch Ina und Sonja, die sich die Zeit genommen haben die Arbeit zu korrigieren und ganz besonders, dass ihr mich immer unterstützt habt, dieses Ziel zu erreichen!!!!
Außerdem möchte ich meinen Eltern danken, die mich während meines gesamten Studiums unterstützt haben.

Die Arbeit wurde mit der Textverarbeitung LaTeX angefertigt.

Erklärung

Hiermit bestätige ich, dass ich die vorliegende Diplomarbeit selbständig verfasst und keine anderen als die angegebenen Quellen und Hilfsmittel verwendet habe.
Ich versichere, dass diese Arbeit noch nicht zur Erlangung eines Diplomgrades an anderer Stelle vorgelegen hat.

Kiel, November 30, 2010

(Sebastian Wache)